Modelling the Fate of Sediments and Micropollutants in Rivers

Dissertation

vorgelegt von

Yan Liu

aus Shaanxi, China

Tübingen

2018

Gedruckt mit Genehmigung der Mathematisch-Naturwissenschaftlichen Fakultät der Eberhard Karls Universität Tübingen.

Abstract

In industrialized countries, the assessment of water quality in rivers remains a timely topic even though problems of eutrophication have been overcome by wastewater treatment. In particular, hydrophobic organic pollutants that typically sorb to suspended sediments (e.g., PAH), and pharmaceuticals that are not included in regular treatment of WWTPs have gained environmental concerns. These pollutants occur at concentrations of nano- to micro-grams per liter in rivers. Continuous monitoring of these compounds is time- and cost-consuming. A modelling approach is advantageous and necessary to understand the interacting environmental processes that determine the fate of micropollutants in river systems.

Sediment transport facilitates the transport of PAH, one group of micropollutants of interest in this thesis. Combining hydrological, hydraulic, and in-stream transport models can give good insights on sediment sources and transport on the catchment-scale, which is essential for investigating the fate of PAH. Therefore, I developed such an integrated sediment transport model to simulate sediment contributions from catchment and in-stream processes under different flow conditions. The characteristics of surface runoff essentially control the sediment supply from urban and rural areas. In the mainly groundwater-fed Ammer catchment, the weak rural surface runoff leads to a small rural sediment supply. By contrast, urban particles dominate the annual sediment load. The flow rate and river geometry determine the deposition and remobilization of sediments in the river. The modelled sediment trapping occurs in very mild reaches of River Ammer.

I extended the integrated sediment transport model to a particle-facilitated pollutant transport model, which considers PAH interaction between water and sediment. This model allows to study the source, turnover, and legacy potential of PAH in river systems. The supply and composition of sediments determine to a large extent the PAH supply to a river. In the Ammer River, the high proportion of urban particles with high PAH content results in the dominant supply of PAH from urban areas. In steep reaches, sediment turnover governs the turnover of PAH, whereas in very mild river segments diffusion of PAH from the river bed to the mobile water is relevant and reduces PAH turnover times.

PAH legacy occurs in river segments with slow sediment turnover. For River Ammer, the simulated sediment trapping reaches have acted as secondary PAH source over 10-20 years after the introduction of environmental regulations in the 1970s.

Pharmaceuticals are emitted to rivers by WWTPs due to incomplete removal. I developed a one-dimensional reactive solute transport model considering transient storage to investigate the transport and fate of these compounds in the WWTP effluent-impacted River Steinlach. The degradation processes are substantially affected by the local conditions. Carbamazepine is relatively conservative, sulfamethoxazole is only biodegradable, while metoprolol and venlafaxine undergo both photo- and bio-degradation. The flow rate influences the relative transient storage and thus pollutant removal decreases with increasing flow rates, particularly under low-flow conditions. The combination of tracer experiments and the Lagrangian sampling approach of pollutants can improve model calibration and diagnose different attenuation mechanisms.

This thesis aims at understanding major controls of transport of sediments as well as dissolved and sediment-bound micropollutants in two exemplary rivers to investigate the long-term fate of sediment-bound micropollutants (PAH) and the transport and transformation dynamics of dissolved micropollutants (pharmaceuticals). While I developed the models to meet measured data in Rivers Ammer and Steinlach, the framework is transferable to other small streams that are affected by anthropogenic micropollutants.

Kurzfassung

In den Industrieländern bleibt die Bewertung der Wasserqualität in Flüssen ein aktuelles Thema, auch wenn die Probleme der Eutrophierung durch die Abwasserbehandlung überwunden worden sind. Insbesondere hydrophobe organische Schadstoffe (z.B. PAK), welche üblicherweise an suspendiertes Sediment sorbieren und Pharmazeutika, die nicht in die reguläre Behandlung von Abwasserbehandlungsanlagen (WWTPs) einbezogen werden sind ein ökologisches Anliegen. Diese Schadstoffe treten in Konzentrationen von Nano- bis Mikrogramm pro Liter in Flüssen auf. Die kontinuierliche Überwachung dieser Verbindungen ist zeit- und kostenintensiv. Der Modellierungsansatz ist zweckmäßig und notwendig für ein Verständnis der interagierenden Umweltprozesse, die das Verhalten der Mikroschadstoffe von Interesse in Flusssystemen bestimmen.

Sedimenttransport fördert den Transport von PAK, einer Gruppe an Mikroschadstoffen von Interesse dieser Arbeit. Die Kombination von hydrologischen, hydraulischen und in Flüssen stattfindenden Transformationsprozessen in einem Transportmodellen kann gute Einblicke in Sedimentquellen und den Transport auf Einzugsgebietsskala liefern, welche für die Untersuchung des Verbleibs von PAK essentiell ist. Aus diesem Grund entwickelte ich ein solches integriertes Sedimenttransportmodell, um Sedimentbeiträge aus Einzugsgebieten und in Flüssen stattfindenden Transformationsprozessen unter verschiedenen Strömungsbedingungen zu simulieren. Die Eigenschaften des Oberflächenabflusses kontrollieren im Wesentlichen die Sedimentversorgung aus städtischen und ländlichen Gebieten. In einem überwiegend grundwasserversorgten Ammer-Einzugsgebiet führt der schwache ländliche Oberflächenabfluss zu einer geringen ländlichen Sedimentversorgung, allerdings dominieren urbane Partikel die jährliche Sedimentfracht. Die Fließgeschwindigkeit und Flussgeometrie bestimmen die Ablagerung und Remobilisierung von Sedimenten im Fluss. Der modellierte Sedimentfang kommt in sehr sanft abfallendenen Flussabschnitten des Ammers vor.

Ich habe das integrierte Sedimenttransportmodell zu einem Partikel-förderndes Schadstofftransportmodell erweitert, das die PAH-Wechselwirkung zwischen Wasser und Sedi-

ment berücksichtigt. Das Modell erlaubt es, Quellen-, Umsatz- und Altlast-Potenzial von PAK in Flusssystemen zu untersuchen. Die Materialzufuhr und Zusammensetzung der Sedimente bestimmen zu einem großen Teil die PAK-Versorgung eines Flusses. In der Ammer führt der hohe Anteil von urbanen Partikeln mit hoher PAK-Kontamination zu einer dominierenden PAK-Versorgung aus städtischen Gebieten. In steilen Flussabschnitten bestimmt der Sedimentumsatz den PAK-Umsatz, während in sehr sanft abfallenden Flussabschnitten die Diffusion von PAK aus dem Flussbett in das mobile Wasser relevant ist und die PAK-Umsatzzeiten reduziert. PAK-Altlasten treten in Flusssegmenten mit einem langsamen Sedimentumsatz auf. Für den Fluss Ammer haben die simulierten Sedimentfanggebiete über 10-20 Jahre nach der Einführung von Umweltreglementierungen in den 1970er Jahren als sekundäre PAK-Quelle gedient.

Arzneimittel gelangen durch Kläranlagen aufgrund unvollständiger Beseitigung dieser Stoffe in Flüsse. Ich entwickelte ein eindimensionales reaktives Transportmodell für gelöste Stoffe unter Einbezug des "Transient Storages", um den Transport und das Verhalten dieser Verbindungen in dem von Abwässern betroffenen Fluss Steinlach zu untersuchen. Die Abbauprozesse werden wesentlich durch die lokalen Bedingungen beeinflusst. Carbamazepin ist relativ konservativ, Sulfamethoxazol ist lediglich biologisch abbaubar, während Metoprolol und Venlafaxin sowohl photolytisch als auch biologisch abbaubar sind. Die Flussrate beeinflusst den "Transient Storage"und somit die Schadstoffentfernung. Diese nimmt mit Zunahme der Strömungsraten ab, insbesondere bei geringen Durchflussbedingungen. Die Kombination von Tracer-Experimenten und Lagrangian-Probenahme von Schadstoffen kann die Modellkalibrierung verbessern und verschiedene Abnahmemechanismen feststellen.

Ziel dieser Dissertation ist ein verbessertes Verständnis der wichtigsten Kontrollmechanismen des Transports von Sedimenten ebenso wie von gelösten und partikelgebundenen Mikroschadstoffen anhand zwei beispielhafter Flüsse und die Untersuchung des Langzeitverhaltens partikelgebundener Mikroschadstoffe (PAK) und der Transport- und Transformationsdynamik gelöster Mikroschadstoffe (Arzneimittel). Obwohl ich die Modelle zur Erfüllung der Messdaten der Flüsse Ammer und Steinlach entwickelte ist der Rahmenplan auf andere kleine von anthropogenen Mikroschadstoffen beeinflussten Flüssen übertragbar.

Acknowledgement

I express my great appreciation to people who gave me help and support during my PhD study and also to the excellent Research Training Group (RTG) "Integrated Hydrosystem Modeling" that provides me funding.

Foremost, I would like to thank my supervisor Prof. Olaf A. Cirpka who gave me instructions to pursue my research. He could always provide me with helpful discussions in the right and possible time. Without his constructive comments on my study and continuous support, I cannot successfully complete my dissertation.

I want to thank my junior supervisor Prof. Christiane Zarfl for her encouragement and support. She gave me advices on how to improve paper for publication and provided various discussions important for my thesis. Talking with her always makes me feel positive and supportive.

I would like to thank my supervisor Prof. Nandita B. Basu from University of Waterloo. During my research stay in Waterloo in 2017, she gave me constructive suggestions on my hydrological and sediment-transport model. She also helps to improve my scientific papers.

I am very grateful to Dr. Marc Schwientek and Dr. Hermann Rügner. They provided me support and discussions on field data, which makes me to better know my study areas.

I want to thank Dr. Chuanhe Lu for the help and advice on my thesis and discussions on numerical problems at the early stage of my study.

I would like to thank all of my colleagues for their help and discussions on scientific research and also for organizing interesting activities in Tübingen and Stuttgart.

I want to thank my family. They gave me unlimited and unconditional support, encouragement and love. I express my great thanks to my father. It is he that raised me up and supports me to pursue what I want. I wish he could have a healthy and peaceful life in another world. Finally, I want to thank my wife Juan Yao. She has been with me all the time and encourages me when I was in the most difficult time.

Contents

List of Figures

List of Tables

Chapter 1

Introduction

1.1 State of Research

1.1.1 Micropollutants

a. Occurrence and Environmental Impacts of Micropollutants

In recent decades, water quality concerns of a river are not only caused by nutrients, but also provoked by the increasing worldwide occurrence of micropollutants in the aquatic environment (Luo *et al.*, 2014; Yang *et al.*, 2017; Schwarzenbach *et al.*, 2006). Micropollutants comprise a vast and expanding group of substances originating from both anthropogenic and natural processes. As the name suggested, they appear in water at small concentrations in the range from nano- to micro-grams per liter (Kim and Zoh, 2016; Kim *et al.*, 2007; Barbosa *et al.*, 2016; Torresi *et al.*, 2017). They are also termerd as emerging contaminants, which are bioactive and persistent contaminants that cannot be fully eliminated by traditional wastewater treatment methods and are not completely biodegradable (Clara *et al.*, 2005; Tiedeken *et al.*, 2017; Reungoat *et al.*, 2010). Micropollutants typically include hydrophobic organic pollutants, pharmaceuticals, personal care products, steroid hormones, industrial chemicals, pesticides and herbicides, and many other compounds (Verlicchi *et al.*, 2012; Luo *et al.*, 2014; Tijani *et al.*, 2013, 2016). The "low concentration" and diversity of micropollutants not only complicate the associated detection and analysis procedures but also create challenges for water and wastewater treatment processes (Luo *et al.*, 2014).

Micropollutants are produced by diverse processes, and then released to different compartments of the environment. The occurrence of micropollutants in aquatic environment

has received increasing attention (Félix-Cañedo *et al.*, 2013; Verliefde *et al.*, 2007; Kim and Zoh, 2016). Studies have shown various detection and contamination levels of micropollutants in the aquatic environment in many countries and regions, which essentially includes studies on influent and effluent of wastewater treatment plants (WWTPs), surfacer water, groundwater and drinking water (Nam *et al.*, 2014; Chiffre *et al.*, 2015; Schwientek *et al.*, 2017; Osenbrück *et al.*, 2007; Benotti *et al.*, 2008).

Almost all kinds of micropollutants can be detected in WWTPs because WWTPs receive domestic and industrial wastewater and also surface runoff during rainfall events that carry the majority of micropollutants (Köck-Schulmeyer *et al.*, 2013; Prieto-Rodríguez *et al.*, 2013; Margot *et al.*, 2013). The traditional WWTPs are incapable to treat these compounds, thus the effluent of WWTPs contains various micropollutant residuals. Studies show significant spatial and temporal variations of micropollutants in WWTP influent and effluent, which is caused by many factors, e.g., influent composition, metabolism (excretion rate), and elimination efficacy of wastewater treatment processes (Petrovic *et al.*, 2009; Luo *et al.*, 2014).

Surface water can be the receiving bodies for micropollutants. In particular, rivers and streams play significant roles in the transport and fate of micropollutants. The effluent from WWTPs and direct surface runoff contribute to the input of micropollutants to rivers and streams, where various attenuation processes take place (Wang and Lin, 2014; Li *et al.*, 2013; Pal *et al.*, 2010). Due to dilution with river water, micropollutant concentrations are smaller in the river than in the WWTP effluent, so that the proportion of WWTP effluent to the river flow is a major controlling factor of micropollutants (Gros *et al.*, 2007). Meanwhile, streams can be temporally sinks or sources of micropollutants due to the sorption/desorption of pollutants onto sediments. The fate of micropollutants in the rivers is important for understanding the environmental impacts, e.g., the overall toxicity of river water. Polycyclic Aromatic Hydrocarbons (PAH) and polychlorinated biphenyls (PCBs) are widely reported in river sediments (Cui *et al.*, 2016; Fadaei *et al.*, 2015; Schwientek *et al.*, 2013b; Liu *et al.*, 2013), which demonstrates the importance of sediment transport hydrophobic micropollutants.

Few studies show that micropollutants are also detected in groundwater (Osenbrück *et al.*, 2007; Phillips *et al.*, 2015; Manamsa *et al.*, 2016), but groundwater is less contaminated with micropollutants than surface water (Vulliet and Cren-Olivé, 2011; Luo *et al.*, 2014). Lapworth *et al.* (2012) conducted a literature review indicating that the vast majority of groundwater resources do not contain micropollutants in concentrations that

would be considered toxic and/or harmful due to natural attenuation and dilution mechanisms. Therefore, the presence of micropollutants is not considered to be significant in groundwater (Stuart *et al.*, 2012). Few studies tried to address the occurrence of micropollutants in drinking water (Vulliet *et al.*, 2011; Luo *et al.*, 2014). These studies show that most micropollutants in drinking water undergoing proper treatment were below the limit of quantitation (Benotti *et al.*, 2008; Huerta-Fontela *et al.*, 2011; Kleywegt *et al.*, 2011; Luo *et al.*, 2014).

Many micropollutants have been detected in the Ammer and Steinlach Rivers, which are the two study rivers of this thesis (details about studied rivers are depicted in Sect. 1.2). Table 1.1 shows some of the measured micropollutants in the two rivers.

Table 1.1: Measured micropollutants in the Ammer and Steinlach Rivers

Group	Compound	River	Reference
Pharmaceuticals	Carbamazepine Diclofenac Metroprolol Venlafaxine Sulfamethoxazole		
Polycyclic musk fragrances	HHCB/HHCB-lactone AHTN OTNE	Steinlach River	(Schwientek *et al.*, 2016) (Guillet *et al.*, 2018)
Phosphorus flame retardants	TCPP TDCPP/TDCP TCEP		
Pesticides	Mecoprop		
Insect repellents	DEET		
PAH	15 priority PAH	Ammer River	(Liu *et al.*, 2013)
PCBs	Some		(Schwientek *et al.*, 2013b)

The increasing number of micropollutant occurrences in receiving water bodies have raised growing concerns on the potential effects of unintended exposure to humans and ecosystems (Kim and Zoh, 2016; Tijani *et al.*, 2016; Schwarzenbach *et al.*, 2006; Yang *et al.*, 2017). Despite the low concentrations in aquatic environment, micropollutants may have adverse impacts on the ecosystem including the following aspects:

- The residues of pharmaceuticals, personal care products, and some persistent organic pollutants can eventually enter into the food chain through effluent discharge and the reuse of treated sewage and sludge for agricultural applications (Yang *et al.*, 2017; Kim and Zoh, 2016; Rajapaksha *et al.*, 2014; Vithanage *et al.*, 2014). These exposures can cause persistent bioaccumulation in wildlife, human tissues, and the ecosystem (Focazio *et al.*, 2008; Tijani *et al.*, 2016). Chronic exposure to the human body can cause potentially unknown long-term health effects (Boxall *et al.*, 2012; Yang *et al.*, 2017).

- The eventual presence of endocrine disrupting compounds, such as steroid estrogens, in the environment poses a significant potential problem of interference with the normal function of the endocrine systems of wildlife, and can thus affect reproduction and development in wildlife (Manickum and John, 2014; Falconer *et al.*, 2006).

- Some persistent organic compounds ubiquitously appearing in the aquatic environment (e.g., PAH) may be potentially toxic, mutagenic, and carcinogenic to human health and aquatic systems (Aziz *et al.*, 2014; Colombo *et al.*, 2006; Yan *et al.*, 2004).

b. Source of Micropollutants

Micropollutants may enter the environment via different pathways, influenced by pollutant properties, management and treatment strategies, and implemented regulations (Barbosa *et al.*, 2016). Depending on the types of micropollutants, i.e., dissolved and particle-facilitated, main contributions of these compounds to river systems can vary between point and non-point sources.

Th main sources and pathways of micropollutants entering aquatic environment are described in Fig. 1.1. They can be summarized as follows: (i) WWTP effluent and overflows of domestic, industrial, and hospital wastewater; (ii) runoff from impervious surfaces (roads and paved areas in urban regions), agriculture, livestock and aquaculture; (iii) landfill leachates (Barbosa *et al.*, 2016; Tijani *et al.*, 2016).

Studies have reported that the release of WWTP effluent into river systems is considered as the main source of pharmaceuticals and personal care products compared with other sources (Alder *et al.*, 2004; Kasprzyk-Hordern *et al.*, 2009; Phillips *et al.*, 2012;
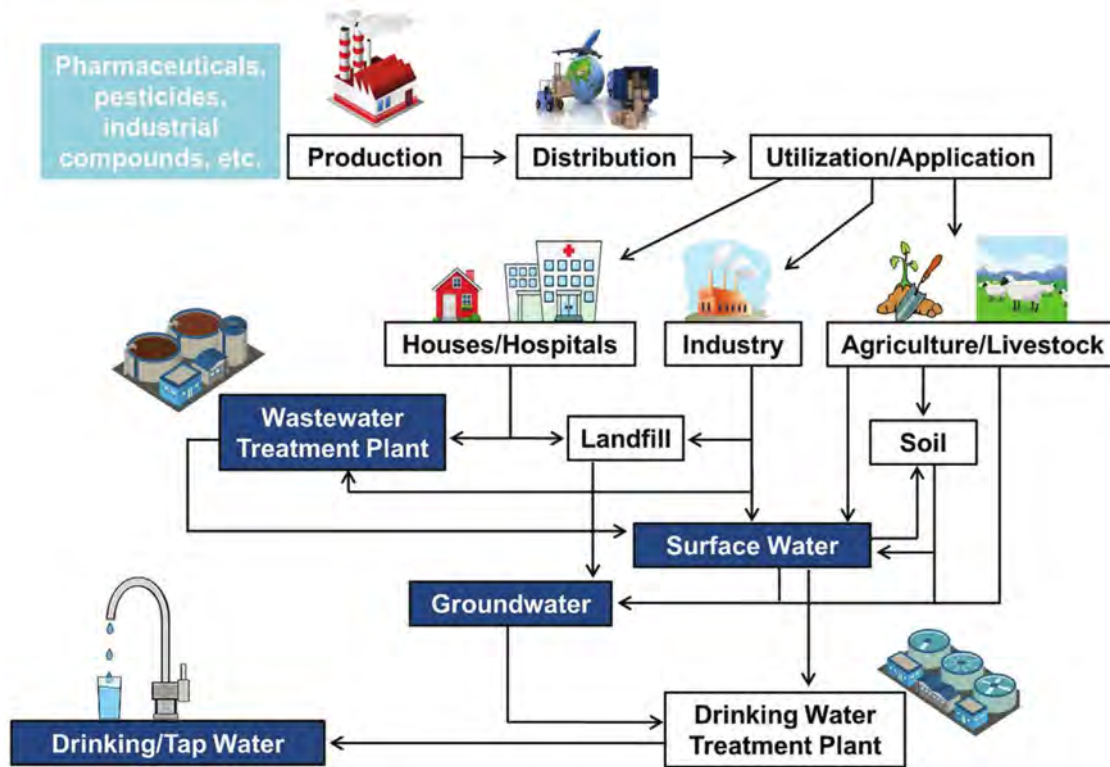
Figure 1.1: Representative sources and routes of micropollutants in the environment

Launay *et al.*, 2016). That is because traditional WWTPs are not designed for the treatment of micropollutants (Aristi *et al.*, 2016; Hughes *et al.*, 2012; Pal *et al.*, 2010). Due to the incomplete removal of these pollutants by WWTPs, the contaminants may at least partially be released into surface water. A certain fraction, however, is retained and adsorbed onto sewage sludge. The sludge is sometimes used by farmers for agricultural soil enrichment, but as it may also contain emerging pollutants, this represents another way how these contaminants get into soil and water (Tijani *et al.*, 2013). Apart from WWTP discharges, other exposure pathways exist, including animal feeding operations, land-applied bio-solids, emissions from manufacturing sites, pharmaceutical industries, mining activities, hospitals and health service centres, agricultural practices, irrigation with wastewater, disposal of unused medicines to landfills, and runoff of veterinary medicines from hard surfaces in farmyards (Boxall *et al.*, 2012; Agunbiade and Moodley, 2014; Kidd *et al.*, 2007; Fick *et al.*, 2009; Price *et al.*, 2010).

Rainfall can dilute concentrations of some micropollutants, e.g., pharmaceuticals. However, rainfall does not always reduce concentrations in rivers, because rainfall events

could intensify combined sewer overflows, resulting in a higher level of contaminant discharge and the untreated overflows can directly reach rivers (Luo *et al.*, 2014). For pesticides and particle-bound micropollutants, e.g., PAH and PCBs, rainfall and surface runoff are identified as the major contributor of the emission to surface water. The contamination level of these pollutants can be influenced by land use (e.g., rural and urban areas), features of the land close to the water bodies (soil use, slope, and distance from water bodies), characteristics of the water bodies (depth and flow rate), crop type, soil properties, and climatic conditions (temperature, rainfall, moisture and wind) (Bermúdez-Couso *et al.*, 2013; Luo *et al.*, 2014). Some studies reveal that chemicals (e.g., bisphenol A and biocides) used in building material (e.g., pavement materials, facades and roof paintings) may leach during precipitation and accumulate to remarkable levels in roof runoff and subsequently end up in surface water (Jungnickel *et al.*, 2008; Schoknecht *et al.*, 2009; Singer *et al.*, 2010; Luo *et al.*, 2014).

In the two studied rivers of this thesis, the focus of investigated micropollutants is different, i.e., sediment-bound compounds (PAH) in the Ammer River and dissolved compounds (pharmaceuticals) in the Steinlach River. Because the transport of PAH is mainly facilitated by sediment transport, the major contribution of PAH to rivers are sediment-related, e.g., surface runoff induced washoff and WWTP emissions. Such pollutants could have a legacy due to the long-term storages of sediments in the river bed. By contrast, the dissolved pharmaceuticals are mainly released as solutes by WWTPs (Schwientek *et al.*, 2016; Guillet *et al.*, 2018).

c. Fate of Micropollutants

The fate of micropollutants in the aquatic systems essentially influences their environmental impacts. Various processes can play roles in the removal of micropollutants including temporary removal, e.g., sorption to sediments and retention in slow-moving/stagnant water bodies and permanent removal, e.g., different natural degradation processes (photolysis and biodegradation) and artificial treatments. Some processes could contribute to the attenuation of concentration, e.g., dilution, dispersion and diffusion. Processes that determine the fate of a micropollutant are typically influenced by individual pollutant properties. Therefore, in the following I discuss the fate of two types of micropollutants i.e., dissolved micropollutants that can undergo degradation and sediment-bound pollutants that are persistent.

For dissolved micropollutants (here focusing on pharmaceuticals), the fate in rivers and streams is controlled by many processes, e.g., dilution, degradation, and retention (Kunkel and Radke, 2008; Wang and Lin, 2014; Li *et al.*, 2013). The degree of dilution is essentially determined by the composition of water flow. With the increase in the fraction of "clean water", the dilution effects become stronger. Degradation mainly consists of photodegradation and biodegradation, for some micropollutions abiotic hydrolysis also plays a role. Photodegradation has been reported as a very important process for the attenuation of many pharmaceuticals in natural waters such as antibiotics, nonsteroidal anti-inflammatory drugs (NSAIDs), -blockers, and chemotherapeutic drugs (Wang and Lin, 2014; Vulava *et al.*, 2016; Schimmelpfennig *et al.*, 2016; Santoke and Cooper, 2017). Photodegradation could be affected by shading of trees, turbidity of the water, and solar radiation intensity. Typically it undergoes a diurnal pattern (Hanamoto *et al.*, 2013) proportional to the solar radiation. Biodegradation is also supposed to be an important removal pathway for pharmaceuticals. It is substantially influenced by microbial activities so that microbial degradation happens in the place that is favorable for microorganisms. Due to the low abundance of microorganisms in river water, biodegradation mainly occurs in the sediment compartment with high density of microorganisms (Kunkel and Radke, 2008), which is also known as a part of the hyporheic zone. Stagnant water zones are good places for microbial to resident in as well (Burke *et al.*, 2014; Kunkel and Radke, 2008). To model degradation processes, first-order kinetics are often assumed with corrections by major environmental factors e.g., temperature and solar radiation intensity (Acuña *et al.*, 2015). The sediment layer of a river and dead water zones make up of the transient storage zone, which is the ideal place for biodegradation as well as for temporary retention of pollutants. After entering these places, they slowly leave to the mobile water, thus the travel time increases and the possibility for biodegradation increases as well.

For sediment-bound micropollutants (PAH), the processes that control their fate in river systems are quite different from pharmaceuticals. PAH are normally persistent in the aquatic system, especially for those with more rings. Degradation processes are seen insignificant. Due to the strong hydrophobicity and low solubility, sorption of PAH to suspended sediments and matters can strongly influence their ultimate fate in the environment (Patrolecco *et al.*, 2010). Sorption to suspended sediments help the removal of PAH from rivers to the receiving water bodies, e.g., lakes and oceans (Wang *et al.*, 2007; Gonzalez-Gaya *et al.*, 2014; Mai *et al.*, 2003), whereas deposition of suspended

sediments in rivers may take PAH to bed sediments that could be eroded and remobilized during big events. Because of the strong sorption of PAH to particles, the transport of PAH from watersheds to river systems and in-stream transport are mainly facilitated by sediment transport (Van Metre and Mahler, 2003; Rügner *et al.*, 2014a). Many studies have reported that suspended-sediment concentrations substantially influence the total PAH concentrations in water (Schwientek *et al.*, 2013a) and suspended sediments from urban surface runoffs show a very high PAH concent (DiBlasi *et al.*, 2009). Some studies also show that the atmospheric deposition rate of PAH is higher in urban areas than in rural regions (Bari *et al.*, 2014; Lang *et al.*, 2007; Liang *et al.*, 2016), which indirectly indicates urban particles may have a high PAH content. Therefore, the pathways for sediments entering streams from urban areas are of high importance for the fate of PAH.

1.1.2 Hydrological Models

Understanding water movement and pollutant transport in a catchment is of great importance. However, it is hardly possible to measure temporally and spatially distributed variables of a system due to high cost and limited techniques (Pechlivanidis *et al.*, 2011). Hydrological models are developed to simulate the water balance of different compartments of a catchment by considering important hydrological exchange processes.

Hydrological models have become a very useful and popular tool to investigate flow generation so that hydrologic systems can be well understood. The strength of hydrological models is that they can provide output at user required resolutions, which enables to study the system on different scales. A good hydrological model is the basis to study pollutant transport. Therefore, having a well verified hydrological model is usually the first step to understand the whole catchment system.

Understanding the current system and making predictions are both valuable. With the changing climate and land use, hydrological models have been developed to explore solutions for sustainable water resources planning, development and management in order to support decision makers and operational water managers (Johnston and Smakhtin, 2014). Hydrological models also receive wide applications to obtain input information for other coupled models such as studying water quality, hydro-ecology and climate response (Liu *et al.*, 2018b; Xu *et al.*, 2017; Teutschbein and Seibert, 2012).

Classification and Comparision of Hydrological Models

Hydrological models can be classified into different groups according to different classification systems. Here I discuss two frequently used classification systems. Based on model structure and applied theory, hydrological models are classified into metric (empirical), conceptual, and physics-based models. Metric models essentially use observed data to find response functions of studied catchments. They are simple to develop, but very much rely on the available data, such as unit hydrograph (UH) theory for event-based catchment-scale simulation (Sherman, 1932; Pechlivanidis *et al.*, 2011) and artificial neural networks (ANNs) to estimate discharge (Tiwari and Chatterjee, 2010; Seo *et al.*, 2015). Conceptual-hydrological models can be understood as conceptualizations of a hydrological system with several components representing interested hydrological processes. Usually not all of the model parameters have a direct physical meaning (i.e. they are not independently measurable). This type of models, e.g., the HBV (Hydrogiska Byråns Vattenbalansavdelning) model (Lindström *et al.*, 1997) varies in complexity by adding storage layers in the model structure, which are used to represent a conceptual view of the important hydrological features (Pechlivanidis *et al.*, 2011). Physic-based models consider physical hydrological processes, e.g., evapotranspiration, infiltration, and different types of flow from catchments using the governing partial differential equations of motion, which are usually solved by numerical methods with spatial discretisation. These models, e.g. HydroGeoSphere (Park *et al.*, 2011) and MIKE-SHE (Rujner *et al.*, 2018), are powerful, but identifying the necessary spatial parameters is difficult. Another classification system is based on spatial distribution. According to that, hydrological models are grouped into lumped models and distributed models. Lumped models represent catchments by spatially averaged parameters that influence hydrologic processes. Therefore, uniform parameter sets are used for the computational unit, which usually is the whole catchment or a sub-catchment so that the variation of spatial characteristics can only be partially included. The number of parameters used in lumped models is relatively small (Hublart *et al.*, 2016; Carpenter and Georgakakos, 2006). Distributed models are capable of considering spatial variability by sub-dividing catchments or sub-catchments into small computational cells. Spatial characteristics, e.g., soil types, land use and vegetation, can be taken into account (Ibarra-Zavaleta *et al.*, 2017; Beven, 2001; Brirhet and Benaabidate, 2016). State variables in each computational cell are locally averaged, the resolution of which depends on the available spatial data. However, obtain-

ing high-resolution data is difficult, which leads to the development of semi-distributed models. These models discretize catchments to a degree that can represent the important features of a catchment, while at the same time require less data and lower computational costs than fully distributed models (Pechlivanidis *et al.*, 2011; De Lavenne *et al.*, 2016).

In this section, I use the second classification system to compare lumped and distributed hydrological models.

As mentioned above, lumped models are used on the catchment or sub-catchment scale. The water balance is the basis, which is calculated for each water storage unit at every computational step. I take the HBV model (Lindström *et al.*, 1997) as an example. The water balance is computed as follows:

$$P - ET - Q = \frac{d}{dt}(SM + Storage) \tag{1.1}$$

in which P is precipitation, ET is evapotranspiration, Q is discharge to rivers, SM represents soil moisture, and *Storage* is water storage in each storage unit. Discharge from each storage layer is linearly relying on the amount of water in each layer.

Distributed models compute the spatial distribution of state variables. Different equations are used for surface and subsurface flow. MIKE-SHE (Ping *et al.*, 2017; Rujner *et al.*, 2018) is taken as an example. It uses the diffusive wave approximation of the Saint Venant equations to calculate the overland flow. Richards equation is used for the unsaturated zone, whereas Darcy's law and continuity equations are used for the saturated zone:

$$\frac{\partial h_{surf}}{\partial t} + \frac{\partial(uh_{surf})}{\partial x} + \frac{\partial(vh_{surf})}{\partial y} = q \tag{1.2}$$

$$\frac{\partial \theta}{\partial t} = \frac{\partial}{\partial z}\left(K(\theta)\frac{\partial K(\theta)}{\partial z}\right) + \frac{\partial K(\theta)}{\partial z} - E(z) \tag{1.3}$$

$$\frac{\partial}{\partial x}\left(K_{xx}\frac{\partial h}{\partial x}\right) + \frac{\partial}{\partial x}\left(K_{yy}\frac{\partial h}{\partial y}\right) + \frac{\partial}{\partial x}\left(K_{zz}\frac{\partial h}{\partial z}\right) - L = S\frac{\partial h}{\partial t} \tag{1.4}$$

in which the horizontal plane coordinates are (x,y), the ground surface level is z, the surface flow depth is h_{surf}, the overland flow velocities in the x- and y-directions are u and v, respectively, and q represents overland flow per unit area. θ is volumetric water content, $K(\theta)$ is unsaturated hydraulic conductivity, and $E(z)$ is a root extraction sink

term. h is hydraulic head, K_{xx}, K_{yy}, K_{zz} are hydraulic conductivities in the $x-$, $y-$ and z directions, respectively, L is a source or sink term, and S is the specific storage coefficient.

Pechlivanidis *et al.* (2011) and Devia *et al.* (2015) compared lumped and distributed models, which I extended in Table 1.2 to show differences between these two types of models.

Table 1.2: Comparisons of lumped and distributed models

Items	Lumped models	Distributed models
Short description	bucket or grey box models	physics-based or white box models
Principle	water balance and empirical equations are used for each reservoir or bucket with or without physical meanings	physical-based partial differential equations e.g., Saint Venant equations, Richards equation, and Darcy's law are used for spatially distributed variables
Parameters	obtained through calibration, usually without physical meaning	can be theoretically obtained from observations, but are typically calibrated
Data requirement	meteorological and discharge data are essential	spatial data e.g., soil characteristics, land use, vegetation, hydraulic head distribution, hydraulic conductivity are required
Advantages	simple to develop, less computational effort, less spatial data requirement	parameters have physical meaning and can be measured, models are valid for a large range of situations
Disadvantages	parameters have hardly any physical interpretation	large computational effort, large spatial data requirement.
Models	HBV model, TOPMODEL	MIKE-SHE, HGS, parflow, OpenGeoSys

1.1.3 Water Quality Models

Drinking water is supplied from groundwater and surface water bodies. The quality of these water resources is crucial for drinking water supply. Furthermore, water quality influences the organisms that live in rivers, lakes and oceans, e.g., fish, and thus impacts

the ecosystem. With demographic and economic growth, more wastewater pollutants are produced and emitted to the receiving water bodies (Wang *et al.*, 2013). Nowadays, apart from nutrients, other new pollutants have been detected in waters that may deteriorate water quality such as pesticides (Chen *et al.*, 2017), pharmaceuticals (Burns *et al.*, 2018) and microplastics(Cole *et al.*, 2015).

Natural water systems are very complicated and environmental factors can influence water quality in different aspects. Pollutant loads entering water systems may exceed the self-purification capacity. The transport and fate of pollutants in the water systems are important for water quality management (Yuceer and Coskun, 2016; Tsakiris and Alexakis, 2012). However, it is time- and cost-consuming and hardly feasible to measure water quality with high spatiotemporal resolution (Wang *et al.*, 2013). Water quality models can be effective tools to simulate and predict pollutant transport and fate in water environment (Álvarez-Romero *et al.*, 2014; Wang *et al.*, 2013), they can therefore support water protection measures.

The governing equations vary among different kinds of water quality models. In general, to capture the main water quality processes, water quality models need hydrologic and hydraulic information representing flow processes. Conservation equations are fundamental, and the advection-dispersion-reaction equation is normally used, which could include biological and chemical reactions. In water quality models, analytical solutions can be obtained only for some simplified water systems. Due to the complexity of the system, numerical methods are widely used to solve the governing equations of the water quality variables in time and space.

Classification of Water Quality Models

Since water quality models are effective tools for water resources management, various models have been developed to simulate the fate and transport of different kinds of pollutants. Based on the model structure, water quality models can be classified into empirical, conceptual, and mechanistic models, which is similar to the first classification system of hydrological models. Empirical water quality models are usually black-box models. The principle is to find the relationship between the interested water quality variables and some state variables that can be easily measured. Then the relationship can be used for prediction by transferring the easily measured variables to the target variable, an example being online probe measurements of turbidity as the proxy for the concentration

of total suspended sediments (Rügner *et al.*, 2013; Schwientek *et al.*, 2013b; Al-Yaseri *et al.*, 2012). The key problem of empirical relationships is they only hold for the investigated system in the range of the observed values so that the transferability is not guaranteed. Conceptual water quality models capture main features of the system, which could take advantages of other models as an ensemble so that the problem of computational costs is solved. The study domain can also be conceptualized based on the scale. To some extent, conceptual water quality models perform quite well or even better than some mechanistic models (Sabiha *et al.*, 2014; Nguyen *et al.*, 2018). However, water quality variables are not independent, the change of one variable could affect a series of other water quality variables. This requires models that can represent the complex system. Mechanistic water quality models consider interactions of different processes to understand the whole mechanism that governs the change of various water quality variables. This kind of models helps to understand the key processes that affect water quality and provide predictive capabilities under changing climate and land use. The second classification is according to the modelled pollutants, i.e., nutrients (Caille *et al.*, 2011; Álvarez-Romero *et al.*, 2014), sediments (Liu *et al.*, 2018b; Nerantzaki *et al.*, 2015), heavy metals (Liu *et al.*, 2007; Sámano *et al.*, 2014) and emerging organic pollutants (Zhu *et al.*, 2019; Osorio *et al.*, 2012). Because of the differences in pollutant properties, the model structure and main processes vary substantially. Regarding the simulated water bodies, water quality models are classified into groups for rivers, lakes and reservoirs, estuaries and oceans, and groundwater. Hydraulics are crucial for modeling river water quality because advection, dispersion, sediment erosion and deposition depend on flow. River water quality models deal with transport and transformations of pollutants in the river system, meanwhile the exchange with atmosphere, sediment and groundwater can be of high importance for some kinds of pollutants (Liu *et al.*, 2018b; Doll and Frimmel, 2003). For modelling suspended sediments in rivers, a surface runoff model is necessary (Liu *et al.*, 2018b). Estuaries are connection zones between rivers and oceans. Thus to model estuaries, the transition from inland river system to tide-affected zones should be included. Hydrodynamics in estuaries is quite different to that in rivers and important for simulating water quality (Liu *et al.*, 2018a). Here salinity is a special variable that is different from modelling in freshwater systems (Chao *et al.*, 2017). Compared to rivers and lakes, tides are the most important transport mechanisms in coastal waters and oceans. Water in lakes and reservoirs is less dynamic. The temperature gradient in the vertical direction is important for mixing transport, and transformation of pollutants. Lakes and

reservoirs can be sinks for many pollutants (Denis *et al.*, 2012; Van Metre and Mahler, 2014). Nowadays lake models are widely used to study the eutrophication in developing countries (Liu *et al.*, 2009b). The contamination of groundwater is of increasing concern since the remediation of groundwater system is very difficult. The groundwater quality models are used to simulate pollutant transport and high contaminated spots for groundwater resources management (Arias-Estévez *et al.*, 2008; Aisopou *et al.*, 2015).

This thesis focuses on water quality modelling in river systems. Some widely used river water quality models are summarised in Table 1.3.

1.2 Studied Rivers

1.2.1 The Ammer River

The Ammer River is a tributary to the River Neckar within the Rhine basin, located in southwest Germany (Fig. 1.2). It is approximately 12 *km* long with a mean discharge of 1 $m^3 s^{-1}$ at the Pfäffingen gauging station. It has two major tributaries, the Kochhart and Käsbach streams and flows through several small cities, e.g., Herrenberg, Gültstein, Altingen, Reusten, Poltringen, and Pfäffingen with a population density of around 600 inhabitants per square kilometer (Liu *et al.*, 2013). No intensive industries exist within the catchment, implying no intensively industrial point sources for pollutant emissions. The studied river reach drains a catchment of approximately 130 km^2 dominated by agricultural land use that accounts for 67 % of the total area. The hydrogeology is dominated by the middle-Triassic Upper Muschelkalk limestone formation which forms the main karstified aquifer (Selle *et al.*, 2013). In this catchment, annual precipitation is $700 - 800$ *mm*. Two WWTPs, Gäu-Ammer and Hailfingen, also contribute flow, suspended sediments, and pollutants to the Ammer River. During dry weather conditions, the discharge of WWTP Gäu-Ammer is $0.10 - 0.12$ $m^3 s^{-1}$, and the effluent turbidity is approximately 3 *NTU* (Nephelometric Turbidity Units). The WWTP in Hailfingen is comparatively small with flow rates of $0.012 - 0.015$ $m^3 s^{-1}$, and its turbidity is in the same range as that of the WWTP Gäu-Ammer.

With the exception of a small stripe at the north-eastern boundary of the Ammer catchment, highlighted by the forest land-use in Fig. 1.2, the topography of the catchment is only slightly hilly (with mean slope of 4.2 degrees), which agrees with the bed rock being a carbonate platform, partially overlain by upper Triassic mudstones and loess.

Table 1.3: Comparisons of river water quality models

Models	Dimension	Simulated pollutants	Characteristics
Streeter-Phelps	1D	DO, BOD	focus on oxygen balance and first-order decay in one-dimensional steady-state
QUAL2K	1D	nutrients, algae	steady state hydraulics, could include tributaries
HSPF	1,2,3D	sediment, nutrients, toxic organic pollutants	combine watershed hydrology and water quality, allow the integrated simulation of land and soil contaminant runoff processes with in-stream hydraulic and sediment-chemical interactions
EFDC	1,2,3D	sediment, nutrients, metals, hydrophobic organic pollutants	provide good grid methods to describe physical characteristics of a waterbody, allow for drying and wetting in shallow areas
SWAT	1,2D	sediment, heavy metals, nutrients, pesticides, bacteria	good for simulation in rural areas, physically based but computationally efficient
SWMM	1,2D	sediment, heavy metals, nutrients, user-defined pollutants	good for sediment and pollutant buildup-washoff process, primary for urban areas
HEC-RAS	1,2D	sediment, nutrients, algae	could provide detailed hydraulic simulation in terms of different flow regimes for natural river profiles

Soils are dominated by luvisols on loess with mostly high probability of deep infiltration and low risk of soil erosion according to the state geological survey of the state of Baden-Württemberg (LGRB, http://maps.lgrb-bw.de).

In the Ammer catchment, Schwientek *et al.* (2013a) and Rügner *et al.* (2014b) have investigated the relationship between total suspended sediment concentrations and turbidity, and Schwientek *et al.* (2013a) established the relationship between hydrophobic organic pollutants and turbidity and urbanity of the catchment. However, a sediment transport model and a particle-facilitated pollutant transport model are still lacking. To develop these models, I divided the Ammer catchment into 14 sub-catchments using the watershed delineation tool of the Better Assessment Science Integrating point & Non-point Sources (BASINS) model (see Fig. 1.2) based on its digital elevation model (DEM). Table 1.4 shows the proportions of different land-use types and the areas of each sub-catchment.
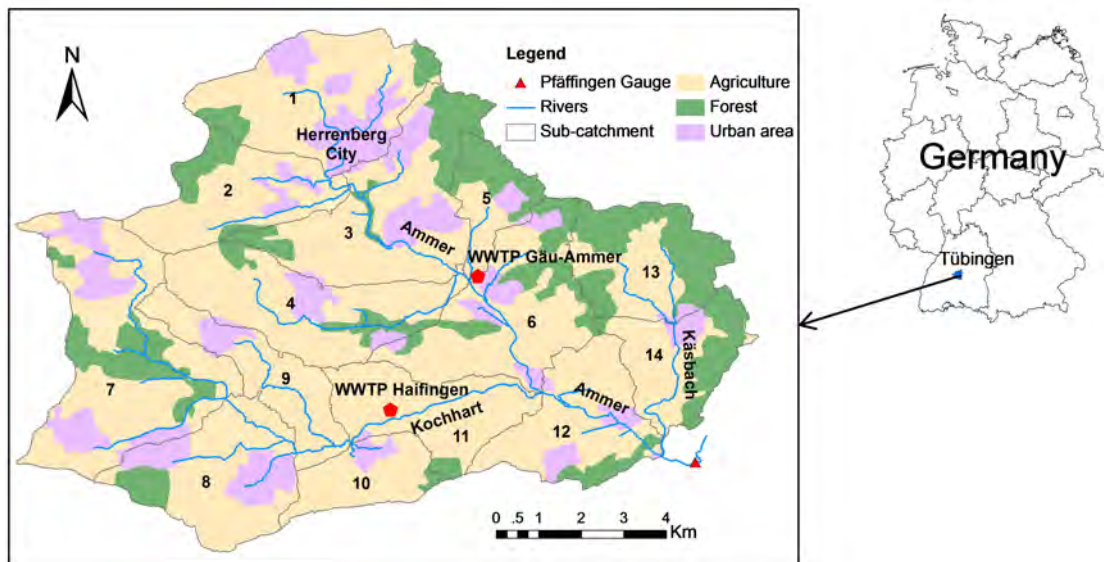
Figure 1.2: Location of the Ammer catchment and its sub-catchments, rivers and land-use. The numbers show identifiers (ID) of 14 sub-catchments that are characterized in more detail in Table 1.4. Two red regular pentagons represent two WWTPs in the study domain. The red triangular indicates the gauge at the catchment outlet.

1.2.2 The Steinlach River

The Steinlach River is located in Tübingen in southwestern Germany (Fig. 1.3), which is a 4th-order tributary of the Neckar River within the Rhine Basin. It receives water from a WWTP named Abwasserverband Steinlach-Wiesaz and from the 140 km^2 hilly catchment (details about the catchment can be found in Schwientek *et al.* (2016)

Table 1.4: Properties of the Ammer sub-catchments.

ID of subcatchment	Area of subcatchment $[km^2]$	Urban area $[km^2]$	Agriculture* $[km^2]$	Forest $[km^2]$
1	12.70	3.78	7.80	1.13
2	8.13	0.70	6.06	1.38
3	13.53	2.47	8.13	2.92
4	11.15	1.19	8.70	1.25
5	3.97	0.46	1.62	1.89
6	11.80	1.53	7.69	2.59
7	17.12	3.30	10.65	3.16
8	10.10	2.41	6.74	0.95
9	6.14	0.66	5.48	0.00
10	4.55	0.50	3.87	0.18
11	7.74	0.05	7.39	0.30
12	8.66	1.04	6.73	0.89
13	8.36	0.21	3.39	4.76
14	6.60	0.58	3.66	2.35
Area of land use $[km^2]$	130.54	18.87	87.92	23.75
Proportion of land use $[\%]$	100	14.45	67.35	18.19

*The agricultural land in the Ammer catchment is dominated by non-irrigated arable land (80.2 % of the total agricultural areas), the crop of which is mainly cereals with annual rotation, and complex cultivation land (e.g., vegetables, 17.5 %). The rest (2.3 %) is principally agricultural area with natural vegetation. Therefore, we summarize the three types of arable land and use the same parameterization to estimate soil erosion.

and Guillet *et al.* (2018)). The mean discharge is 1.84 m^3s^{-1} (http://www.hvz.baden-wuerttemberg.de). The WWTP (red pentagon in Fig. 1.3) treats an inhabitant equivalent of 99000 including domestic and industrial wastewater, which releases the mean effluent of 0.26 m^3s^{-1} to the river. The Steinlach river is very dynamic, the flood of 2-year return period reaches 38.4 m^3s^{-1}, whereas during the dry weather season the flow rate can drop to 0.1-0.2 m^3s^{-1}. This makes the pollutant concentration and the removal of organic compounds in the river quite different under different flow conditions. In particular, when the discharge is very small, the influence of WWTP may be substantially amplified. The average bed slope of the river is 7 ‰ and the bed material is mainly composed of medium sized gravel to larger cobbles (Schwientek *et al.*, 2016). Some even larger stones also exist in the channel. It makes the transient storage (mainly hyporheic

zone and stagnant pools) more important when the flow rate is very small.

In the Steinlach river, Schwientek *et al.* (2016) have applied tracer tests and Lagrangian samplings to assess persistence and transport characteristics of micropollutants, and Guillet *et al.* (2018) used transfer functions to interpret the fate and removals of micropollutants. However, a solute reactive transport model is lacking for in-depth understanding of the processes controlling the fate of dissolved micropollutants.
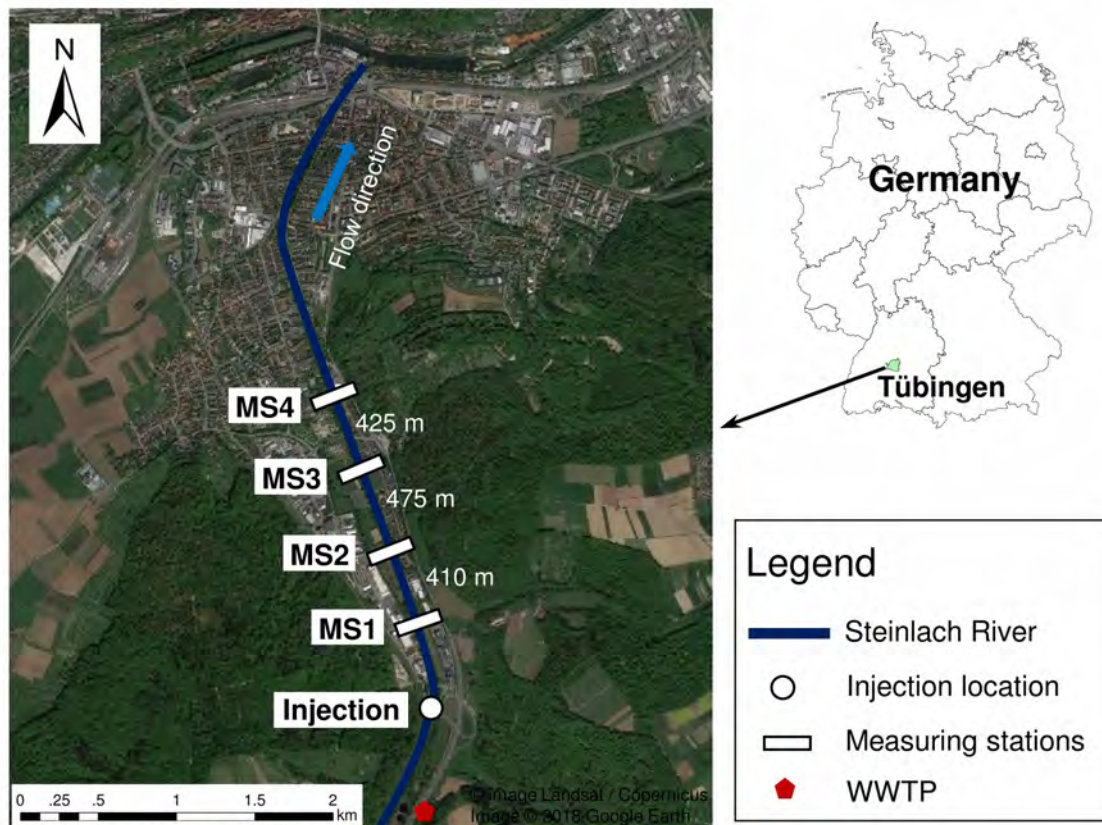
Figure 1.3: Schematic map of the studied river segment showing the river location, tracer injection site and measuring stations (MS1-MS4) of tracer and pollutants.

1.3 Motivation of the Thesis

In industrialized countries, water quality concerns of a river have shifted from nutrients and industrial contaminants to micropollutants in recent years, e.g., persistent compounds (such as PAH and PCBs) and pharmaceuticals. As reviewed in Sect. 1.1.1, they

potentially have adverse effects on aquatic systems and humans (Gelsleichter and Szabo, 2013; Grabicova *et al.*, 2017; Yan *et al.*, 2004). Understanding the transport and fate of these contaminants is of great importance.

Persistent compounds are typically hydrophobic and strongly sorb to particles. In urbanized and industrialized regions, they are mainly emitted via anthropogenic activities (Zhang *et al.*, 2009; Schwientek *et al.*, 2017). Pharmaceuticals appear in streams typically at concentrations in the nanogram-per-liter range (Li *et al.*, 2016; Acuña *et al.*, 2015), which are mainly released by WWTPs (Musolff *et al.*, 2009; Phillips *et al.*, 2012; Launay *et al.*, 2016) since pharmaceuticals are currently not the target of routine wastewater treatment. Because the input of micropollutants to rivers is temporally variable and the transport processes are substantially affected by river discharge, the thorough understanding of micropollutant dynamics requires mechanistic numerical models of flow, sediment transport, particle-facilitated pollutant transport, and reactive solute transport.

Transport of PAH in rivers is mainly facilitated by sediment transport (Van Metre and Mahler, 2003; Rügner *et al.*, 2014a). Particles with different origins essentially determine the contamination level of PAH, which are redistributed in the river channel. Without a sediment transport model considering catchment and in-stream processes, the fate of PAH cannot be understood. The linear relationship between suspended-sediment concentrations and turbidity was reported to be robust in the Ammer River (Rügner *et al.*, 2013, 2014b), which allows to feasibly validate a sediment transport model that is the basis for PAH transport. To further understand the behavior and fate of PAH in a river system, the partitioning of PAH between water, suspended sediments, and bed sediments is necessary. Due to the environmental regulation in 1970s, continuous declines of PAH emissions was observed (Lima *et al.*, 2003; Purcaro *et al.*, 2013; Shen *et al.*, 2011), however the legacy of PAH in rivers is not clear.

With improved analytical methods, compounds at very small concentrations have come into the focus of water-quality monitoring (Schwarzenbach *et al.*, 2006). But only few reactive-transport models exist for micropollutants in streams (Riml *et al.*, 2013), such as for pharmaceuticals. The river discharge is a mixture of WWTP effluents and water from the catchment, which controls the river hydrodynamics and thus substantially affects transport and degradation of contaminants within the river (Cranswick *et al.*, 2014; Lewandowski *et al.*, 2011). Under low-flow conditions, the fraction of WWTP effluents to the total river discharge becomes larger, then flow and pollutant transport may behave differently than under medium to high flow conditions e.g., the ratio of stagnant

water and hyporheic zones to the mobile water increases. Degradation processes and pollutant removals may change as well. Reactive transport models with tracer experiments could provide possible ways to quantitatively investigate the attenuation processes of dissolved micropollutants in rivers.

Understanding the long-term fate of sediment-bound micropollutants (e.g. PAH) and the transport and transformation dynamics of dissolved micropollutants (e.g. pharmaceuticals) is useful to develop appropriate river management strategies and provides insights to evaluate their environmental exposure to river systems.

1.4 Objectives

In this PhD thesis, I want to use a modelling approach to understand the complex environmental processes that determine sediment transport and the fate of micropollutants of interest in river systems. Through this dissertation, I want to achieve the following objectives:

- I will develop numerical models as the basis to investigate chemical fate in river systems. First, develop an integrated sediment-transport model that is able to capture different sediment production processes, i.e., surface runoff related soil erosion in rural areas and particle build-up and wash-off in urban areas and that can also differentiate bed and bank erosion within the river channel based on river hydraulics. Then, extend it to a particle-facilitated pollutant model that is able to estimate PAH input to a river from different origins and simulates dissolved, suspended sediment-bound, and bed sediment-bound PAH. Third, propose a reactive transport model with transient storage that differentiates different attenuation processes in mobile water and transient storage zones and can be used to estimate pollutant removals.

- I want to understand the combined contributions from catchment and in-stream processes to suspended-sediment transport by using the integrated sediment transport model, which allows to study the fate of sediment-bound PAH. Specifically, I will answer what are the main contribution processes to annual suspended sediment load in the groundwater-fed Ammer catchment, how does flow conditions influence the contributions of catchment and in-stream processes to sediment trans-

port, and where are hotspots of bed erosion located and what is the controlling factor.

- I will investigate the fate of the sum of 15 priority PAH in the Ammer River to answer the following research questions: what is the main contribution process to the annual PAH load, what are the turnover differences between bed sediments and attached PAH and how does sediment turnover affect PAH turnover, whether the PAH legacy exists in the Ammer River and where are the locations and how long would it last.

- I will model the fate of some representative pharmaceuticals in the Steinlach River by combining tracer experiments and the proposed modelling approach and answer the following research questions: how does river hydraulic parameter change with flow rates and how do flow rates affect transient storage related parameters, what are the main attenuation processes and removal rates of the representative pharmaceuticals, and how do flow rates affect the pharmaceutical removals.

1.5 Outline of the Thesis

In this PhD dissertation, I developed sediment and pollutant transport models, and applied these numerical simulation models to investigate the fate of two different kinds of micropollutants, i.e., sediment-bound (PAH) and dissolved (representative pharmaceuticals). The dissertation is outlined as follows:

- **Chapter 1:** A general introduction is presented in this chapter. It reviews micropollutants from the following aspects: describing their occurrence and environmental impacts, listing the main sources for different types of micropollutants, and comparing the effects of different processes on the fate of micropollutants. This chapter also provides an overview of hydrological and water-quality models, which describes model application and classification and shows the comparison of widely used models. The studied rivers, i.e., the Ammer and Steinlach Rivers are described in details. This chapter provides the basic information for the following chapters to understand the processes controlling the fate of the studied micropollutants. This chapter also describes the motivation and objectives of this thesis.

- **Chapter 2:** This chapter depicts the fundamental knowledge that is used to develop appropriate models in this thesis so that the behaviors of studied contaminants can be well reproduced. It presents a catchment hydrological model to predict discharge, describes the theory of quasi-steady state flow implemented in HEC-RAS to obtain river hydraulics, proposes an integrated sediment transport model to simulate sediment production from catchment and sediment transport in streams, extends the sediment transport model to the particle-facilitated pollutant model that considers dissolved, suspended sediment-bound, and bed sediment-bound PAH, and presents a one-dimensional reactive transport model for a stream considering the exchange of pollutants between the main channel (continuous flow) and the transient storage zone (hyporheic zones and stagnant water). This chapter also shows methods that are used for parameter estimation.

- **Chapter 3:** In this chapter, the parameters for generations of sediments in the catchment and for sediment transport in the river are calibrated and validated. Then the integrated sediment transport model is applied to the Ammer catchment to investigate the annual and monthly suspended-sediment load, to analyze the main processes for sediment contributions, to model the effects of flow rates on different processes, and to identify potential sediment trapping areas, which is important to address the legacy problems of PAH in chapter 4. This model is the basis for developing the particle-facilitated pollutant transport model to understand the fate of sediment-bound micropollutants in chapter 4.

- **Chapter 4:** This chapter describes details of PAH production from the catchment and transport in the River Ammer. Based on the integrated sediment transport model, the particle-facilitated pollutant transport model is verified. The validated model is then applied to investigate the annual PAH contribution from wet and dry seasons, in dissolved and sediment-bound forms, and from different processes, to calculate the mean turnover time of sediments and attached PAH in order to find the controlling factor for PAH turnover along the river, to understand the function of bed sediments on PAH transport under different flow conditions, and to simulate the legacy potential of PAH after the introduction of environmental regulations in the 1970s.

- **Chapter 5:** This chapter presents the model settings and calibration of the one-

dimensional reactive transport and transient storage model. Combined with day and night tracer experiments, the model is used to differentiate photodegration and biodegradation. It is fitted to time series of tracer concentrations in order to obtain river hydraulic parameters. Then the model is applied to the WWTP-affected Steinlach River to investigate the main degradation processes and the removal of representative pharmaceuticals, and to study the effects of flow rates on pollutant removals.

- **Chapter 6:** This chapter summarizes the main conclusions of the PhD thesis, and proposes topics for future studies.

Chapter 2

Methods

The content in this chapter contains materials published in "Liu, Y., Zarfl, C., Basu, N. B., Schwientek, M., and Cirpka, O. A. (2018). Contributions of catchment and in-stream processes to suspended sediment transport in a dominantly groundwater-fed catchment. Hydrology and Earth System Sciences, 22(7), 3903-3921." and materials submitted in "Liu, Y., Zarfl, C., Basu, N. B., and Cirpka, O. A. (2019). Turnover and legacy of sediment-associated PAH in a baseflow-dominated river. Science of the Total Environment."

This chapter introduces models and fundamental theories that are used for investigating the fate of micropollutants in chapters 3-5. They include the catchment hydrological model, the river hydraulic model, the sediment transport model, the particle-facilitated pollutant transport model, and the reactive solute transport model. The methods used for parameter estimation are also described here.

2.1 Catchment Hydrological Model

The hydrological model provides the water fluxes needed for modelling sediment transport and water quality in rivers. To account for the special base-flow behavior of the Ammer River (Sect. 1.2.1), I developed a catchment-scale hydrological model based on the HBV model (Lindström *et al.*, 1997). It is composed of three storage zones in the vertical direction with a quick recharge component and an urban surface runoff component (Fig. 2.1). This model considers three different types of land use: urban area, agriculture and forest. For the urban area, effective urban areas (e.g., roads and roofs) and inef-

fective urban areas (e.g., parks and gardens) are differentiated. Detailed processes are shown below.
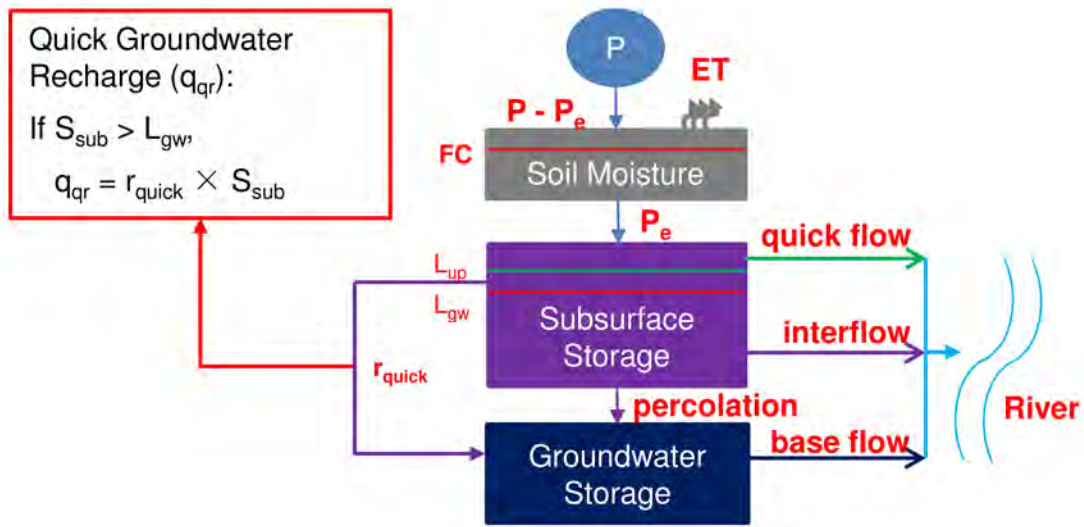
Figure 2.1: The hydrological model of the Ammer catchment with three storage zones (soil moisture, subsurface storage and groundwater storage), a quick groundwater recharge and an urban surface runoff component.

The effective urban area is used for urban surface runoff component, the ratio is calculated by:

$$r_{eff} = A_{eff}/A_{urb} \tag{2.1}$$

in which $r_{eff}\,[-]$ is the ratio of effective urban area over total urban area, $A_{eff}\,[km^2]$ and $A_{urb}\,[km^2]$ represent the areas of effective and total urban area, respectively.

The effective precipitation to the subsurface storage for agriculture, forest and ineffective urban area is calculated by:

$$P_e = \left(\frac{SM}{FC}\right)^{\alpha} P \tag{2.2}$$

in which $P_e\,[mmd^{-1}]$ indicates effective precipitation, $P\,[mmd^{-1}]$ is total precipitation, $SM\,[mm]$ and $FC\,[mm]$ are soil moisture and the maximum soil storage capacity, respectively, the exponent $\alpha\,[-]$ is a shape factor.

The long-term monthly mean evapotranspiration is used to calculate the actual evapotranspiration with a temperature adjustment.

$$L_{et} = FCc_{et} \tag{2.3}$$

$$ET_t = [1 + c_t(T - T_m)]ET_m \tag{2.4}$$

$$ET_a = \begin{cases} ET_t & if\, SM \geq L_{et} \\ \frac{SM}{L_{et}}ET_t & SM < L_{et} \end{cases} \tag{2.5}$$

in which $L_{et}\,[mm]$ is a threshold for maximum evapotranspiration, $c_{et}\,[-]$ is a factor to calculate L_{et}. $ET_t\,[mmd^{-1}]$ represents the maximum evapotranspiration at temperature $T\,[^\circ C]$. $ET_m\,[mmd^{-1}]$ and $T_m\,[^\circ C]$ indicate long-term monthly mean evapotranspiration and long-term monthly mean temperature, respectively, $c_t\,[^\circ C^{-1}]$ is a temperature adjustment factor. $ET_a\,[mmd^{-1}]$ represents actual evapotranspiration, which reaches maximum evapotranspiration when soil moisture is greater than the threshold for maximum evapotranspiration. Otherwise, it increases linearly with soil moisture.

The top storage layer, soil moisture, is calculated by:

$$\frac{dSM}{dt} = P - P_e - ET_a \tag{2.6}$$

in which $\frac{dSM}{dt}\,[mmd^{-1}]$ represents the rate of change of soil moisture. It is used for agriculture and forest. The change of soil moisture is urban area is $\frac{dSM}{dt}(1 - r_{eff})$ since precipitation on the effective urban area is assumed to directly become urban surface runoff.

The surface runoff in the effective urban area, overflow and interflow are calculated by:

$$q_{effurb} = P \tag{2.7}$$

$$q_{of} = \begin{cases} 0 & if\, S_{up} < L_{of} \\ k_o f(S_u p - L_o f) & if\, S_{up} \geq L_{of} \end{cases} \tag{2.8}$$

$$q_{if} = k_{if}S_{up} \tag{2.9}$$

$$q_{bf} = k_{bf}S_{gw} \tag{2.10}$$

in which $q_{effurb}\,[mmd^{-1}]$ is surface runoff in the effective urban area. $q_{of}\,[mmd^{-1}]$ represents overflow when the subsurface storage $S_{up}\,[mm]$ exceeds the overflow threshold $L_{of}\,[mm]$. It is used for agriculture, forest and ineffective urban area. $q_{if}\,[mmd^{-1}]$ represents interflow. $k_{if}\,[d^{-1}]$ is a rate constant. $q_{bf}\,[mmd^{-1}]$ represents base flow, $S_{gw}\,[mm]$ is groundwater storage, and $k_{bf}\,[d^{-1}]$ is a base flow recession coefficient.

The two equations below are used to calculate percolation and quick recharge:

$$q_{perc} = k_{perc}S_{up} \tag{2.11}$$

$$q_{qr} = \begin{cases} 0 & if\ S_{up} < L_{qr} \\ k_{qr}(S_{up} - L_{qr}) & if\ S_{up} \geq L_{qr} \end{cases} \tag{2.12}$$

in which $q_{perc}\,[mmd^{-1}]$ represents percolation from soil moisture to the subsurface storage. $k_{perc}\,[d^{-1}]$ is a rate constant. $q_{qr}\,[mmd^{-1}]$ represents quick recharge, which occurs when subsurface storage reaches the threshold $L_{qr}\,[mm]$ of quick recharge. $k_{qr}\,[d^{-1}]$ is a rate constant.

The subsurface storage and groundwater storage are calculated by:

$$\frac{dS_{up}}{dt} = \begin{cases} P_e - q_{perc} - q_{qr} - q_{of} - q_{if} & \text{agriculture and forest} \\ P_e(1 - r_{eff}) - q_{perc} - q_{qr} - q_{of} - q_{if} & \text{urban area} \end{cases} \tag{2.13}$$

$$\frac{dS_{gw}}{dt} = q_{perc} + q_{qr} - q_{bf} \tag{2.14}$$

in which $\frac{dS_{up}}{dt}\,[mmd^{-1}]$ is the rate of change of subsurface storage. In the urban area, only precipitation in the ineffective area contributes to recharge to the subsurface storage. $\frac{dS_{gw}}{dt}\,[mmd^{-1}]$ represents the rate of change of groundwater storage.

2.2 River Hydraulic Model

One focus of this thesis is on the behavior of sediment-bound pollutants (PAH) in a river. River hydraulic information including river stage, cross-sectional area, velocity, and bottom shear stress are essential for the transport of sediments and attached pollutants. Some existing models (Morgan *et al.*, 1998; Neitsch *et al.*, 2011) use simplified cross sections to estimate average hydraulics, which may be feasible in estimating annual sediment and pollutant load. However, such approaches neglect detailed information, e.g., variable velocity and bottom shear stress, which are very important to simulate the dynamics of sediments and attached pollutants in a river since they control the onset of longitudinally variable deposition and erosion (Zhang and Yu, 2017; Siddiqui and Robert, 2010). In particular, various sediment and particle-facilitated transport models require detailed river hydraulics regarding cross sections along a river so that the immobile sediments and pollutants in the river bed can be coupled with the transport in the mobile phase.

The Hydrologic Engineering Center's River Analysis System (HEC-RAS) (Brunner, 2016) is widely used to simulate river hydraulics and can further be used for sediment transport. HEC-RAS accepts any shapes of river cross sections, if detailed profile data is available. HEC-RAS solves full one-dimensional St. Venant equations for any given river profiles depending on the user defined flow characteristics. It also provides several modes for simulating different flow regimes i.e., sub-critical, super-critical and mixed flow including cases with changes in flow regimes under different boundary conditions. The built-in algorithms e.g., geometry interpolation help to obtain the necessary spatial resolution. HEC-RAS yields the water-filled cross-sectional area, water depth, flow velocity, and shear stress and other useful information. With these detailed hydraulic parameters, the in-stream processes for sediment and pollutant transport can be well addressed.

2.2.1 Theory

HEC-RAS computes one-dimensional water profiles and related parameters for gradually varying steady and unsteady flow. The theory described in this section is mainly adopted from the reference manual of HEC-RAS (Brunner, 2016).

The gradually varying steady flow is mainly computed by solving the energy equation with an iterative procedure called the standard step method. However, when the transition

of flow regimes between subcritical and supercritical occurs or the mixed flow regime is applied, the energy equation is not applicable, and the momentum equation must be solved. The energy equation reads as:

$$Z_2 + Y_2 + \frac{a_2 V_2^2}{2g} = Z_1 + Y_1 + \frac{a_1 V_1^2}{2g} + h_e \tag{2.15}$$

in which indices 1 and 2 refer to two subsequent cross-section, $Z_1\,[m]$ and $Z_2\,[m]$ are the corresponding elevations of the main channel bed; $Y_1\,[m]$ and $Y_2\,[m]$ represent average depths of water at the cross sections; $V_1\,[ms^{-1}]$, $V_2\,[ms^{-1}]$ indicate average velocities (total discharge/ total flow area); $a_1\,[-]$ and $a_2\,[-]$ are velocity weighting coefficients; $g\,[ms^{-2}]$ is the gravitational acceleration constant; and $h_e\,[m]$ is the energy head loss due to friction and contraction or expansion.

The energy head loss is calculated as follows:

$$h_e = L\bar{S}_f + C \left| \frac{a_2 V_2^2}{2g} - \frac{a_1 V_1^2}{2g} \right| \tag{2.16}$$

in which $L\,[m]$ is discharge weighted reach length; $\bar{S}_f\,[-]$ is the representative friction slope between two sections (see below), and $C\,[m]$ represent expansion or contraction loss coefficient.

HEC-RAS subdivides the cross section according to the change of Manning's roughness coefficient. Then the total conveyance and velocity coefficient are determined. Within each subdivision, Manning's equation is used:

$$Q = K S_f^{1/2} \tag{2.17}$$

$$K = \frac{1}{n} A R^{2/3} \tag{2.18}$$

in which $K\,[m^3 s^{-1}]$ is conveyance, $n\,[-]$ is Manning's roughness coefficient, $A\,[m^2]$ is flow area, and $R\,[m]$ is the hydraulic radius (area / wetted perimeter).

When computing gradually varying unsteady flow, the one-dimensional St. Venant equations are used, the momentum equation of which is also applied for solving flow transitions. Some assumptions should be fulfilled: (i) one-dimensional flow of an incom-

pressible fluid (water in this case) with negligible vertical accelerations; (ii) the bottom slope of the channel is small; and (iii) the resistance can be described by Manning's and Chezy's equations. The one-dimensional St. Venant equations consist of continuity and momentum equations:

$$\frac{\partial A_T}{\partial t} + \frac{\partial Q}{\partial x} + q_l = 0 \tag{2.19}$$

$$\frac{\partial Q}{\partial t} + \frac{\partial QV}{\partial x} + gA_T \left(\frac{\partial z}{\partial x} + S_f \right) = 0 \tag{2.20}$$

in which $A_T [m^2]$ and $q_l [ms^{-1}]$ denote total flow area and the lateral inflow per unit length.

2.2.2 Quasi-Steady State Flow

HEC-RAS provides an option to compute quasi-steady state flow, which is beneficial for sediment transport. Because the simulation of unsteady state flow requires much more computational time. The quasi-steady state simplifies the flow calculation by approximating a continuous hydrograph with a series of discrete steady flow profiles. During each discrete time window, flow remains constant so that the computation is faster. I have used this hydrodynamic simplification to obtain river hydraulics for sediment transport and further for particle-facilitated pollutant transport.

For sediment transport, each discrete steady flow can be subdivided upon the temporal resolution of the simulation. They are defined in HEC-RAS as flow duration and computation increment (Fig. 2.2).

The flow duration is the coarsest time step, which represents the length of time over which all hydraulic parameters stay constant. This is normally determined by the temporal resolution of the measured river discharge. The computational increment is achieved by subdividing the flow duration, which is a shorter block of time for computing sediment transport. Even though the hydraulic parameters remain the same during the flow duration, it is necessary to achieve the temporal resolution for sediment transport.
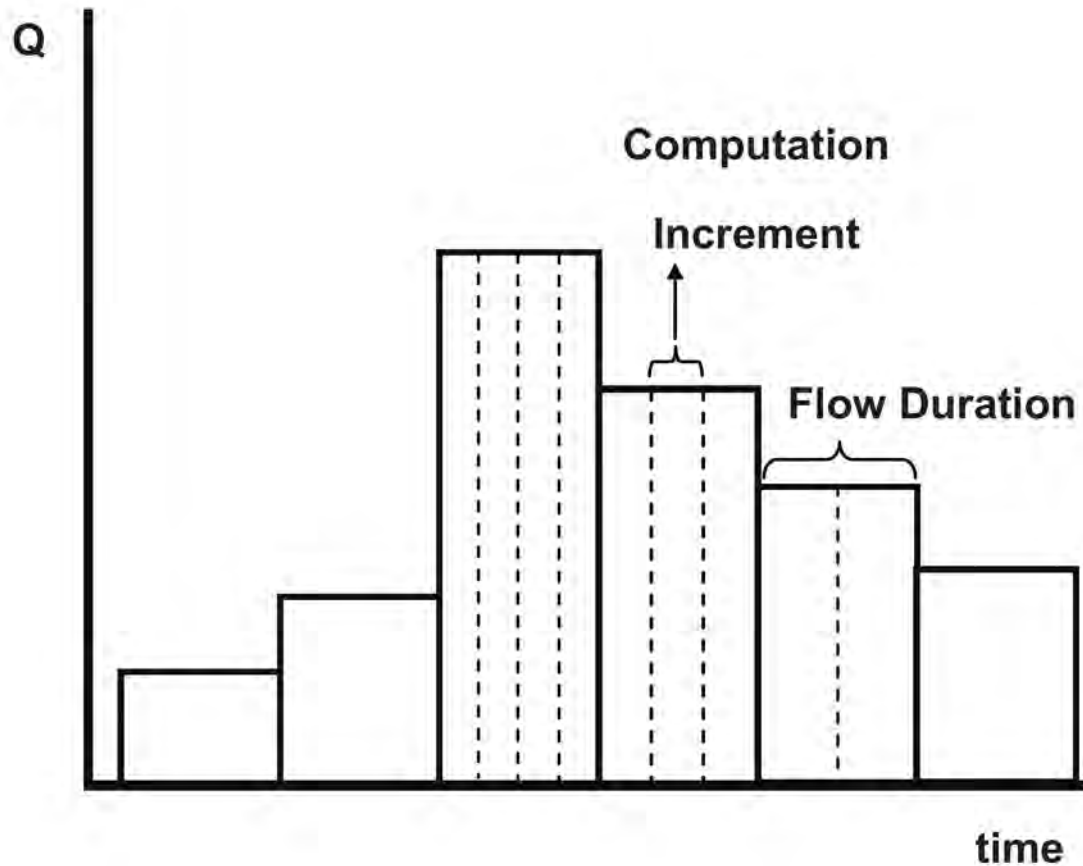
Figure 2.2: Flow duration and computation increment of quasi-steady flow in HEC-RAS.

2.3 Sediment Transport Model

Based on the catchment-scale hydrological model and the river hydraulic model, I propose an integrated sediment-transport model (Fig. 2.3), which considers sediment generating from urban and rural areas of the catchment and in-stream transport processes. Mobilization of particles from different sources varies substantially, e.g., input of urban particles depends on build-up and wash-off processes, rural particles rely on soil erosion, whereas bed and bank erosion are dramatically affected by river hydraulics. Therefore, different approaches are used for reproducing these processes.
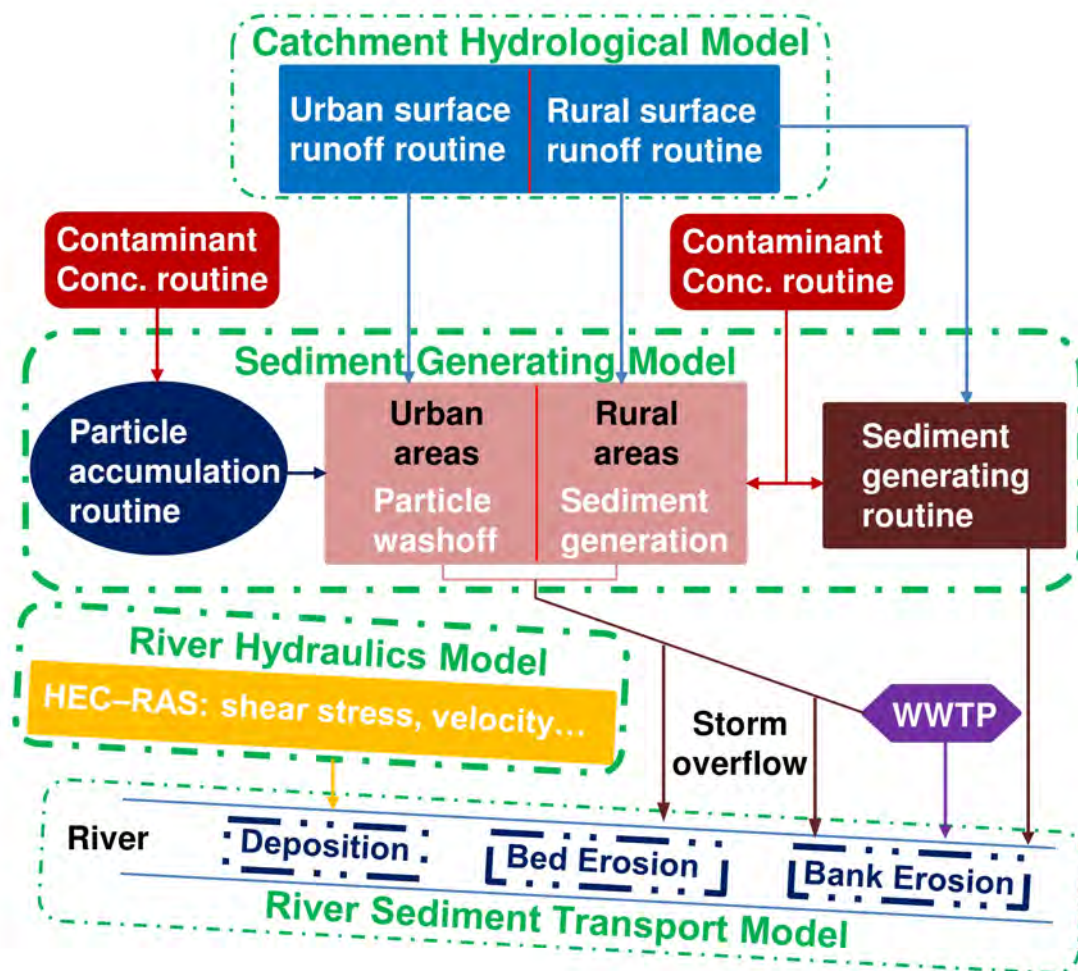
Figure 2.3: Integrated sediment transport model, consisting of a catchment-scale hydrological model, a river-hydraulic model, a sediment-generating model, and a river sediment-transport model.

2.3.1 Sediment Generation in the Catchment

The land use is classified into urban, rural areas, and forested areas. Impervious surfaces such as roads and roofs are regarded as urban areas, while rural areas consist of pervious surfaces such as gardens, parks, and agricultural land. The sediment generating processes are different for these two types of land use. Sediment generation in forested areas is considered to be negligible.

a. Urban Areas

The urban-area algorithm of SWMM performs well with respect to particle build-up and wash-off for urban land use (Wicke *et al.*, 2012; Gong *et al.*, 2016). Thus, I use it to describe sediment generation from urban areas. The corresponding processes are described below.

(1) Particle Accumulation

An exponential function is used to simulate particle accumulation during dry periods under the assumption that particles in the urban areas have a capacity, which is governed by the accumulation process during dry periods:

$$\frac{dM}{dt} = kM_{max}e^{-kt} \tag{2.21}$$

in which $M\,[gm^{-2}]$ and $M_{max}\,[gm^{-2}]$ represent the particle build-up at the current time and the maximum build-up (particle mass per unit area), respectively; $k\,[s^{-1}]$ is the rate constant for particle accumulation, and $t\,[s]$ denotes time since the last wash-off event.

(2) Particle Wash-Off

A power function is used to simulate particle wash-off during rain periods. The particle wash-off quantity is a function of surface runoff and the initial buildup of the corresponding rain period.

$$\frac{dM}{dt} = r_w = -k_w q^{n_w} M \tag{2.22}$$

$$c_{sw} = -\frac{r_w}{q} \tag{2.23}$$

in which $r_w\,[gm^{-2}s^{-1}]$, $q\,[ms^{-1}]$, and $c_{sw}\,[mgL^{-1}]$ are the rate of wash-off, the surface runoff velocity, and the concentration of washed suspended sediment, respectively; k_w $[s^{n_w-1}m^{-n_w}]$ and $n_w\,[-]$ represent a wash-off coefficient and a wash-off exponent.

b. Rural Areas

In contrast to urban areas, the supply of suspended sediments from rural areas can be seen as "infinite" because they mainly originate from eroded soils. Soil erosion is assumed to linearly depend on shear stress, provided that the shear stress generated by surface runoff is larger than a critical shear stress. The sediment generation from rural areas is based on the study of Patil *et al.* (2012).

$$\tau = \rho_w g R_{surface} \tan \theta \tag{2.24}$$

$$y_h = \begin{cases} C_h(\tau - \tau_c) & if \ \tau > \tau_c \\ 0 & \text{otherwise} \end{cases} \tag{2.25}$$

$$c_{sed} = \frac{y_h}{q} \tag{2.26}$$

in which $\tau \ [Nm^{-2}]$ is the mean shear stress generated by the average depth of surface runoff $R_{surface} \ [m]$, $\tan \theta \ [-]$ is the mean slope of the sub-catchment, $\rho_w \ [kgm^{-3}]$ is the density of water, and $g \ [ms^{-2}]$ is the gravitational acceleration constant. The rural sediment load $y_h \ [kgm^{-2}s^{-1}]$ is directly proportional to the difference between the mean shear stress τ and the critical rural shear stress $\tau_c \ [Nm^{-2}]$. $C_h \ [sm^{-1}]$ is a proportionality constant. $c_{sed} \ [kgm^{-3}]$ is the concentration of sediment generated in rural areas, and $q \ [ms^{-1}]$ is, like above, the surface runoff velocity.

2.3.2 Sediment Transport in the River

Two types of sediment are considered, namely suspended sediments in the aqueous phase (mobile component) and bed sediments (immobile component). Fig. 2.4 shows a schematic of the river sediment-transport model, which considers advection, dispersion, deposition, bank erosion, bed erosion, and lateral input of suspended sediments. This model calculates the average concentration of the mobile component and the mass of the immobile component for every computational cell (formed by two cross-sections) every hour.

(1) Mobile Component
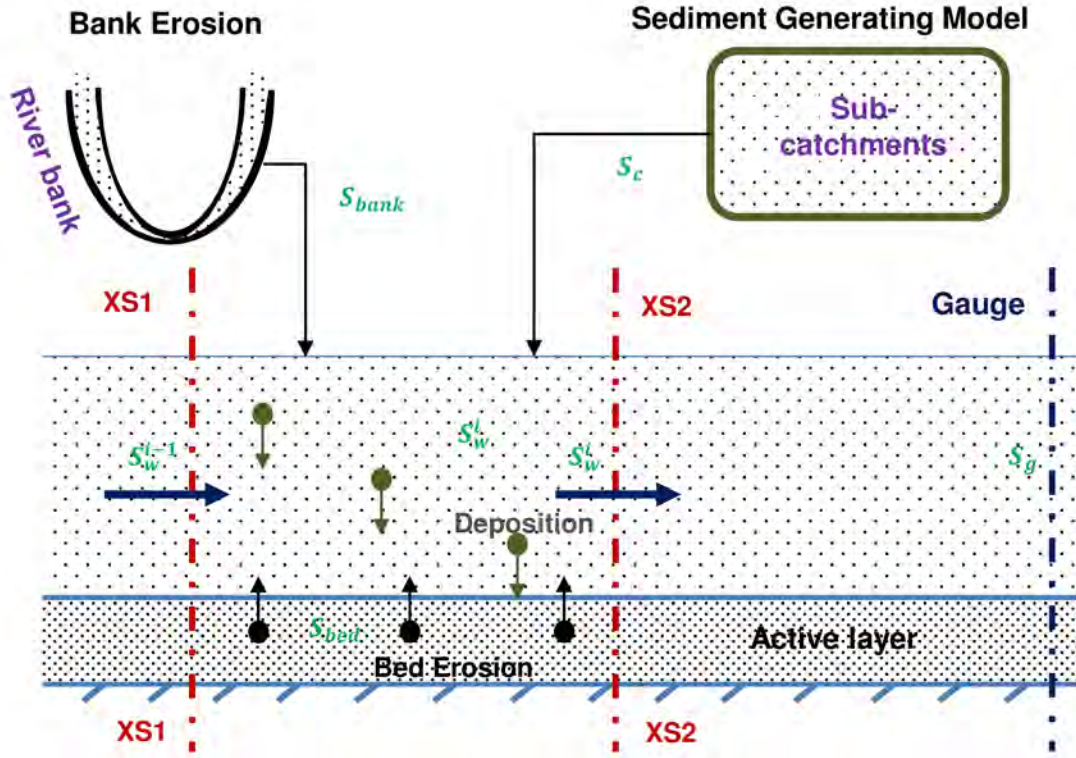
Figure 2.4: In-stream processes of the river suspended-sediment transport model considering deposition, bed erosion, bank erosion, and input from the catchment. XS1 and XS2 are the two cross sections bounding a cell in a Finite Volume scheme. S_c and S_{bank} are sediments from the catchment and bank erosion. S_{bed} indicates the bed sediment mass. S_w^i stands for the concentration of suspended sediments in the i-th cell. S_g is the suspended-sediment concentration at a river gauge.

A Finite Volume discretization is applied for suspended-sediment transport for the main channel, considering storage in the aqueous phase, advection, dispersion, bed and bank erosion, deposition, and lateral inputs (tributaries and WWTPs):

$$\frac{\partial(c_w V)}{\partial t} = -\frac{\partial(c_w Q)}{\partial x}\Delta x + AD\frac{\partial^2 c_w}{\partial x^2}\Delta x + (r_{bed} + r_{bank})\Delta x - r_d V + \sum(c_{lat}^i Q_{lat}^i) \quad (2.27)$$

in which $c_w\,[mgL^{-1}]$ is the suspended-sediment concentration; $V\,[m^3]$ is the cell volume; $x\,[m]$ is the cell length; $Q\,[m^3s^{-1}]$ and $A\,[m^2]$ are the flow rate and cross sectional area; $D\,[m^2s^{-1}]$ is the dispersion coefficient; $c_{lat}^i\,[mgL^{-1}]$ and $Q_{lat}^i\,[m^3s^{-1}]$ rep-

resent the suspended-sediment concentration and flow rate of the i-th lateral inflow; $r_d\,[mgL^{-1}s-1]$, $r_{bank}\,[gm^{-1}s^{-1}]$, and $r_{bed}\,[gm^{-1}s^{-1}]$ indicate the deposition, bed-erosion, and bank-erosion rates, respectively. For the advective term, upstream weighting is used, whereas the second derivative of concentration appearing in the dispersion term is evaluated by calculating diffusive fluxes.

(2) Immobile Component

For bed sediments, I made the simplification of accounting for a single active layer only in the bed sediment per cell and considering only the average grain size. Deposition of suspended sediments leads to a mass flux from the aqueous phase to the bed layer, whereas bed erosion causes a mass flux in the opposite direction:

$$\frac{\partial M_{bed}}{\partial t} = r_d \frac{V}{\Delta x} - r_{bed} \qquad (2.28)$$

in which $M_{bed}\,[gm^{-1}]$ is the sediment mass per unit channel length in the active layer on the river bed.

(a) Deposition

The deposition rate r_d of particles can be calculated by (Krone, 1962):

$$r_d = \begin{cases} (1 - \frac{\tau_b}{\tau_e})\frac{v_s c_w}{y} & if\ \tau_b > \tau_e \\ 0 & \text{otherwise} \end{cases} \qquad (2.29)$$

in which $\tau_b\,[Nm^{-2}]$ and $\tau_e\,[Nm^{-2}]$ represent the bottom shear stress of the river and the threshold shear stress of particle erosion (see below); $y\,[m]$ denotes the water depth; and $v_s\,[ms^{-1}]$ is the settling velocity.

(b) Bed Erosion

Two types of bed erosion are considered, namely particle erosion and mass erosion, which correspond to two thresholds of the bottom shear stress. The bed erosion rate r_{bed} can be calculated by (Partheniades, 1965):

$$r_{bed} = \begin{cases} M_{me}(\frac{\tau_m}{\tau_e} - 1) & if \ \tau_b > \tau_m \\ M_{pe}(\frac{\tau_b}{\tau_e} - 1) & if \ \tau_e < \tau_b \le \tau_m \\ 0 & \text{otherwise} \end{cases} \tag{2.30}$$

in which $r_{bed}\,[gm^{-1}s^{-1}]$ is bed erosion rate; $\tau_m\,[Nm^{-2}]$ represents the mass erosion threshold; whereas $M_{pe}\,[gm^{-1}s^{-1}]$ and $M_{me}\,[gm^{-1}s^{-1}]$ are rate constants, denoting the specific rates of particle and mass erosion.

(c) Bank Erosion

The bank erosion rate r_{bank} is calculated by:

$$r_{bank} = \begin{cases} \kappa \rho L y(\tau_{bank} - \tau_{bc}) & if \ \tau_{bank} > \tau_{bc} \\ 0 & \text{otherwise} \end{cases} \tag{2.31}$$

in which $r_{bank}\,[Nm^{-2}]$ and $\tau_{bc}\,[Nm^{-2}]$ are the bank shear stress and critical shear stress for bank erosion. $\kappa\,[m^3N^{-1}s^{-1}]$ is the erodibility coefficient. $\rho\,[kgm^{-3}]$ is density of bank material. $L\,[km]$ is length of the river bank.

2.4 Particle-Facilitated Pollutant Transport Model

PAH are a group of hydrophobic organic pollutants, the transport of which in streams is mainly facilitated by sediment transport and the degradation can be neglected in rivers (Rakowska *et al.*, 2014). Therefore, to investigate the fate of PAH, a particle-facilitated pollutant transport model is developed based on the integrated sediment transport model (Liu *et al.*, 2018b). Fig. 2.5 shows the conceptual model, which consists of a catchment input module and a river pollutant transport module. The catchment input module is used to obtain the pollutant flux from sub-catchments, while the river transport module solves pollutant transport in the river channel by considering advection, dispersion, deposition, bed and bank erosion, sorption/desorption between dissolved and suspended sediment-bound pollutants, and exchange between dissolved and sediment-bound pollutants. In this section, I explain the details of the particle-facilitated pollutant transport model.

(1) Dissolved and Suspended Sediment-Bound Pollutants
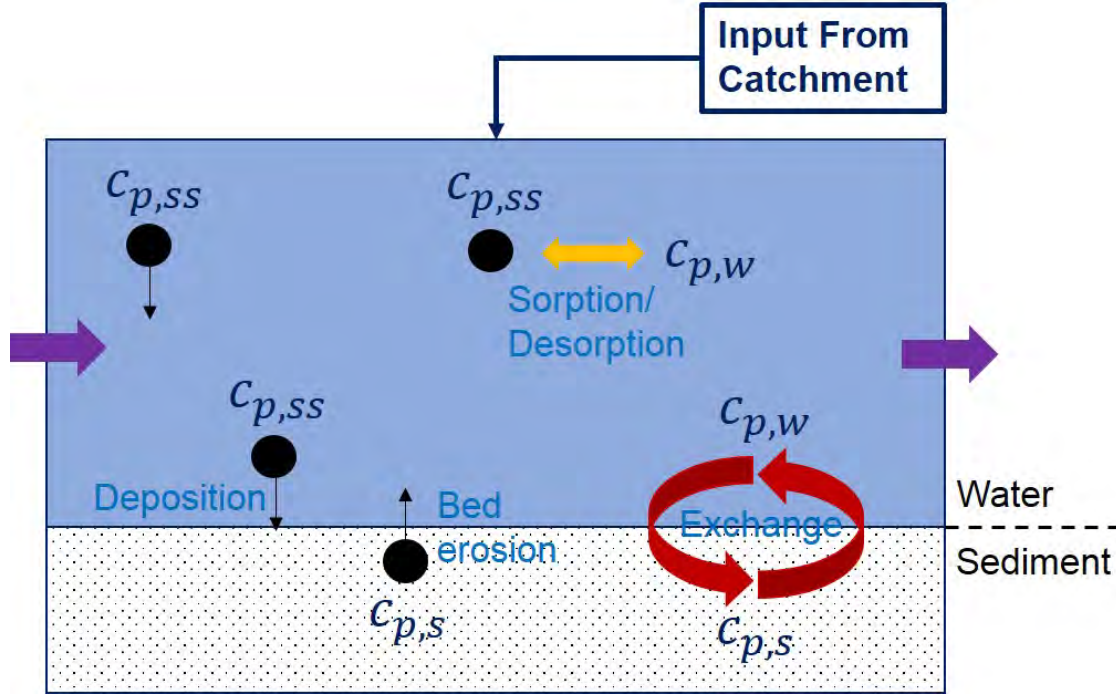
Figure 2.5: Conceptual model for the particle-facilitated pollutant transport, $c_{p,w}$, $c_{p,ss}$, and $c_{p,s}$ represent the dissolved, suspended sediment-bound, and bed sediment-bound pollutant concentrations, respectively.

Bank materials are seen clean compared with bed sediments and surface-runoff generated particles in terms of the studied pollutants. Besides advection, dispersion, erosion, sorption/desorption, and exchange process, the storage of dissolved and suspended sediment-bound pollutants in the aqueous phase are also considered. The following equations calculate concentrations of dissolved and suspended sediment-bound pollutants.

$$c_{p,tot} = c_{p,w} + c_{p,ss}c_{ss} \tag{2.32}$$

$$\frac{\partial(c_{p,tot}V)}{\partial t} = \frac{\partial(c_{p,w}V)}{\partial t} + \frac{\partial(c_{p,ss}c_{ss}V)}{\partial t} \tag{2.33}$$

$$\frac{\partial(c_{p,w}V)}{\partial t} = -\frac{\partial(c_{p,w}Q)}{\partial x}\Delta x + AD\frac{\partial^2 c_{p,w}}{\partial x^2}\Delta x + r_s V + r_e V + \sum c^i_{p_{lat},w}Q^i_{lat} \tag{2.34}$$

$$\frac{\partial(c_{p,ss}c_{ss}V)}{\partial t} = -\frac{\partial(c_{p,ss}c_{ss}Q)}{\partial x}\Delta x + AD\frac{\partial^2(c_{p,ss}c_{ss})}{\partial x^2}\Delta x - r_sV - r_dc_{p,s}V$$
$$+ r_{bed}c_{p,s}\Delta x + \sum c^i_{p_{lat},ss}c^i_{lat,ss}Q^i_{lat} \quad (2.35)$$

in which $c_{p,w}$ $[ng\,L^{-1}]$, $c_{p,ss}$ $[mg\,kg^{-1}]$, and $c_{p,tot}$ $[ng\,L^{-1}]$ represent concentrations of dissolved, suspended sediment-bound, and total mobile (the sum of dissolved and suspended sediment-bound) pollutants, respectively. $c_{p,s}$ $[mg\,kg^{-1}]$ indicates pollutant concentrations on bed sediments. c_{ss} $[mg\,L^{-1}]$, r_d $[mg\,L^{-1}\,s^{-1}]$, and r_{bed} $[g\,m^{-1}\,s^{-1}]]$ are the suspended sediment concentration in the aqueous phase, deposition rate of suspended-sediments, and bed erosion rate, respectively, which are obtained from the sediment transport model. r_s $[ng\,L^{-1}\,s^{-1}]$ and r_e $[ng\,L^{-1}\,s^{-1}]$ indicate the sorption/desorption rate and the exchange rate between mobile and immobile phases. V $[m^3]$ and Δx $[m]$ are the cell volume and length. Q $[m^3\,s^{-1}]$, A $[m^2]$, and D $[m^2\,s^{-1}]$ are the flow rate, cross-sectional area, and dispersion coefficient at the cell interfaces. $c^i_{p_{lat},w}$ $[ng\,L^{-1}]$, $c^i_{p_{lat},ss}$ $[mg\,L^{-1}]$, $c^i_{p_{lat},ss}$ $[mg\,kg^{-1}]$, and Q^i_{lat} $[m^3\,s^{-1}]$ represent dissolved pollutant concentrations, lateral suspended sediment concentrations, the attached pollutant concentrations, and flow rates of the i-th lateral flow, respectively.

(2) Sediment-Bound Pollutants

As described in the sediment transport model in Sect. 2.3, the bed sediments are represented by to a single active layer. Therefore, I compute the average pollutant concentrations on bed sediments only. Except for deposition and bed erosion, the diffusive exchange process causes a mass flux of pollutants between the river bed and mobile water, which direction depends on the concentration gradient. The mass change of sediment-bound pollutants is calculated by:

$$\frac{\partial(c_{p,s}c_s\Delta x)}{\partial t} = r_dc_{p,ss}V - r_{bed}c_{p,s}\Delta x - r_eV \quad (2.36)$$

in which $c_{p,s}$ $[mg\,kg^{-1}]$ represents the pollutant concentrations on bed sediments. c_s $[g\,m^{-1}]$ is the sediment mass per unit channel length in the active layer of the river

bed.

(a) Sorption/Desorption

Film diffusion is used to model sorption/desorption between dissolved and suspended sediment-bound pollutants.

$$r_s = k \frac{6}{\rho_{ss} d_{ss}} c_{ss} (\frac{c_{p,ss}}{K_s} \times 10^6 - c_{p,w}) \qquad (2.37)$$

in which k $[m\,s^{-1}]$ and K_s $[L\,kg^{-1}]$ denote the mass transfer coefficient and the combined partition coefficient. ρ_{ss} $[kg\,m^{-3}]$ and d_{ss} $[mm]$ are the density of suspended sediment and average grain size. c_{ss} $[mg\,L^{-1}]$ is the suspended-sediment concentration. The factor of 10^6 stems from unit conversion (from $[mg\,L^{-1}]$ to $[ng\,L^{-1}]$).

(b) Exchange Between Dissolved and Sediment-Bound Pollutants

I assume that sediment-bound and dissolved pollutants in sediment pores are in a local equilibrium. A mass flux of pollutants is induced by the concentration gradient between dissolved pollutants in the water phase and free pollutants in sediment pores. Then local sorption and desorption occur between free pollutants in sediment pores and sediment-bound pollutants. These detailed processes are simplified in the model by assuming a mass exchange between dissolved pollutants in the aqueous phase and sediment-bound pollutants. The exchange rate is computed by:

$$r_e = k_e (\frac{c_{p,s}}{K_s} \times 10^6 - c_{p,w}) \qquad (2.38)$$

in which k_e $[s^{-1}]$ is the exchange rate constant. The factor of 10^6 stems from unit conversion (from $[mg\,L^{-1}]$ to $[ng\,L^{-1}]$).

2.5 Solute Reactive Transport Model

To investigate the fate of dissolved micropollutants in rivers, I developed a one-dimensional transport model for solutes in streams (Fig. 2.6). It consists of two compartments, the main channel and the transient storage area. Water in the main channel is mobile, which

forms the continuous flow. Whereas the transient storage area is mainly composed of the hyporheic zone and stagnant pools, the water in which is considered immobile. Therefore, processes of advection and dispersion only happen in the main channel, but different reaction activities can occur in both compartments and the exchange process between the main channel and the transient storage area is approximated by a linear driving-force expression. Some assumptions are made for this model:

- Solutes are well-mixed in the transverse direction, therefore only longitudinal dispersion is considered;

- Photo-degradation only takes place in the main channel, where water can receive solar radiation. The average photo-degradation rate in vertical direction is used in my study;

- Bio-degradation only occurs in the transient storage area because microorganisms live in the hyporheic zone and on the bed of stagnant pools.

The governing equations read as:

$$\frac{\partial c_m}{\partial t} = -v\frac{\partial c_m}{\partial x} + D\frac{\partial^2 c_m}{\partial x^2} - f_{im}k_{ex}(c_m - c_{im}) - k_{pho}c_m \tag{2.39}$$

$$\frac{\partial c_{im}}{\partial t} = k_{ex}(c_m - c_{im}) - k_{bio}c_{im} \tag{2.40}$$

in which $c_m\left[\mu mol L^{-1}\right]$ and $c_{im}\left[\mu mol L^{-1}\right]$ denote the concentration of dissolved compounds (e.g., tracer and pollutants) in the main channel and the transient storage area, respectively; $t\left[s\right]$ and $x\left[m\right]$ are time and the length of the computational cells; $v\left[ms^{-1}\right]$ and $D\left[m^2s^{-1}\right]$ are the flow velocity and the longitudinal dispersion coefficient; $f_{im}\left[-\right]$ represents the ratio of the cross-sectional area in the transient storage over that of the main channel; $k_{ex}\left[s^{-1}\right]$ is the first-order exchange rate constant between the main channel and the transient storage area. $k_{pho}\left[s^{-1}\right]$ and $k_{bio}\left[s^{-1}\right]$ represent rates of photo-degradation in the main channel and bio-degradation in the transient storage area.

$$f_{im} = \frac{A_{im}}{A_m} \tag{2.41}$$
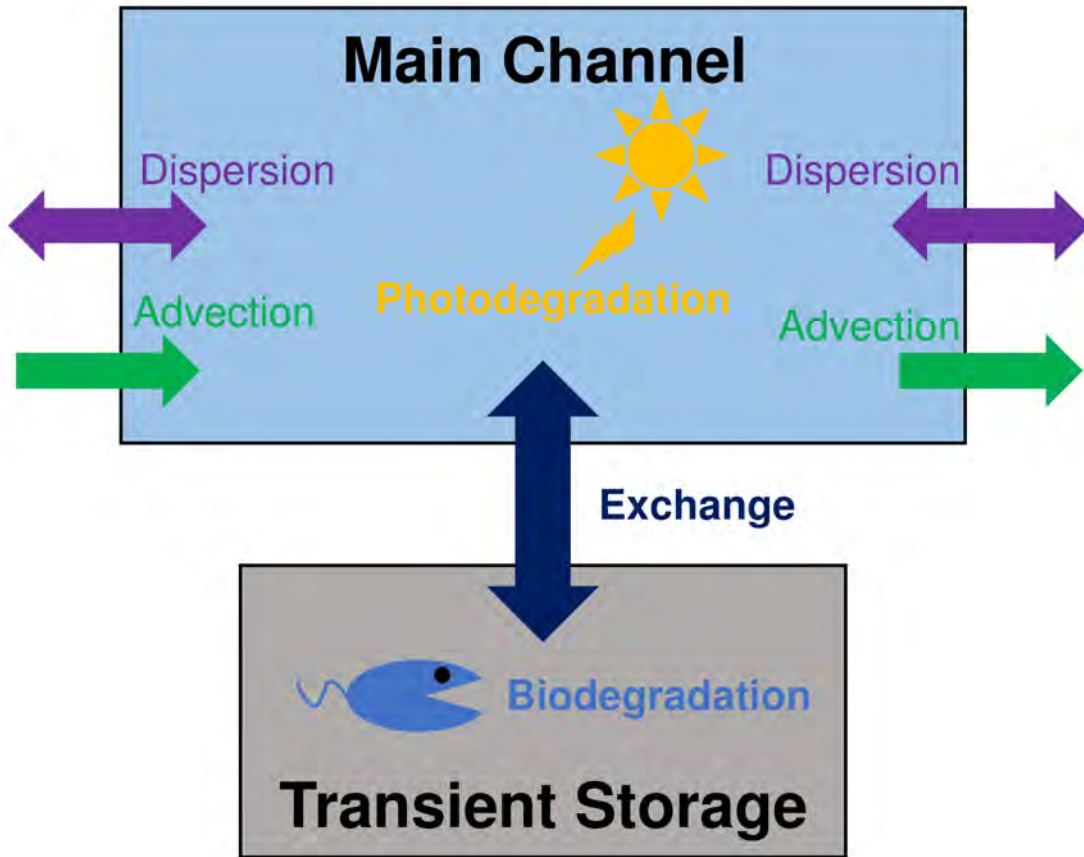
Figure 2.6: Conceptual model for the solute transport with transient storage in streams.

$$k_{pho} = f_{cor} k_{pho,0} \qquad (2.42)$$

$$f_{cor} = \frac{J(t)}{J_{pho,0}} \qquad (2.43)$$

in which $A_m \, [m^2]$ and $A_{im} \, [m^2]$ represent the cross-sectional areas of the main channel and the transient storage, respectively; $k_{pho,0} \, [s^{-1}]$ denotes the reference photo-degradation rate under the reference solar radiation, $J_{pho,0} \, [Jm^{-2}s^{-1}]$ (500 $Jm^{-2}s^{-1}$); $f_{cor} \, [-]$ is the correction factor for photo-degradation because of the time-variable solar radiation, $J(t)$ $[Jm^{-2}s^{-1}]$.

2.6 Parameter Estimation

Models are widely used to simulate the behavior of complex systems in order to understand the system and make predictions. Generally, model parameters can be hardly measured, especially for spatially-distributed, spatially-averaged, and those without any physical meanings. Therefore, it is important to obtain both fitting and reliable model parameters with limited number of measurements.

From the view of computational cost, parameter estimation methods can be classified into automatic and manual approaches. Automatic methods normally need many model simulations to find optimal parameters or target parameter distribution. Therefore, the predictive forward model should run fast so that enough simulations can be achieved within acceptable time. In nonlinear models with many variables in space and time, a model run may take hours to days, which makes the automatic parameter estimation unfeasible. Thus, manual model calibration is implemented. For this type of models, here a preceding sensitivity analysis can help to find sensitive parameters so that the number of parameters to be calibrated can be reduced.

2.6.1 DREAM$_{(ZS)}$

The aim of model calibrations is to find optimal parameters to well represent the simulated systems so that the model output and state variables can fit the observed system behavior as closely and consistently as possible (Vrugt, 2016). Bayesian methods have been widely used for parameter calibration. They are based on Bayes' law:

$$p\left(x|\widetilde{Y}\right) = \frac{p(x)\,p\left(\widetilde{Y}\,|x\right)}{p\left(\widetilde{Y}\right)} \tag{2.44}$$

in which $p(x)$ and $p\left(x|\widetilde{Y}\right)$ are the prior and posterior parameter distribution, respectively, $p\left(\widetilde{Y}\,|x\right) \equiv L\left(x|\widetilde{Y}\right)$ is the likelihood function, and $p\left(\widetilde{Y}\right)$ is the evidence, a normalization constant. $L\left(x|\widetilde{Y}\right)$ represents the distance between model simulations and corresponding observations. For a preset model structure, all statistical inferences about $p\left(x|\widetilde{Y}\right)$ can be made from the unnormalized density:

$$p\left(x|\,\widetilde{Y}\right) \propto p\left(x\right)L\left(x|\,\widetilde{Y}\right) \tag{2.45}$$

Based on Bayes theorem, the posterior distribution of model parameters can be obtained by conditioning model simulations to measurements. The Monte Carlo method is a basic method and widely used to draw samples from a given prior distribution.

Vrugt *et al.* (2008, 2009) proposed a DiffeRential Evolution Adaptive Metropolis (DREAM$_{(ZS)}$) algorithm for Bayesian inference, which is a multi-chain Markov chain Monte Carlo simulation algorithm that provides full distributions of parameters conditioned on the measurements (Knapp *et al.*, 2017). It adopts Differential Evolution Markov chain (DE-MC) (Ter Braak, 2006) but uses subspace sampling and outlier chain correction so that it can automatically tunes the scale and orientation of the proposal distribution to the target distribution, thus speeds up the convergence.

DREAM$_{(ZS)}$ has exhibited an excellent performance on a wide range of problems involving nonlinearity, high-dimensionality, and multimodality and has received many applications in hydrological and pollutant transport models (Vrugt *et al.*, 2008; Knapp *et al.*, 2017), which demonstrates its efficiency for parameter optimization. In this thesis, I used DREAM$_{(ZS)}$ to fit the model parameters of a one-dimensional pollutant transport with transient storage in a small river (described in Chapter 5).

2.6.2 Sensitivity Analysis

The sensitivity analysis investigates how the variation in the output of a numerical model can be attributed to variations of its input factors (Pianosi *et al.*, 2016; Norton, 2015). It studies the relative importance of input factors on model output, whereas an uncertainty analysis focuses on quantifying the uncertainty of the model output.

Sensitivity analyses have a wide range of applications. To understand a system, the mechanism that controls system behavior should be properly identified. In practice, the mechanitic model includes many processes. The sensitivity analysis is very helpful for identifying parameters that influence the model outcome, thus reducing the complexity when calibrating the model (Shin *et al.*, 2013; Norton, 2015; Butler *et al.*, 2014). It is important to ensure that the model does not exhibit strong dependence on supposedly non-identifiable parameters (Campolongo and Saltelli, 1997; Butler *et al.*, 2014). Moreover, sensitivity analysis is an effective tool for decision support since it can provide

appropriate insights into studied problems (Singh *et al.*, 2014; Pianosi *et al.*, 2016).

Local and global sensitivity analyses differ by perturbing either one parameter at a time, or all parameters jointly. Local sensitivity analysis considers the output variability against variations of an input factor around a specific value, i.e., how model performance changes when moving away from some optimal or reference parameter set (Pianosi *et al.*, 2016; Castaings *et al.*, 2009). Global sensitivity analysis considers variations within the entire space of variability of input factors, i.e., how the combination of all input factors affect the model output (Song *et al.*, 2015; Castaings *et al.*, 2009).

To perform a sensitivity analysis, firstly select one output of interest (pollutant concentration, water level, flow rate, et al) or an objective function (goodness of fit), then choose the input factors of interest, thirdly define sensitivity analysis scenarios (variation of one factor of interest for local sensitivity analysis, sampling of all input factors for global sensitivity analysis), fourthly perform the model simulation with the sensitivity analysis scenarios, finally evaluate the model simulation and identify the important (sensitive) input factors. I applied a sensitivity analysis for parameter calibration of the sediment and particle-facilitated pollutant transport models (Chapter 3 and 4) in my thesis.

For the estimation of parameters, the well-known Nash-Sutcliffe Efficiency (NSE) is often used as model performance criterion:

$$NSE = 1 - \frac{\sum_{i=1}^{n}(O_i - M_i)^2}{\sum_{i=1}^{n}(O_i - \bar{O})^2} \tag{2.46}$$

in which O_i and M_i are the i-th observed and modelled values, $\bar{O}$ is the mean of all observed values. An NSE-value close to unity indicates good agreement between model and data, whereas NSE values smaller than zero imply that the model performs worse than taking the mean of all observations.

Chapter 3

Hybrid Model for Simulating Sediment Transport in River Ammer

Suspended sediments impact stream water quality by increasing the turbidity and acting as a vector for strongly sorbing pollutants. Understanding their sources is of great importance to understand the fate and transport of sediments and sediment-bound pollutants, and thus to develop appropriate river management strategies. In this chapter, I apply the integrated sediment transport model to investigate the sediment contributions from the catchment and in-stream processes in the Ammer River close to Tübingen in South-West Germany. I analyze the annual load and seasonal variations of suspended sediments from different processes by means of monthly mean suspended-sediment load. I quantify the contributions of catchment and in-stream processes to the total loads by model simulations under different flow conditions. The evaluation of shear stresses by the river-hydraulics model allows identifying hotspots and hot moments of bed erosion for the main stem of the Ammer River.

3.1 Introduction

Suspended sediments are comprised of fine particulate matter (Bilotta and Brazier, 2008), which is an important component of the aquatic environment (Grabowski *et al.*, 2011). Sediment transport plays significant roles in geomorphology, e.g., floodplain formation (Kaase and Kupfer, 2016), and transport of nutrients, such as particulate phosphorus and nitrogen (Haygarth *et al.*, 2006; Slaets *et al.*, 2014; Scanlon *et al.*, 2004). Fine sediments are important for creating habitats for aquatic organisms (Amalfitano *et al.*, 2017; Zhang *et al.*, 2016). Conversely, high suspended-sediment concentrations can have negative impacts on water quality, especially, by facilitating transport of sediment-associated contaminants, such as heavy metals (Mukherjee, 2014; Peraza-Castro *et al.*, 2016; Quinton and Catt, 2007) and hydrophobic organic pollutants such as polycyclic aromatic hydrocarbons (PAH) (Rügner *et al.*, 2013; Schwientek *et al.*, 2013a; Dong *et al.*, 2015, 2016), polychlorinated biphenyls (PCB), and other persistent organic pollutants (Meyer and Wania, 2008; Quesada *et al.*, 2014). Without understanding the transport of particulate matter, stream transport of strongly sorbing pollutants cannot be understood.

An efficient approach to estimate suspended-sediment loads is by rating curves, relating concentrations of suspended sediments to discharge. By this empirical approach, however, we cannot gain any information on the sources of suspended sediments, which is important for the assessment of particle-bound pollutants. Therefore, a model considering the various processes leading to the transport of suspended sediments in streams is needed. Numerous sediment-transport models have been developed during the past decades, including empirical and physically based models. Commonly used empirical models include the Universal Soil Loss Equation (USLE) (Wischmeier and Smith, 1978) and the Sediment Delivery Distributed (SEDD) model (Ferro and Porto, 2000). The USLE was designed to estimate soil loss on the plot scale. It is incapable to deal with heterogeneities along the transport pathways of soil particles and thus cannot be applied to entire sub-catchments. The SEDD model considers morphological effects at annual and event scales. The two models cannot distinguish between different in-stream processes. Among the models simulating physical processes, the Water Erosion Prediction Project (WEPP) (Flanagan and Nearing, 1995), the EUROpean Soil Erosion Model (EUROSEM) (Morgan *et al.*, 1998), the Soil and Water Assessment Tool (SWAT) (Neitsch *et al.*, 2011), the Storm Water Management Model (SWMM) (Rossman and Huber, 2016), the Hydrological Simulation Program Fortran (HSPF) model (Bicknell *et al.*,

2001), and the Hydrologic Engineering Center's River Analysis System (HEC-RAS) (Brunner, 2016) are widely used. WEPP and EUROSEM are applied to simulate soil erosion from hillslopes on the timescale of single storm events. The two models do not have the capability of estimating urban particles. SWAT uses a modified USLE method to calculate soil erosion from catchments. SWMM aims at simulating runoff quantity and quality from primarily urban areas, including particle accumulation and wash-off in urban areas. HSPF considers pervious and impervious land surfaces. All of these models estimate sediment productions from the catchment and model the transport in the river channel with simplified descriptions of in-stream processes by simplifying the shape of cross sections. Various sediment-transport models for river channels exist that rely on detailed river hydraulics, particularly the bottom shear stress, which controls the onset of erosion and the transport capacity of a stream for a given grain diameter (Zhang and Yu, 2017; Siddiqui and Robert, 2010). HEC-RAS solves the full 1-D St. Venant equation for any type of cross-section including cases with changes in the flow regime, which is beneficial to obtain detailed information on river hydraulics. Therefore, using an integrated sediment transport model combining advantages of abovementioned models can help to well understand the sediment transport in rivers.

3.2 Available Data

Hourly precipitation and air-temperature data are the driving forces of the hydrological model. Hourly precipitation data is obtained from the weather station Herrenberg, operated by the German weather service DWD (CDC, 2017), whereas air temperatures are taken from the weather station Bondorf of the agrometerological service Baden-Württemberg (BwAm, 2006). The generation and transport of sediments behave differently for different land use and topography, thus the digital elevation model with 10 *m* resolution and land-use map of the state topographic service of Baden-Württemberg and Federal Agency for Cartography and Geodesy (BKG, 2009; LGRB, 2011; UBA, 2009) are used. The river-hydraulics model requires bathymetric profiles of River Ammer and its main tributaries. 230 profiles at 100 *m* spacing are available, obtained from the environmental protection agency of Baden-Württemberg (LUBW, 2010).

Only one gauging station is installed in the main channel of the Ammer River at the outlet of the studied catchment in Pfäffingen (red triangle in Fig. 1.2); here, hourly dis-

charge and turbidity measurements are available, which are used for model calibration and validation. The water levels and turbidity data were measured by online probes (UIT GmbH, Dresden, Germany). The hydrograph was converted to discharge time series by rating curves, whereas the suspended-sediment concentrations are derived from continuous turbidity measurements (Rügner *et al.*, 2013). The linear relationship between suspended-sediment concentrations and turbidity with a conversion factor of 2.02 ($mgL^{-1}NTU^{-1}$) has been reported to be robust in the Ammer River (Rügner *et al.*, 2013, 2014b).

The simulation period covers the years 2013-2016. In this time, the maximum discharge reflected an event with 2-10 year return period according to the long-time statistics of the gauging station (LUBW, http://www.hvz.baden-wuerttemberg.de/).

3.3 Model Setup

The integrated sediment transport model was applied to the Ammer catchment, located in southwest Germany. The river discharge, sediment production from catchment and transport in the river are simulated by the following sub-models.

3.3.1 Catchment-Scale Hydrological Model

The main Ammer springs are fed by groundwater from the karstified middle-Triassic Muschelkalk formation. The measured hydrograph indicates a rapid increase of base flow in sporadic events. This special behavior is explained with the catchment-scale hydrological model (details are given in Sect. 2.1) that contains three storages of water in the subsurface: soil moisture in the top soils, a subsurface storage in the deeper unsaturated zone, and groundwater in the karstic aquifer. It assumes water storage in the deep unsaturated zone, which spills over when a threshold value is reached, causing quick groundwater recharge to occur which then leads to a rapid increase of base flow. An urban surface runoff component is used to obtain surface runoff depths in urban areas in order to simulate particle wash-off from urban land surface. The catchment-scale hydrological model was used to simulate discharge contributions from the 14 sub-catchments of the Ammer catchment (shown in Sect. 1.2.1), the temporal resolution of which is one hour.

3.3.2 River-Hydraulics Model

In order to better understand in-stream processes, the discharge data of the hydrological model is fed into the river-hydraulics model HEC-RAS (see Sect. 2.2). The HEC-RAS model simulates hourly quasi-steady flow using the hourly discharge of the 14 sub-catchments simulated by the hydrological model as change-of-discharge input. The locations where the discharge from 14 sub-catchments enters into the main channel are set to the corresponding cross sections. The upstream boundary condition was set to time-series of flow and the downstream one to normal depth. There are 258 measured cross section profiles and the built-in interpolation algorithm in HEC-RAS was used to obtain the additional cross sections, which results in totally 385 cross sections for the entire river network. The distances between computed cross sections range from 10 *m* to 100 *m* depending on the changes of river bathymetry. The model requires river profiles in cross-sections along the river channel and yields the water-filled cross-sectional area, the water depth, flow velocity, and shear stress, among others, as model output, which are needed in the river sediment-transport model.

3.3.3 Sediment-Generating Model

The sediment-generating model is used to obtain hourly sediments of urban and rural particles from the 14 sub-catchments. The sediment generating processes are different for the two types of land use, i.e., urban and rural areas.

For urban particles, particle accumulation and wash-off are simulated by the urban algorithm of the catchment sediment generating model. The maximum build-up depends on the location because the particle production (such as traffic density, population density, and industry density) and cleaning frequency (removing urban particles) differ in different urban areas. In the model it is obtained as uniform value for the entire catchment by calibration. The particle accumulation is restarted at the beginning of every accumulation period considering remaining particles after the flush period. The particle wash-off quantity is a function of surface runoff and the initial buildup of the corresponding rain period.

For rural particles, based on the prior knowledge of the Ammer catchment, soil erosion is very limited (the information supporting this statement will be discussed in Sect. 3.4.2), thus a simplified rural algorithm of the catchment sediment generating model was

used to estimate the average sediment delivery from rural areas to streams. It does not explicitly consider all processes on the hillslope scale. In particular, the dependence of the coefficients on the crop type and time-dependent phenology of the crops are not considered. Instead, all rural areas are treated the same. This strong simplification is justified by an overall low sediment input from rural areas discussed further in the following sections. In catchments with larger sediment load from rural areas, distinctions should be made.

3.3.4 River Sediment Transport Model

The river sediment-transport model is used to simulate in-stream processes (advection, dispersion, deposition, as well as bank and bed erosion) in hourly resolution. This model requires the sediment concentrations in the lateral inputs (tributaries and WWTPs) as boundary conditions. The lateral inputs are computed by the sediment-generating model. For the sediment input by the Ammer spring, we consider the turbidity of 3 *NTU* measured under base-flow conditions. Rügner *et al.* (2013) showed that the karst springs in the Ammer catchment contribute to turbidity, which is in agreement with many previous studies showing that karst systems can contribute suspended sediments (Bouchaoua *et al.*, 2002; Meus *et al.*, 2013). Thus, the turbidity under base-flow conditions is potentially generated by subsurface flow through the karst matrix. The karstic sediment flux was calculated by subsurface flow rates and constant suspended sediment concentrations. Wastewater treatment plants (WWTPs) are treated as point inputs with constant discharge and sediment concentration during dry weather periods. Under low-flow conditions, when no soil erosion and urban particle wash-off occur and the suspended sediment concentrations in the streams are relatively small, a constant concentration is assumed to represent the sediment input under these conditions.

3.3.5 Parameter Estimation

For the estimation of parameters, the well-known Nash-Sutcliffe Efficiency (NSE, described in Sect. 2.6.2) is chosen as the model performance criterion. The best set of parameters is obtained by systematically scanning the parameter space.

The hydrological model was applied to 14 sub-catchments. Each sub-catchment has three types of land use: agricultural areas, forest, and urban areas. daily average dis-

charge data of $2013 - 2014$ and $2015 - 2016$ were used for calibration and validation, respectively. 1000 realizations of the 14 parameters were generated by Latin Hypercube Sampling (LHS) and the corresponding NSE-value for each parameter set was calculated as well. If NSE was ≥ 0.55, the parameter set was regarded acceptable. In the same way, the accepted parameter sets were used for validation. Subsequently the 90 % confidence intervals and the NSE value for high flows (flow rate greater than the mean discharge) were computed using the accepted parameter-sets. Finally, the best-fit parameter values was identified.

For the calibration and validation of the sediment generating and the river sediment-transport models, I performed a literature survey to identify a reference range of each parameter. Then I conducted a manual calibration for the corresponding parameters with the given range to fit the modelled and measured suspended-sediment concentrations at the river gauge. Subsequently, I used the identified parameter-set as base values in a local sensitivity analysis, the details of which are given in Table A1 of Appendix A. Within the given parameter variations, the manually calibrated parameter-sets were confirmed as optimal. The parameters of the sediment-generating model and the river sediment-transport models are listed in Tables 3.1 and 3.2, respectively.

3.4 Results and Discussion

3.4.1 Quality of Model Calibration and Validation

The best-fit parameter set of the hydrological model resulted in NSE values of 0.63 and 0.59 for calibration and validation, respectively. Fig. 3.1 shows the measured and simulated hydrographs for the calibration and validation periods with 90 % confidence intervals. It can be seen that the discharge was reproduced quite well, both in the general trend and the dynamics. The measured discharge data almost all fall within the 90 % confidence interval of the simulation. The NSE value for high flows (greater than the mean discharge, $1\ m^3 s^{-1}$) of the simulation period is 0.43, implying an acceptable fit of high flows. Only few events cannot be reproduced by the model. These events occurred in the summer months and probably resulted from thunderstorms, which are very local and precipitation measurements may miss them, so that the resulting flow peaks could not be predicted by the hydrological model.

Figure 3.2 depicts measured suspended-sediment concentrations and the simulation

Table 3.1: Parameters of the sediment-generating model

Parameter symbol	Definition	Unit	Range	Reference	Value
M_{max}	Maximum accumulation load	$g\,m^{-2}$	$7.5 - 50$	(Piro and Carbone, 2014; Modugno *et al.*, 2015; Bouteligier *et al.*, 2002)	23
k	Accumulation rate constant	d^{-1}	$0.16 - 0.46^a$	(Rossman and Huber, 2016)	0.33
K_w	Wash-off coefficient	$d^{0.5}\,m^{-1.5}$	$50 - 500^b$	(Rossman and Huber, 2016)	80
n_w	Wash-off exponent	–	$0 - 3$	(Wicke *et al.*, 2012; Modugno *et al.*, 2015; Rossman and Huber, 2016))	1.5
C_h	Proportionality constant	$s\,m^{-1}$	$0.0003 - 0.05$	(Gilley *et al.*, 1993; Romero *et al.*, 2007)	0.001
τ_c	Critical rural shear stress	$N\,m^{-2}$	$0 - 10^c$	(Bones, 2014; Léonard and Richard, 2004)	0.3

a. The range of k is calculated under the assumption that it takes $5 - 30$ days to reach 90 percent of the maximum buildup;

b. The range of K_w, $50 - 500$, is sufficient for most urban runoff;

c. It is for the most of time, but depends on soil properties.

results of the sediment-transport model during the calibration (year 2014) and validation (year 2016) periods. The corresponding NSE values are 0.46 and 0.32, respectively, which indicates an acceptable fit, albeit not as good as for the hydrograph. The integrated sediment transport model can capture the dynamics of the suspended sediment concentrations. Especially, the model captures the concentration peaks well. However, two events, one in the calibration and the other in the validation period, were not well fitted. These are events which were also not captured by the hydrological model, occurring in

Table 3.2: Parameters of the river sediment-transport model

Parameter symbol	Definition	Unit	Range	Reference	Value
v_s	Settling velocity	$m\,s^{-1}$	10^{-6} —10^{-4}*	(Brunner, 2016)	4×10^{-6}
τ_e	Particle erosion threshold	$N\,m^{-2}$	0.1 —5	(Winterwerp *et al.*, 2012)	2.5
τ_m	Mass erosion threshold	$N\,m^{-2}$	$> \tau_e$	(Partheniades, 1965; Brunner, 2016)	3.5
M_{pe}	Particle erosion rate	$kg\,m^{-1}\,d^{-1}$	0.8 —43.2	(Brunner, 2016)	30
M_{me}	Mass erosion rate	$kg\,m^{-1}\,d^{-1}$	$> M_{pe}$	(Partheniades, 1965; Brunner, 2016)	40
κ	Erodibility coefficient	$m^3\,N^{-1}\,d^{-1}$	0.0001 —0.32	(Clark and Wynn, 2007; Hanson and Simon, 2001)	0.0018
τ_{bc}	Critical bank shear stress	$N\,m^{-2}$	0 —21.91	(Clark and Wynn, 2007)	5
ρ	Density of bank material	$kg\,m^{-3}$	2190 —2700	(Clark and Wynn, 2007)	2650

* This range is calculated for the suspended sediment with average diameter $1-50\,\mu m$.

the summer months and were caused by thunderstorms.

3.4.2 Annual and Monthly Suspended Sediment Loads from Different Processes

After calibration and validation, the model results can be used to analyze the importance of different sediment sources. Fig. 3.3 displays the modelled annual suspended-
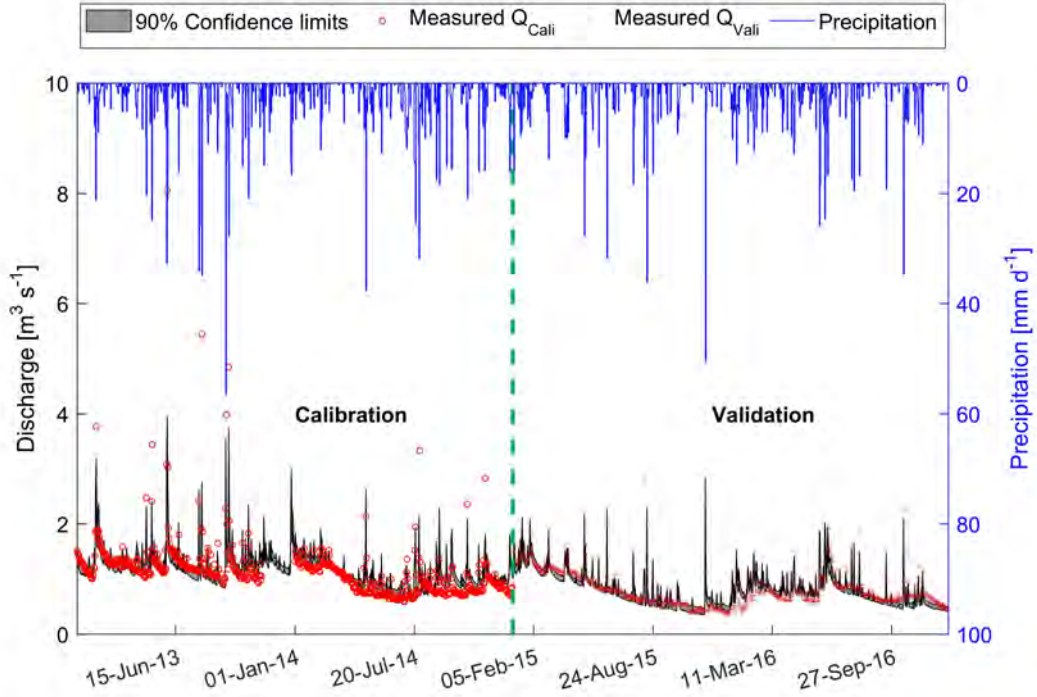
Figure 3.1: Calibration (left, year $2013-2014$) and validation (right, year $2015-2016$) of hydrological model, Q_{Cali} and Q_{Vali} are measured discharges used for calibration and validation, respectively.

sediment loads from catchment and in-stream processes for the entire Ammer River network. The annual suspended-sediment load at the gauge ranges between 410 and 550 $ton\,yr^{-1}$. Equation 3.8 describes the overall mass balance of sediments in the entire catchment:

$$
\begin{aligned}
Load_{gauge} =& (Load_{urban} + Load_{rural} + Load_{karst})_{Catchment} \\
&+ (Load_{bde} + Load_{bke} - Load_{dep} - \Delta S)_{Stream}
\end{aligned}
\tag{3.1}
$$

in which $Load_{gauge}\,[ton\,yr^{-1}]$ indicates the suspended-sediment load at the river gauge. $Load_{urban}\,[ton\,yr^{-1}$, $Load_{rural}\,[ton\,yr^{-1}]$, and $Load_{karst}\,[ton\,yr^{-1}]$ denote the suspended-sediment loads from urban areas generated by surface runoff and WWTP effluent, rural areas generated by soil erosion, and karst system carried by subsurface flow, respectively. These three terms represent the catchment processes. $Load_{bde}\,[ton\,yr^{-1}]$,
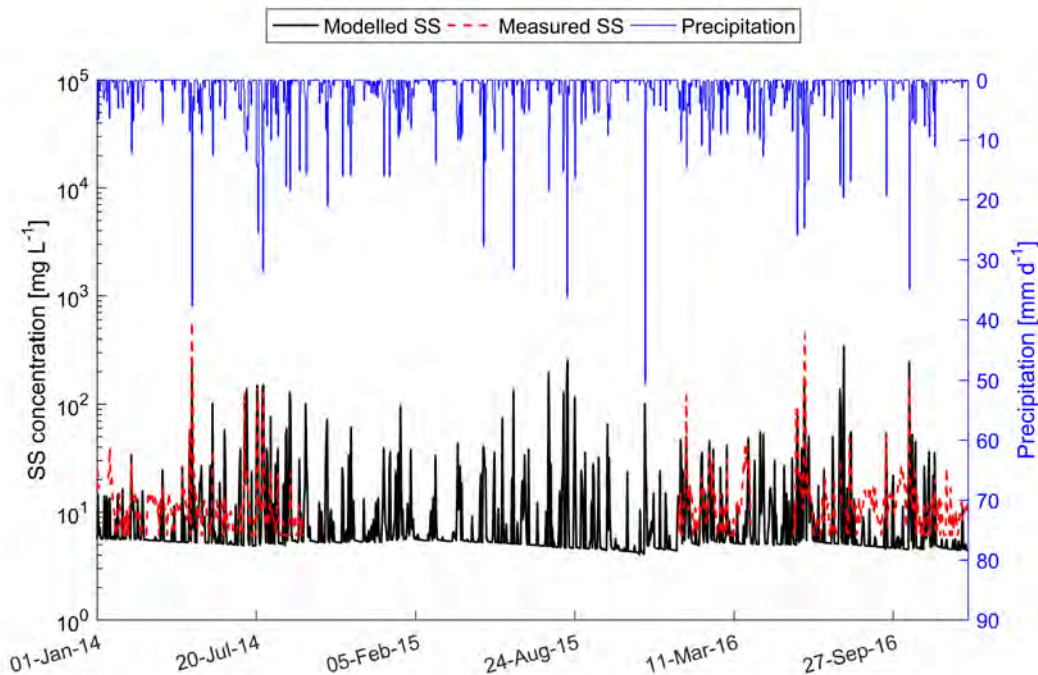
Figure 3.2: Modelled and measured suspended sediment concentrations used for calibration (year 2014) and validation (year 2016) of the sediment transport model. A data gap exists for year 2015.

$Load_{bke}$ [$ton\,yr^{-1}$], $Load_{dep}$ [$ton\,yr^{-1}$], and ΔS [$ton\,yr^{-1}$] are the suspended-sediment loads from bed erosion, bank erosion, deposition, and the change of sediment storage in the entire river channel, respectively. These four terms represent the in-stream processes.

In the Ammer catchment, urban particles (266 —337 $ton\,yr^{-1}$) and the sediment input from the karst system (106 —160 $ton\,yr^{-1}$) dominate the annual suspended sediment load, accounting for 59.1 % and 24.9 %, respectively. Bed erosion, bank erosion, and rural sediment contribute much less, namely 6.2 %, 6.3 %, and 3.5 % of the total annual load, respectively. The contribution of rural runoff sediment in the Ammer catchment was very small, which may occur surprising at first. There are several independent lines of evidence that support these findings and are included them in the Appendix A:

- The suspended sediments of the Ammer River are strongly contaminated by PAH and other hydrophobic organic pollutants (Schwientek *et al.*, 2013a). Table A2 and Equation A1-A7 of Appendix A present an end-member-mixing analysis indicating a fraction of rural particles amounting to only 3%, see also Chapter 4.

- The state geological survey of the state of Baden-Württemberg has developed a soil-erosion risk map shown Fig. A1, putting most of the Ammer catchment into the class of lowest soil-erosion risk. This is so because the surface runoff from agricultural areas is small due to a comparably flat topography. The same agency associates most of the catchment with deep infiltration as main discharge mechanism.

- Schwientek *et al.* (2013b) found a lacking connection between soils and streams in the Ammer catchment. The catchment has a large water storage capacity due to the karst and the slopes of this catchment being mild. During the simulation period, the precipitation intensity was not large enough to exceed the maximum infiltration rates or to reach storage capacity of the subsurface. Compared with literature values of maximum infiltration rates, 10-20 mmh^{-1} and 5-10 mmh^{-1} for loamy and clay loamy soil, respectively (http://www.fao.org/docrep/S8684E/s8684e0a.htm.), only few events exceed 10 mmh^{-1} of with the precipitation intensity during the simulation period. Thus, hardly any surface runoff occurred in the rural area, so that sediment generation and transport from rural areas to the river channel were small.

- The comparably flat topography can be explained by the geological formation. The Muschelkalk limestone is a carbonate platform that is partially overlain by mudstones of the upper Triassic. Along the Ammer main stem, there is only a small stretch where the river is somewhat deeper incised into the limestone rock. The river has lost its former headwater catchment in the early Pleistocene to river Nagold so that the currently existing small river has a too wide valley given its discharge.

As discussed above, a simplified approach is used to simulate the average sediment delivery from rural areas because the contribution of rural areas to sediment delivery was so small. In particular, the model does not distinguish between different crop types and seasons, but estimates the average sediment load that reaches the streams instead. In other catchments, where the rural contributions to the sediment load are considerably higher, the description of soil erosion processes would require more differentiations.

To identify seasonal variations of suspended-sediment loads originating from different processes, I used the model results of $2014 - 2016$ to analyze the monthly mean sus-
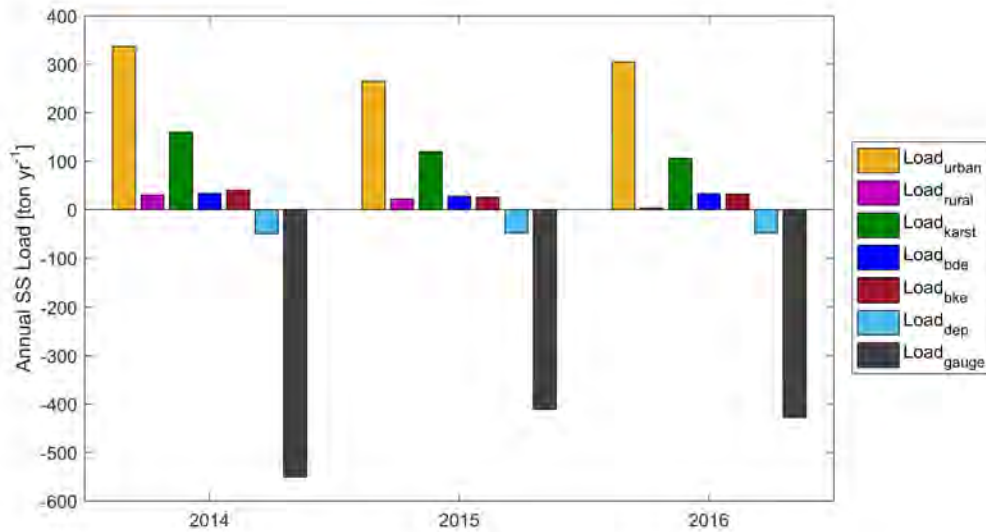
Figure 3.3: Annual suspended sediment loads from different processes. *Load*$_{gauge}$ is calculated by modelled discharge and suspended sediment concentrations at catchment outlet. *Load*$_{urban}$, *Load*$_{rural}$, and *Load*$_{karst}$ are calculated using the results of sediment generating model. *Load*$_{dep}$, *Load*$_{bde}$, and *Load*$_{bke}$ are the sum of deposition load, suspended sediments eroded from river bed and river bank of the entire river network for a whole year, respectively. In this figure, the positive values represent sediment input to the river channel, while negative values denote sediment output from the river channel.

pended sediment loads from the urban areas, rural areas, karst system, bed erosion, bank erosion, and deposition (Fig. 3.4). More suspended-sediment loads from urban areas and at the gauge can be observed in June and July (summer months). In summer months events with high rain intensity are more common than in winter months, which results in higher discharge peaks, more sediments generated in urban areas, and higher suspended-sediment loads at the gauge. Monthly suspended-sediment loads at the gauge have similar dynamics as the monthly urban particle contributions. The suspended-sediment load from the karst system is higher in winter months because the subsurface flow in the Ammer catchment is higher in winter months. Rural particles contribute to the overall particle flux only during few months because annual precipitation and rainfall intensity were relatively small so that surface runoff generated from rural areas was also low.

In the model simulation period, the seasonal patterns of bed erosion and bank erosion are obvious. High bed erosion and bank erosion occur from June to August due to increased bed shear occurring during big events. The area above the line of *Load*$_{gauge}$

indicates net deposition, which shows small variations with a slight increase in July and August. The slight increase in summer is due to increased suspended-sediment concentrations during summer months. Comparing monthly mean bed erosion and deposition shows that bed erosion was greater than deposition in July, which indicates that accumulated bed sediment can be partly eroded in July.
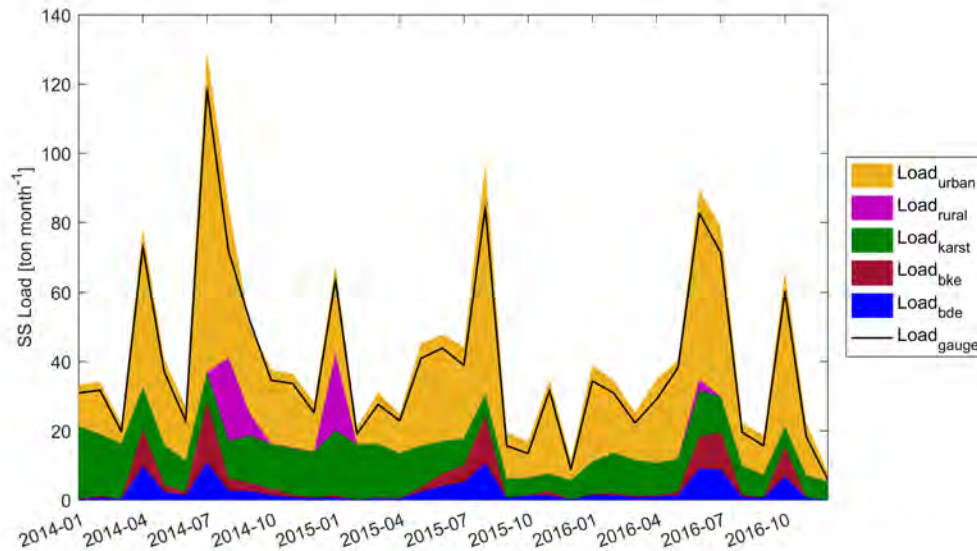
Figure 3.4: Monthly mean suspended-sediment load from different processes, calculated using the model results of 2014-2016. $Load_{gauge}$, $Load_{urban}$, $Load_{rural}$, and $Load_{karst}$ are the monthly mean suspended-sediment load at the gauge and from urban areas, rural, and karst system. $Load_{bke}$ and $Load_{bde}$ represent monthly mean suspended-sediment load from bank erosion and bed erosion for the entire river network, respectively. The area above the line of $Load_{gauge}$ is the monthly mean deposition, $Load_{dep}$.

3.4.3 Suspended-Sediment Sources under Different Flow Conditions

Figure 3.5 shows the relationship between hourly mean discharge and the simulated hourly suspended sediment loads from catchment, bed erosion, and bank erosion. The hourly suspended-sediment load from the catchment monotonically increases with increasing hourly mean discharge by a power-law relationship (Fig. 3.5a), which is consistent with the particle wash-off rate being a power-law function of discharge. Bed erosion requires that the bed shear stress exceeds a critical value, so that bed erosion is almost 0 when hourly mean flow is smaller than 1.5 m^3s^{-1}, namely 1.5 times mean discharge

(Fig. 3.5b). For discharge larger than this threshold (1.5 $m^3 s^{-1}$), bed erosion increases approximately linearly with discharge. The simulated hourly bed-erosion loads for a given flow rate vary substantially because bed erosion is not only influenced by the shear stress, which directly depends on discharge, but also on the bed sediment storage, which depends on previous deposition and erosion events. Bank erosion occurs when the hourly mean flow rate is larger than 2.5 $m^3 s^{-1}$, i.e., 2.5 times mean discharge (Fig. 3.5c). The relationship between bank-erosion related loads and discharge is more unique than that of bed-erosion loads because I assume an infinite sediment supply for bank erosion.

Figure 3.6 shows the suspended sediment loads from in-stream (bed erosion and bank erosion) and catchment processes (input from karst system, urban areas, and rural areas) under different flow regimes. The fractions of suspended-sediment contributions from different processes change with flow regimes. The contributions of in-stream processes are negligible in the flow regime of discharge smaller than 5 $m^3 s^{-1}$. With the discharge increasing, the contributions of in-stream processes increase. The in-stream processes play significant roles in high flow regimes, which contribute 23 % and 34 % of total suspended sediment loads under flow regimes of $10 \leq Q\,[m^3 s^{-1}] < 15$ and $Q\,[m^3 s^{-1}] \geq 15$, respectively. The relative contribution of the karst system is high in the low-flow regime ($Q\,[m^3 s^{-1}] < 5$), while it can be neglected under high-flow regimes ($Q\,[m^3 s^{-1}] > 10$). With the increase in flow rates, the contribution of urban particles becomes dominant in terms of catchment processes, especially when discharge is larger than 10 $m^3 s^{-1}$.

From above observations, it can be seen that the sources of suspended sediments differ under different flow conditions. Table 3.3 lists the various regimes.

3.4.4 Hotspots and Hot Moments of Bed Erosion in the Ammer River

The annual mean rates of bed erosion and deposition (mass per unit length per year) along the main channel can be used to identify hotspots of bed erosion and net sediment trapping (Fig. 3.7). The rates of deposition and bed erosion vary substantially along the main stem, ranging from essentially zero to a maximum of 8.6 $kgmyr^{-1}$ and 8.0 $kgmyr^{-1}$, respectively. Bed erosion is higher in the river segment close to the gauge because the flow rate is higher due to the contributions of the tributaries. Bed erosion is rather low in the river segments of $5-6.5\,km$, $7-8\,km$, $8.5-9\,km$, and $10-11\,km$ to the gauge, where the channel slope is very mild. The river sections with the steepest channel
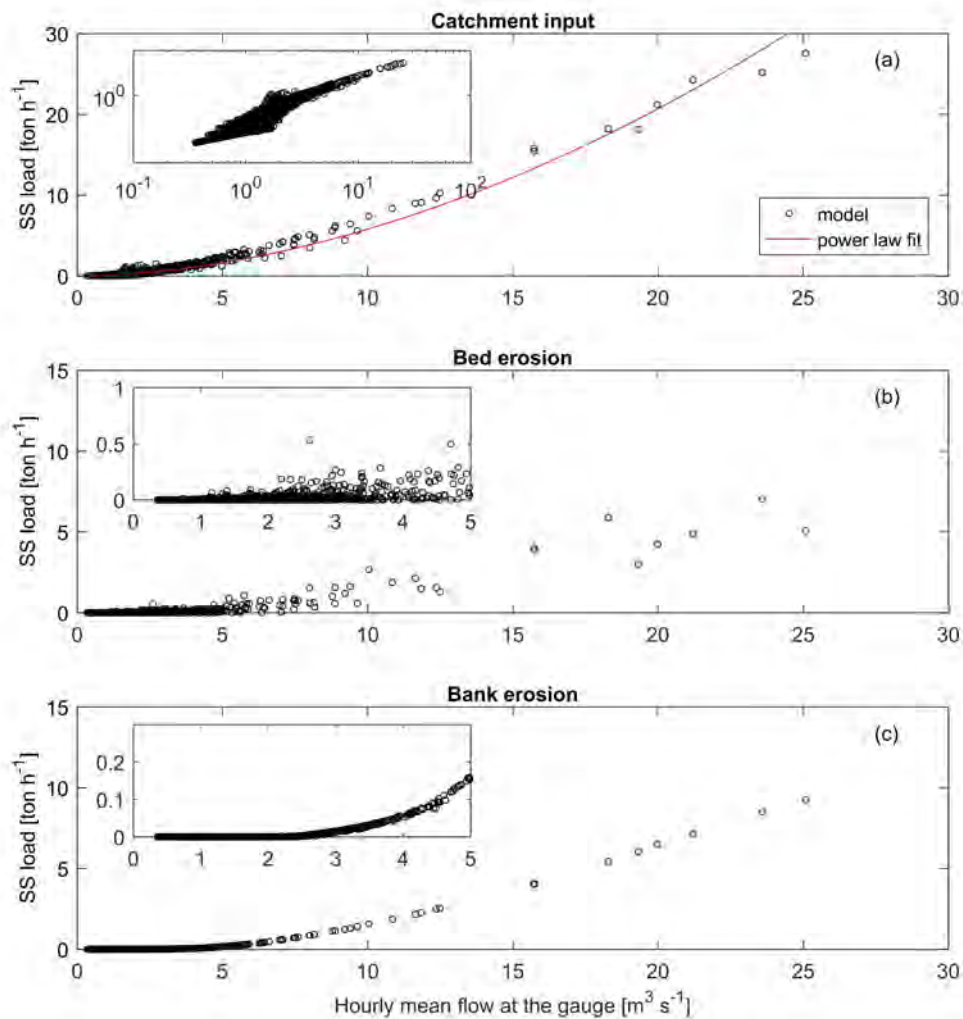
Figure 3.5: Relationship between simulated hourly mean flow and hourly suspended-sediment loads from the catchment (a), bed erosion (b), and bank erosion (c), in which bed erosion and bank erosion are sums over all computation cells. Loads from catchment is the sum of contributions from urban areas, non-urban areas, and karst system.

slope typically do not show the highest bed erosion because there is not enough sediment available for erosion, which is caused by insufficient deposition. Fig. 3.7 also shows that when the channel slope is very mild, the deposition rate is very high, while the bed erosion rate is nearly zero. These are sections where net sediment trapping (blue dash-dotted line) was observed. With increasing channel slope, bed erosion rates increase and
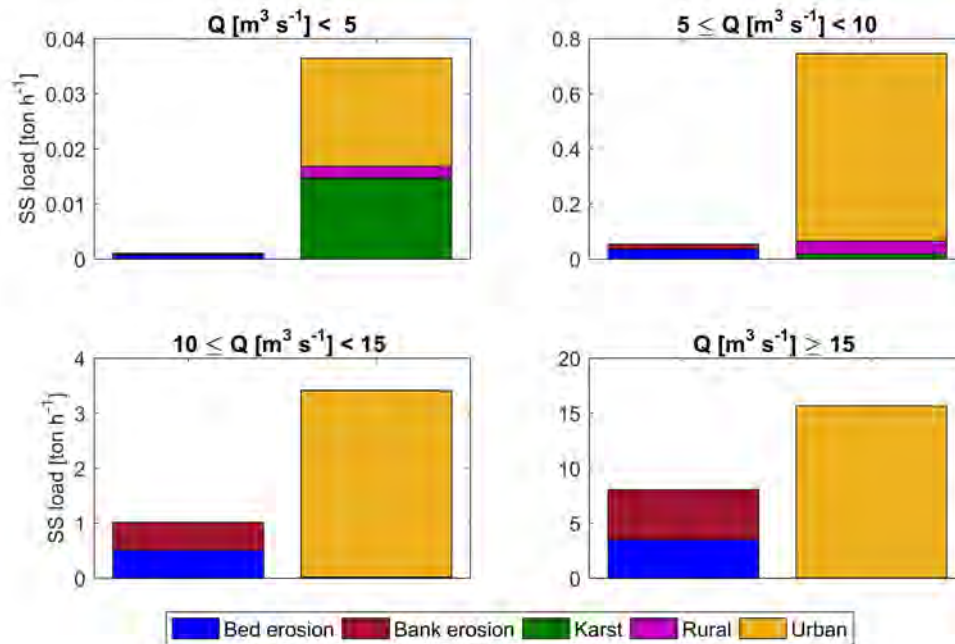
Figure 3.6: Simulated suspended sediment load from bed erosion, bank erosion, karst system, rural areas, and urban areas (including suspended sediment from WWTPs) under different flow regimes, the suspended sediment loads are the mean values for the specific flow regimes.

deposition rates decrease. In a small range of channel slopes, deposition rates equal the erosion rates, resulting in a local steady state. If the channel slope continues increasing, the erosion rate will be higher than the deposition rate, which results in net sediment erosion if the sediment storage in the channel is large enough (red dash-dotted line in Fig. 3.7). Where the channel slope is very steep, both sediment deposition and erosion rates are very small.

Figure 3.8 shows monthly means of the bed erosion rates along the Ammer main stem, computed for the simulated years 2014 to 2016. Bed erosion is stronger in the summer months, especially in July, which is consistent with the monthly load of suspended sediments discussed in Sect. 3.4.2. The hot moments of bed erosion are the extreme events caused by summer thunderstorms. The downstream river segments close to the gauge show higher bed erosion rates than the sections further upstream because flow rates and thus bed shear stresses are higher even with identical channel slope.

Table 3.3: Summary of suspended-sediment sources under different flow conditions.

Flow (Q) [$m^3 s^{-1}$]	Description of main suspended-sediment sources
$Q < 1.5$	Suspended sediment load is dominated by contributions from the catchment (karst system, rural areas, and urban areas), while bed erosion and bank erosion can be neglected.
$1.5 \leq Q < 2.5$	Bed erosion starts contributing.
$2.5 \leq Q < 5$	Bank erosion starts contributing, but the contributions from bed and bank erosion are still negligible. Contributions from urban areas and karst system are dominant.
$5 \leq Q < 10$	Bed and bank erosion contributes more, but the major contribution is still from catchment, especially from urban areas. Bed erosion contributes less than 5 % and bank erosion contributes less than 3 %. The relative contribution from karst system becomes very small.
$Q \geq 10$	Suspended sediment contributions from bed and bank erosion are significant. The contribution of in-stream processes can be up to 35 % of the total suspended sediment load when discharge is larger than 15 $m^3 s^{-1}$. The contribution from urban areas is largest, which dominates the catchment input.

3.5 Summary and Conclusion

Suspended sediment transport is of great importance for river morphology, water quality, and aquatic ecology. In this chapter, I applied an integrated sediment-transport model to the Ammer catchment, which combines a conceptual hydrological model with a river-hydraulics model, a model of sediment generation, and a shear-stress dependent sediment-transport model within the river. This framework enables to investigate the major contributors to the suspended-sediment loads in different river sections under different flow conditions.

In the mainly groundwater-fed Ammer catchment, annual suspended-sediment load is dominated by the contributions of urban particles and sediment input from the karst system. The contribution from rural areas is small because the topography is comparably flat and the infiltration capacity of the soils is high in this region resulting in a very weak surface runoff from rural areas, thus very few rural particles are generated and transported to the river channel. In-stream processes, i.e. bed erosion and bank erosion, play significant roles under high-flow conditions ($Q > 10 m^3 s^{-1}$). The flow rate governs
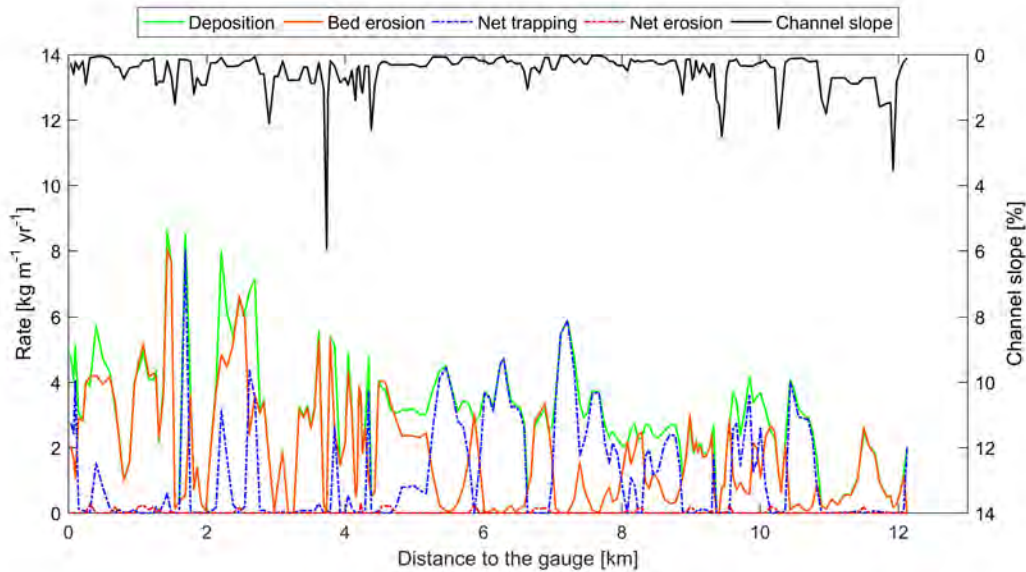
Figure 3.7: The distribution of the annual mean deposition, bed erosion, net sediment trapping, net sediment erosion, and channel slope along the main channel of the Ammer River (flow direction from right to left). The blue and red dash-dotted lines highlight net sediment trapping and net erosion, respectively.

the contributions of different processes to the suspended sediment loads. Especially, bed erosion and bank erosion take place when flow rates reach the corresponding thresholds, which are 1.5 and 2.5 times the mean discharge, respectively. The channel slope has a significant effect on the deposition and bed erosion rates. Net sediment trapping was modelled in the river segments with very mild channel slopes in the Ammer River during the simulation period with events of a 2-year to 10-year return period. Finally, the river hydraulics model is necessary to differentiate sediment sources and sinks of in-stream processes i.e. shear stress related deposition, bed erosion and bank erosion.

The model and results of sediment transport in this chapter are useful and essential for studying the fate and particle-facilitated transport of hydrophobic pollutants like PAH in the following chapter, and for the design of optimal sampling regimes to capture the different processes that drive particle dynamics. In addition, the analysis of deposition and bed erosion in the Ammer main stem provides information on the distribution of net sediment trapping within the channel, which would be a good indicator for channel dredging to improve water quality.
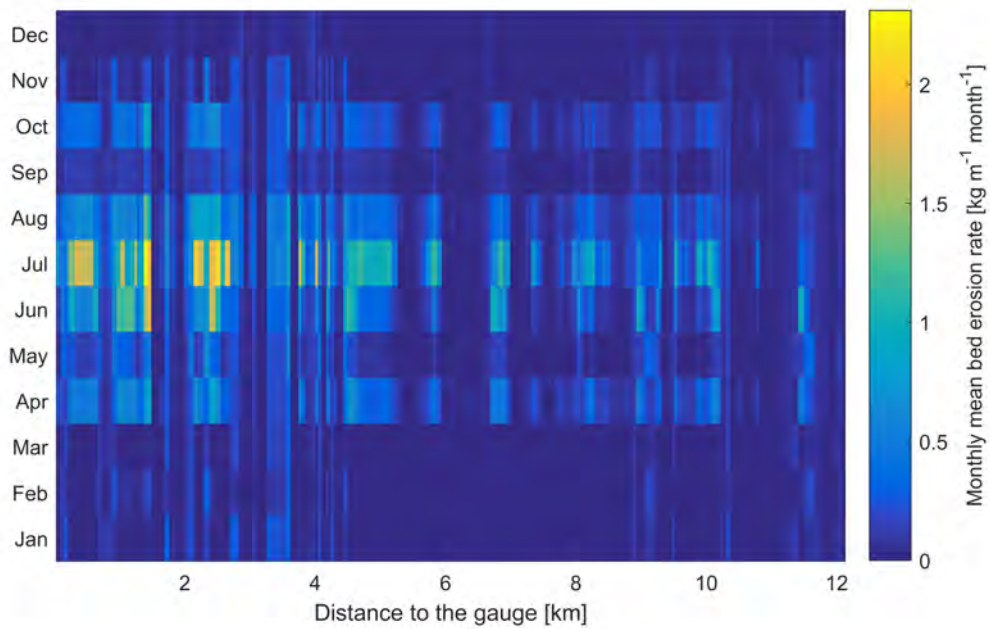
Figure 3.8: Monthly mean bed erosion along the channel of the Ammer River upstream of the gauge (flow direction from right to left).

Chapter 4

Fate of Sediment-Associated Micropollutants in River Ammer

The content in this chapter contains materials submitted in "Liu, Y., Zarfl, C., Basu, N. B., and Cirpka, O. A. (2019). Turnover and legacy of sediment-associated PAH in a baseflow-dominated river. Science of the Total Environment."

Polycyclic Aromatic Hydrocarbons (PAH) ubiquitously occur in rivers and threaten the aquatic system. Understanding the behavior and fate of PAH in a river system can help to improve management strategies. In this chapter, I apply the particle-facilitated pollutant transport model to investigate the turnover and legacy of sediment-bound PAH in a baseflow-dominated river system, the Ammer river. I identify PAH contributions from dissolved/sediment-bound, wet/dry weather periods, and catchment/in-stream processes by model simulations. The average turnover time of sediments and attached PAH in the Ammer main stem is investigated by analyzing in-stream processes. I study the legacy of sediment-bound PAH through a model scenario in which I assume a 50% reduction in PAH emissions after the implementation of environmental regulations in the 1970s.

4.1 Introduction

PAH ubiquitously occur in the environment, and pose threats to human health and aquatic systems due to potentially toxic, mutagenic, and carcinogenic properties (Aziz *et al.*, 2014; Colombo *et al.*, 2006; Yan *et al.*, 2004). The US Environmental Protection Agency

(USEPA) has listed 16 species of PAH with 2-6 fused aromatic rings as priority pollutants (Bojes and Pope, 2007). An increasing number of studies have been conducted on these priority PAH, such as the detection of occurrence (Chiffre *et al.*, 2015; Yang *et al.*, 2008), the monitoring of concentrations (Oros *et al.*, 2007; Kasiotis and Emmanouil, 2015), and the diagnosis of potential sources (Christensen and Bzdusek, 2005; Zhang *et al.*, 2012). PAH are emitted into the environment to a small extent via natural processes, such as biomass burning, volcanic eruptions, and diagenesis (Tobiszewski and Namies-nik, 2012), but they are mainly caused by anthropogenic activities in the urbanized and industrialized regions including vehicle exhaust and tire degradation, industrial emissions, and home heating (Zhang *et al.*, 2009; Schwientek *et al.*, 2017). PAH reach lakes and oceans through atmospheric deposition and transport by river water (Wang *et al.*, 2007; Gonzalez-Gaya *et al.*, 2014; Mai *et al.*, 2003). Owing to the strong hydrophobicity and low solubility, PAH strongly sorb to particles in the aquatic environment (Patrolecco *et al.*, 2010), and are thus transported over long distances in rivers by sediment transport (Van Metre and Mahler, 2003; Rügner *et al.*, 2014a). Schwientek *et al.* (2013a) reported that total PAH concentrations in rivers linearly scale with the concentration of suspended solids and the contamination of particles correlates with the degree of urbanization in the catchment. DiBlasi *et al.* (2009) revealed that the PAH in the influent of an urban stormwater bioretention facility show a strong affiliation with runoff suspended solids. The deposition rates of PAH are higher close to emission sources, e.g., urban areas and industrial regions (Bari *et al.*, 2014; Lang *et al.*, 2007; Liang *et al.*, 2016; Schwientek *et al.*, 2017), thus soils are less contaminated with PAH in remote rural areas compared to urban particles. Doong and Lin (2004) and Liu *et al.* (2013) demonstrated that PAH concentrations on bed sediments vary substantially along river channels. Therefore, the origins of particles essentially determine the contamination level by PAH, i.e., high contamination of urban particles, low contamination of rural sediments, and variable contamination of bed sediments. Particles with different PAH content can be redistributed in the river channel. To understand the behavior and fate of PAH in a river system, a particle-facilitated transport model considering particles from different origins and their redistributions by in-stream processes is necessary, which can also help to investigate the turnover of sediments and attached PAH.

Many historical studies on PAH demonstrated that PAH fluxes and concentrations in Europe and the US increased significantly from the 1860s to the 1960s because of the massive usage of fossil fuels since the Industrial Revolution (Lima *et al.*, 2003; Yan *et al.*,

2014), and reached the peak in the 1960s and 1970s (Fernández *et al.*, 2000; Wakeham *et al.*, 2004). In the late 20th century, continuous declines of PAH concentrations and fluxes have been observed due to cleaner fuels, technological progress, e.g., particle filters for vehicles, and the implementation of environmental legislations (Lima *et al.*, 2003; Purcaro *et al.*, 2013; Shen *et al.*, 2011). Bao *et al.* (2015) reported that the role of soils changed from sinks to sources of phenanthrene for a duration of over two decades after the implementation of environmental regulations in the 1970s. In a river system, highly PAH-polluted particles may have been stored in bed sediments before the 1970s, and become a secondary source for PAH afterwards. It is not well understood whether sediment-bound PAH have legacy effects in the Ammer River and similar streams and how long the legacy effects would remain in such rivers.

4.2 Model Setup

I apply the particle-facilitated pollutant transport model to the Ammer river to simulate dissolved, suspended sediment-bound, and sediment-bound PAH concentrations (here the PAH concentration is the sum of 15 individual PAH concentrations, see Sect. 4.2.2) using a temporal resolution of one hour. Considering catchment and in-stream processes in the particle-facilitated pollutant transport model helps to diagnose PAH sources and investigate the behavior and fate of PAH in rivers.

4.2.1 Particle-Facilitated Pollutant Transport Model

a. PAH Emission From the Catchment

The catchment input module of this model assumes local equilibrium between dissolved and sediment-bound PAH. The main driving forces for PAH generation are surface runoff and point-source emissions. Therefore, PAH within the catchment are emitted essentially via urban and rural surface runoff, contributions from the karst system, and WWTP effluents.

The total PAH content in the water phase is determined by the dissolved and suspended sediment-bound concentrations. Total PAH concentrations from different sources are catchment-specific. It is assumed that PAH concentrations on particles vary from different origins, which can be obtained through measurements. Because of the assumption

of a local equilibrium between dissolved and particle-bound PAH, the dissolved PAH concentrations from lateral flows can be calculated through the following equation:

$$c^i_{p_{lat},w} = \frac{c^i_{p_{lat},ss}}{K_s} \times 10^6 \tag{4.1}$$

in which, $c^i_{p_{lat},w} \, [ng\,L^{-1}]$, and $c^i_{p_{lat},ss} \, [mg\,kg^{-1}]$ are the dissolved and suspended sediment-bound PAH concentrations from the i-th lateral source, respectively. $K_s \, [L\,kg^{-1}]$ denotes the partition coefficient. Given sediment fluxes from the catchment (Liu *et al.*, 2018b), the total PAH flux from sub-catchments can be achieved.

b. PAH Transport in the River

The in-stream transport module is formulated for the main stem of the river. No flow diversion exists, and tributaries and WWTP effluents are regarded as lateral flows. I use a Finite Volume discretization to model two types of pollutants, mobile components (i.e., dissolved and suspended sediment-bound PAH), and an immobile component (i.e., sediment-bound PAH). Because the studied river is small and 12-km long, I assume that dissolved PAH and suspended-sediments with attached PAH in the water phase are well mixed such that the in-stream transport module of the model simulates the average concentrations. For bed sediments, average sediment-bound PAH concentrations are calculated without considering a potential vertical gradient.

I performed a sensitivity analysis on the sorption/desorption process, which demonstrates that the dissolved and suspended sediment-bound PAH can reach equilibrium within 20 minutes. The temporal resolution of my particle-facilitated pollutant transport model is one hour. Therefore, the model is not sensitive to the parameters regarding kinetic sorption/desorption. The parameters are set as following: $k = 10^{-5} \, [m\,s^{-1}]$, $\rho_{ss} = 1800 \, [kg\,m^{-3}]$, and $d_{ss} = 5 \times 10^{-2} \, [mm]$.

4.2.2 Studied Pollutants and Turnover Time

a. Studied Pollutants

I study priority PAH, excluding naphthalene, with the model approach. Since naphthalene is relatively volatile, considerable transport can occur via the atmosphere. In

addition, it is comparably well biodegradable (Schwientek *et al.*, 2013a). The 15 studied PAH include acenaphthylene (AcNy), fluorene (Fl), acenaphthene (AcNe), phenanthrene (PhA), anthracene (An), fluoranthene (FlA), pyrene (Py), benz[a]anthracene (BaA), chrysene (Chy), benzo[b]fluoranthene (BbF), benzo[k]fl-uoranthene (BkF), benzo[a]pyrene (BaP), indeno[1,2,3-cd]pyrene (IP), benzo[ghi]perylene (BghiP), and dibenz[a,h]anthracene (DBahA). This study does not focus on each individual PAH, but on the total PAH concentrations in dissolved, suspended sediment-bound, and sediment-bound forms, attributing average properties to the total sum.

b. Mean Turnover Time

The mean turnover time has been used to investigate water storage dynamics in a hillslope (Amvrosiadi *et al.*, 2017; Bishop *et al.*, 2011). I use a similar concept, also mean turnover time, to quantify the renewal of sediments and attached PAH in rivers. The smaller the turnover time, the faster the renewal rate. The mean turnover time is expressed as follows:

$$\overline{t_{t,s}} = \frac{\overline{M_s}}{\overline{r_{bed}}} \tag{4.2}$$

$$\overline{t_{t,p}} = \frac{\overline{M_p}}{\overline{r_{bed}^p} + \overline{r_{e-}^p}} \tag{4.3}$$

in which, $t_{t,s}$ [s] and $t_{t,p}$ [s] represent the mean turnover times of sediments and attached PAH. $\overline{M_s}$ [$g\,m^{-1}$] and $\overline{M_p}$ [$\mu g\,m^{-1}$] are the average sediment and PAH storage amounts per unit river length for the simulation period, respectively. $\overline{r_{bed}}$ [$g\,m^{-1}\,s^{-1}$], $\overline{r_{bed}^p}$ [$\mu g\,m^{-1}\,s^{-1}$], and $\overline{r_{e-}^p}$ [$\mu g\,m^{-1}\,s^{-1}$] indicate the average bed erosion rate of sediments, the erosion rate of PAH, and the exchange rate of PAH from sediments to the water phase, respectively.

4.2.3 Model Verification and Scenarios

a. Parameter Estimation

Parameters concerning the sediment transport model have been discussed in details in Sect. 3.3.5. Table 4.1 lists the six parameters required for the particle-facilitated pollu-

tant transport model. The first four parameters are PAH concentrations on particles from different origins, which are normally catchment-specific. I used measurements in the Ammer catchment and literature values to estimate these four parameters. I conducted a literature survey to determine a reference range of the combined partition coefficient of the investigated PAH (K_s) and the exchange rate constant (k_e). Then I performed a sensitivity analysis to identify the optimal values of the two parameters, in which the relationship between total PAH concentrations and total suspended-sediment concentrations (Rügner *et al.*, 2014a; Schwientek *et al.*, 2013a) was used as the reference. Knowing the organic carbon content of the sediments in the Ammer River, 2-4 % (Schwientek *et al.*, 2013a), K_s was also estimated based on the composition of the 15 PAH (Liu *et al.*, 2013) and the octanol-water partition coefficient (K_{ow}) of the individual PAH compounds. Details on the sensitivity analysis and the K_s estimation are provided in Appendix B. The sensitivity analysis indicates that k_e is not sensitive to the hourly total PAH concentrations, whereas it substantially affects the turnover of sediment-bound PAH. In the following model simulations, I used the median values of k_e from the reference range.

Table 4.1: Estimated parameters of the particle-facilitated pollutant transport model

Parameters	Unit	Value	Comment
PAH concentration on urban particles	$mg\,kg^{-1}$	8.1	(Gocht *et al.*, 2005)
PAH concentration on rural particles	$mg\,kg^{-1}$	1 [a]	Field measurements
PAH concentration on karst particles	$mg\,kg^{-1}$	1	Set the same as rural particles
PAH concentration on WWTP particles	$mg\,kg^{-1}$	13	(Launay *et al.*, 2016)
Combined partition coefficient, K_s	$L\,kg^{-1}$	10^5	See Supporting Material
Exchange rate constant, k_e	s^{-1}	5×10^{-9} [b]	(Rakowska *et al.*, 2014)

a represents the average PAH concentration on rural particles.
b indicates the median value of the reference range.

b. Model Verification

Measuring PAH is time-consuming and expensive so that a time-series of PAH measurements is hardly possible. The developed particle-facilitated pollutant transport model will overcome this issue and use easily measured parameters (e.g., precipitation and turbidity) to investigate the fate of PAH. Only few measurements of total PAH concentrations are available in the Ammer River, which means that the typical calibration-validation method is inappropriate. However, these available measurements and information on pollutant patterns can help to verify the model. Rügner *et al.* (2014a) and Schwientek *et al.* (2013a) reported a linear relationship between total PAH concentrations and suspended-sediment concentrations in the Ammer River, which can be used as a reference to evaluate the particle-facilitated pollutant transport model.

c. Simulation Scenario for PAH Legacy Effect

To investigate whether a PAH legacy exists in the Ammer River, a model scenario is used to simulate the general trend of sediment-bound PAH concentrations from 1960 to 2010. The environmental regulation of PAH became effective in 1970 which resulted in the reduction in PAH and particle emissions after 1970. Thus, the simulation period is divided into the pollution period (1960-1970) and the environmental-regulation period (1970-2010). Bao *et al.* (2015) assumed a 50% reduction of the phenanthrene concentration in the atmosphere for the environmental regulation period after 1970 to investigate the role of soils in the soil-atmosphere exchange of phenanthrene. The same concept is used here, i.e., particle and PAH emission for the pollution period is twice as high as during the regulation period.

4.3 Results and Discussion

4.3.1 Model Performance

Figure 4.1 shows the modelled and measured total PAH concentrations at the gauge. It can be seen that the modelled total PAH concentrations for the event in July 2013 are in the same order of magnitude as the measurements, especially the shape of the event measurement is simulated well by the model. In addition, the relationship regressions between total PAH concentrations and suspended-sediment concentrations of the model

and the reference study (Rügner *et al.*, 2014a; Schwientek *et al.*, 2013a) are in good agreement (Table 4.2). This indicates that the model setting is feasible for the particle-bound PAH simulation in the Ammer River.
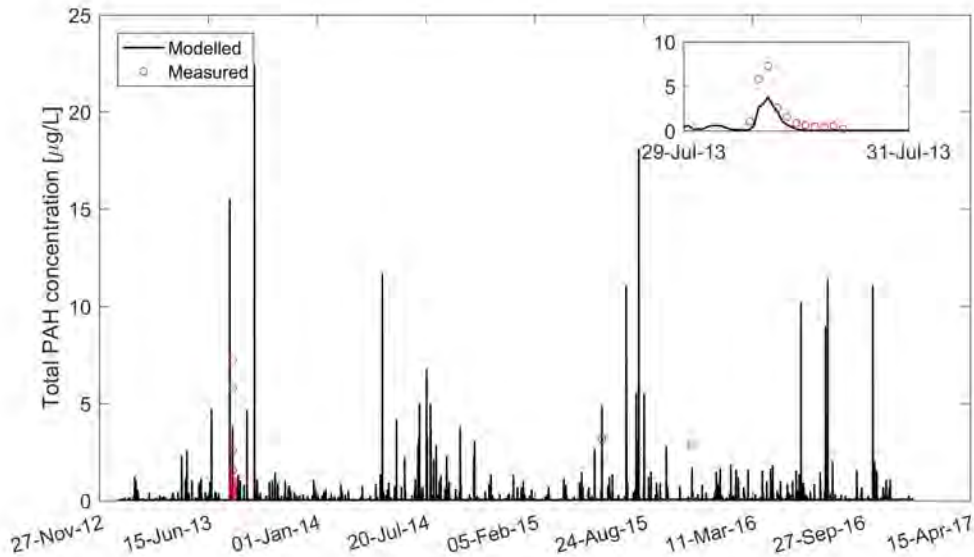
Figure 4.1: Modelled and measured total PAH concentrations (dissolved + suspended sediment-bound) in the aqueous phase at the gauge.

Table 4.2: PAH concentrations on suspended sediments and distribution coefficients (logarithm form) from the reference and model simulation

Parameters	Reference value	Model value
PAH concentrations on SS [$mg\,kg^{-1}$]	5.8 ± 0.3	5.7
Log (K_{ss} [$L\,kg^{-1}$]) [a]	5.3 [b]	5.6 [c]

a. K_{ss} represents the distribution coefficient, the ratio of the suspended sediment-bound PAH concentration ($mg\,kg^{-1}$) over the dissolved PAH concentration ($mg\,L^{-1}$).
b. it shows the distribution coefficient of Fluoranthene.
c. it is the combined distribution coefficient of 15 investigated PAH.

4.3.2 Annual PAH Load

Figure 4.2 shows the modelled contributions of dissolved and suspended sediment-bound PAH, as well as the contributions of wet and dry periods to the annual PAH load for the

years 2014-2016 in the Ammer River. The suspended sediment-bound PAH account for approximately 75% of the total annual load, and dissolved PAH constitute about 25% (Fig. 4.2(a)). This demonstrates that the transport of PAH in the Ammer River is mainly facilitated by suspended-sediment transport. Hwang and Foster (2006) investigated PAH sources in the Anacostia River suggesting that PAH in storm flow were significantly enriched in the particle phase with 68-97% (median = 87%) of the total PAH. Our simulated fraction of particle-bound PAH falls within the corresponding range, which indicates a good agreement. Because the Ammer catchment is dominantly groundwater-fed, the low flow accounts for a very big proportion of the flow duration curve, which results in a relatively high fraction of dissolved PAH since dissolved PAH were predominant under base-flow conditions (Hwang and Foster, 2006). Fig. 4.2(b) depicts contributions of PAH during wet periods (with precipitation) and dry periods (without precipitation). Seventy percent of the total PAH load is contributed by wet periods. The contribution of dry periods (30%) is surprisingly large because the Ammer River has a rather high suspended sediment contribution under low-flow conditions and WWTPs also emit PAH to the river during dry periods, which reflects that the pattern of suspended-sediment transport substantially affects the PAH transport.
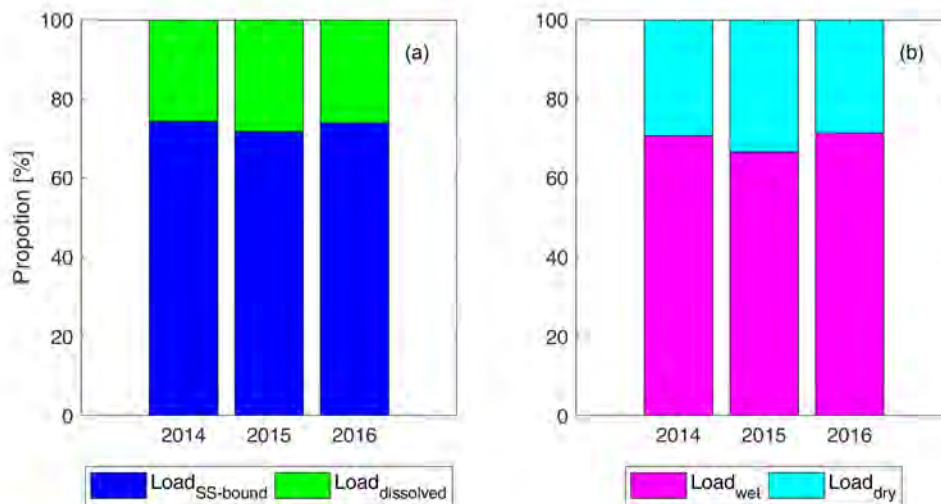
Figure 4.2: The contribution of dissolved and suspended sediment-bound PAH (a), wet and dry periods (b) to the annual PAH load.

PAH from different processes were analyzed by model simulations (Fig. 4.3). In the

Ammer River, urban PAH (2.6 *kg* per year) dominate the total PAH load, accounting for over 74%, followed by the contribution from the karst system, constituting 19%. Bed erosion induces 4% of the total PAH load from bed sediments, namely 0.13 kg per year. PAH contributions from different processes demonstrate a similar pattern as for suspended sediments (Liu *et al.*, 2018b). A big urban contribution was observed because urban particles are typically more contaminated by PAH due to anthropogenic activities than rural particles (see also Table 4.1). Zhang *et al.* (2012) revealed that car emissions were the most significant source of PAH in Lake Taihu (53.6-54.3%), followed by coal combustion (23.8-28.8%) and wood combustion (11.9-16.0%). The sum of car emissions and coal combustion (84.0-88.1%) could represent the urban signals. Stein *et al.* (2006) demonstrated that high-molecular-weight PAH compounds, which mainly have a pyrogenic source, account for 74% of the total PAH concentrations in the Dominguez channel watershed in Los Angeles, USA. My model results are consistent with these studies.
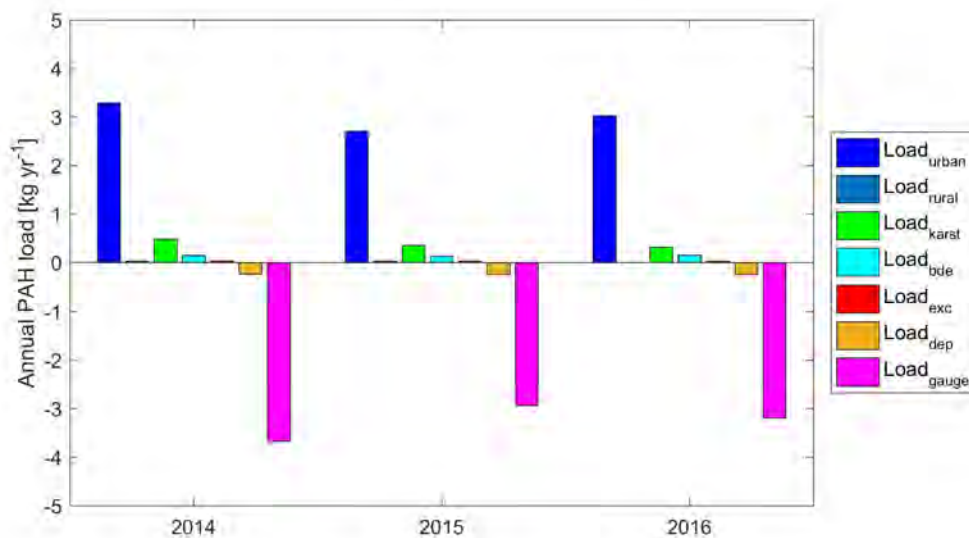
Figure 4.3: Annual PAH load from different processes. $Load_{gauge}$ is the PAH load at the gauge calculated by modelled discharge and PAH concentrations. $Load_{urban}$, $Load_{rural}$, and $Load_{karst}$ represent PAH load from urban areas, rural regions, and the karst system. $Load_{bde}$, $Load_{dep}$, and $Load_{exc}$ are the PAH load from bed erosion, deposition and exchange between water and sediments for the entire river channel. The positive values indicate PAH input to the water phase of the river channel, while negative values denote PAH load leaving the river channel.

4.3.3 Turnover of Sediments and Attached PAH

The length profile of turnover time was simulated for bed sediments and attached PAH for the years 2014-2016 (shown in Fig. 4.4). It varies substantially along the river channel, namely $10\text{-}10^6$ days and $10\text{-}10^4$ days for sediments and sediment-bound PAH, respectively. The turnover time of sediments is longer than that of sediment-bound PAH, particularly in the mild river reaches with long sediment turnover time. Because the turnover of sediments is driven only by bed erosion, whereas the turnover of sediment-bound PAH is also affected by the PAH exchange between the water phase and sediments. As seen in Fig. 4.4, no significant difference of turnover time for sediments and attached PAH can be observed in river segments with steep slopes, which indicates that for steep river reaches, turnover of sediments determines the turnover of attached PAH. By contrast, in the very mild river segments, the turnover time of sediments is 1-2 orders of magnitude longer than that of the attached PAH. This is because bed erosion in mild river reaches is so small that the diffusive PAH exchange between water and sediments dominate the overall transfer from the bed to the mobile water. Reaches with long sediment turnover time are sediment storage pools, where old and highly PAH-polluted particles may cumulate. These locations could release PAH under low-flow conditions due to the diffusion of PAH from sediments to water. Therefore, the PAH legacy may exist in very mild river reaches (further discussion will be included in Sect. 4.3.5).

4.3.4 Role of River Beds as PAH Sources or Sinks

Flow rates influence the PAH flux between water and the river bed, Fig. 4.5 demonstrates the relationship between modelled PAH flux of the entire river and flow rates. A positive PAH flux (from water to the river bed) when the flow rate is small, typically smaller than $2\ m^3\,s^{-1}$, indicates that the river bed functions as PAH sink for the entire river under low-flow conditions. Deposition of suspended sediments dominates when discharge is small, which leads to the deposition of suspended sediment-bound PAH. With the increase of discharge to the range of 2-5 $m^3\,s^{-1}$, the PAH flux becomes nearly zero so that a temporary steady state is formed since deposition and erosion of PAH are balanced for the whole river within this range of flow rates. When flow rates are larger than 5 $m^3\,s^{-1}$, the overall PAH flux is oriented from the river bed to the mobile water due to the strong erosion of bed sediments, denoting that the river bed becomes a PAH source under
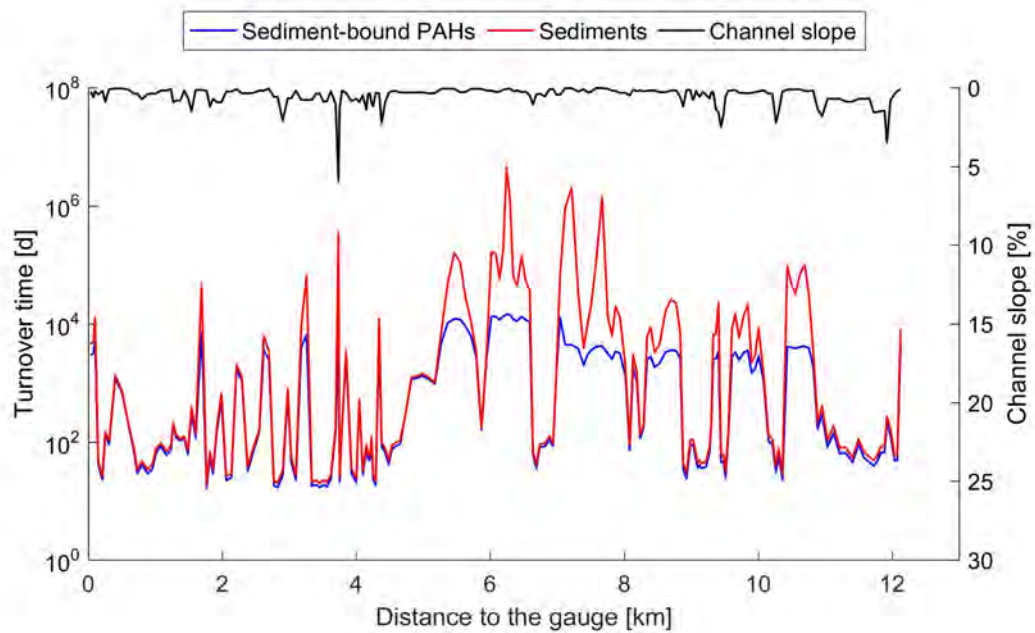
Figure 4.4: Average turnover time of sediments and sediment-bound PAH along the main stem of the Ammer River based on the simulation from 2014 to 2016 (flow direction from right to left).

high-flow conditions. To large extent, the PAH flux is related to the flux of sediments.

With the length profiles of deposition, bed erosion, and exchange of PAH, I can identify potential spots of PAH legacy. The length profile with channel slopes is shown in Fig. 4.6. The net deposition and flux of PAH from the river bed to the mobile water vary significantly along the Ammer main stem. The net PAH deposition shows a similar pattern as the net sediment deposition (Liu *et al.*, 2018b), i.e., the net deposition occurs in the very mild reaches, which indirectly reflects the strong particle-facilitated transport characteristic of PAH. The main difference is that PAH are released from sediments to water in sediment trapping pools. These reaches may carry the signals of old sediments and thus attached PAH. Because of the weak erosion in mild river reaches, the exchange of dissolved and sediment-bound PAH becomes relevant. Therefore, net sediment trapping pools may be long-term PAH sources even after a significant reduction of the PAH load in the water entering the river.
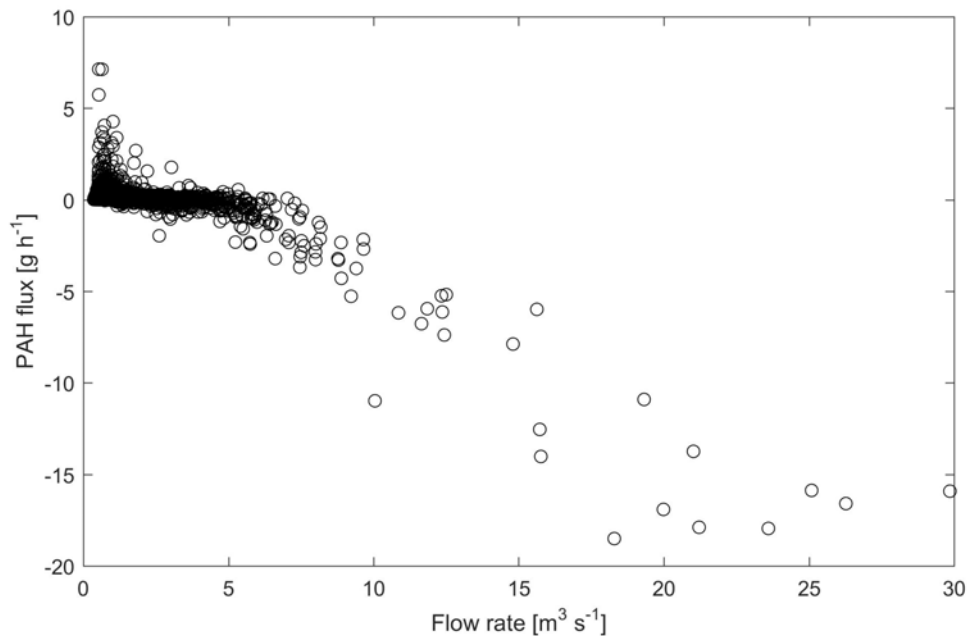
Figure 4.5: PAH flux between the river bed and the mobile water for the entire river. Positive (+) values indicate PAH flux from water to the river bed, while negative (-) values indicate the opposite direction.

4.3.5 Legacy of Sediment-Bound PAH

The emission level of PAH influences the concentration distribution and the contamination level of sediments in rivers. Fig. 4.7 displays the simulated time series of sediment-bound PAH concentrations at three locations (locations are marked in Fig. 4.6) before and after the pollution regulation came into effect in the 1970s assuming a 50% reduction in PAH emission and particle production. Higher sediment-bound PAH concentrations were simulated for all three locations before 1970 because higher emissions before the regulation period result in particles with higher PAH content. After the regulation became effective, a very fast decrease of sediment-bound PAH concentrations is modelled at location A. This is because the deposition and bed erosion rates at location A are approximately the same leading to a fast sediment turnover and erasing historical PAH concentrations. At location B and C, however, the simulated bed sediment-bound PAH concentrations only gradually decrease, taking 10-20 years. Here, the deposition rate is larger than the bed erosion rate, which results in the trapping of sediments with their historical PAH contamination. Over time the cumulated old sediments with high-content
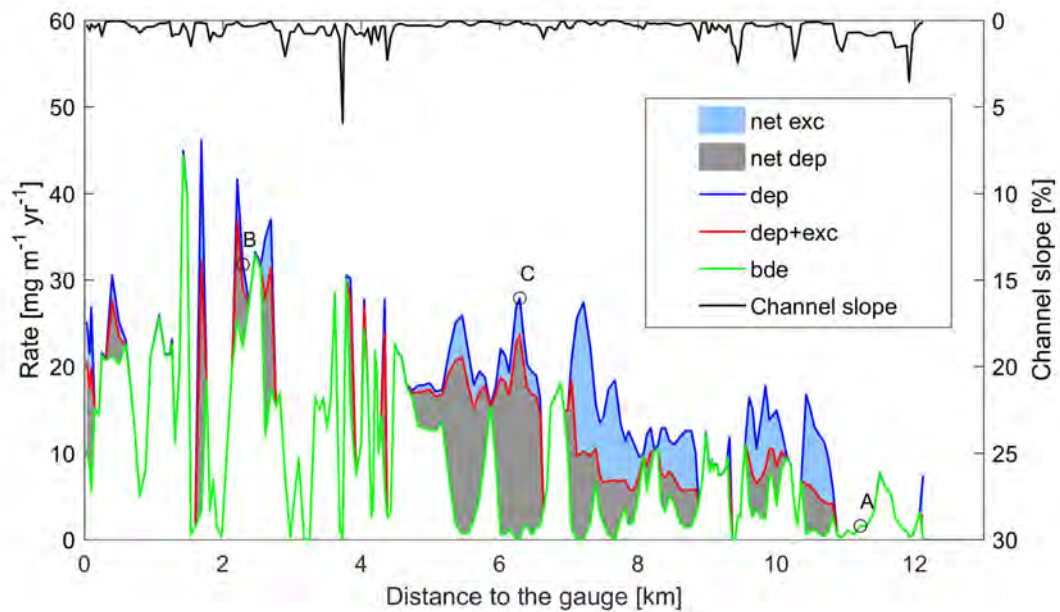
Figure 4.6: The distribution of PAH deposition (dep), deposition + exchange (dep+exc), bed erosion (bde), net exchange (net exc), and net deposition (net dep) along the channel of the Ammer River.

of PAH are diluted by the less-contaminated newer sediments. As discussed above, the diffusion of PAH from river-bed sediments to the mobile water is relevant in the sediment trapping locations. The concentration decrease of bed sediment-bound PAH at location B is faster than that at location C since the sediment trapping in location B is smaller than that at location C. Therefore, in these locations (representing reaches with sediment trappings), the PAH legacy is relevant, which can extend 10-20 years.

Figure 4.8 shows the time series of modelled sediment-bound PAH mass and modelled diffusive PAH fluxes between the mobile water and the river bed at three representative locations. At location A, the modelled bed sediment-bound PAH mass (Fig. 4.8(a)) immediately drops to a lower level after 1970 (the environmental regulation is assumed to be effective in 1970) because the turnover of sediments and PAH at location A is very fast, and the PAH flux (Fig. 4.8(b)) due to the exchange process between water and the river bed remains around 0, which indicates that the diffusion of PAH at location A is not relevant. This finding is consistent with the statement that the sediment turnover determines PAH turnover at location A. By contrast, at location B and C, Fig. 4.8(a)
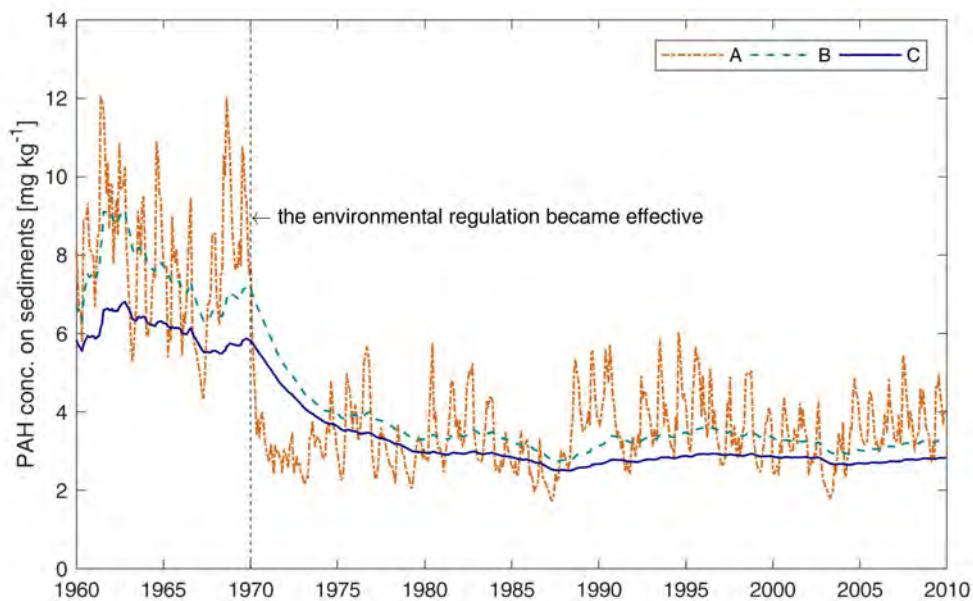
Figure 4.7: The change of PAH concentrations on sediments for locations A, B, and C (shown in Fig. 4.6) along the river before and after the pollution regulation in 1970. A: deposition $\approx$ erosion, B: deposition $>$ erosion, C: deposition $\gg$ erosion.

shows a continuous decrease of modelled bed sediment-bound PAH mass from 1970 to 1980 due to the introduction of the environmental regulation. This can be explained by the input of particles to the river becoming less and particles becoming "cleaner" after 1970 compared to that in the pollution period before 1970, which induces the river bed switched from the sink to the source of PAH in the Ammer river at the early time after the simulated drop in PAH load. The model simulates small increases and decreases of bed sediment-bound PAH mass between 1980 and 1990. During this period, the diffusion of PAH from the river bed to the water becomes smaller because of the continuous decrease of bed sediment-bound PAH concentrations but is still so significant that the deposition of PAH and the release of PAH from the river bed to the mobile water are balanced. From 1990 I can see a continuous increase of bed sediment-bound PAH mass at location B and C from the model simulation because the bed sediment-bound PAH concentration decreases to the same level as the input PAH such that the river bed becomes the sink of PAH at the two locations. This is supported by Fig. 4.8(b), my model simulates a significant diffusive mass flux from the river bed to the water over a time period of 10-

20 years after the change of the input into the river at location B and C, followed by a regime in which the flux fluctuates and changes direction. The latter implies that in River Ammer the legacy of PAH remained over 10-20 years, which is in good agreement with the change of sediment-bound PAH concentrations.

4.4 Summary and Conclusion

The transport of PAH is mainly facilitated by sediment transport due to the strong hydrophobicity of these compounds. In this study, I presented a particle-facilitated pollutant transport model, which simulates dissolved and sediment-bound PAH from different origins (i.e., urban regions, rural areas, and the river channel) with variable PAH contamination and considers PAH interactions between water and sediment. With this model I investigated the turnover of sediment-bound PAH and their legacy potential in a river.

In the Ammer River, sediment-bound PAH contribute approximately 75% to the annual PAH load, whereas, in other rivers this fraction has been reported to vary substantially (Hwang and Foster, 2006; Schwientek *et al.*, 2017). The supply and composition of the sediments determine to a large extent the PAH supply to a river. In steep reaches, sediment turnover governs the turnover of PAH, whereas in very mild river segments diffusion of PAH from the river bed to the mobile water is relevant and significantly reduces PAH turnover times. As the turnover of sediments is affected by the flow rate, this also holds for the redistribution of PAH. This study indicates that PAH legacy occurs in sediment trapping reaches. For River Ammer, we simulated that the river bed may have acted as secondary PAH source over 10-20 years after the environmental regulation in 1970s, which supports the hypothesis of Liu *et al.* (2013) on PAH legacy pollution in industrialized countries.

This study demonstrates how the PAH turnover and the legacy potential varies along the simulated river, which is useful and helpful for the management of persistent pollutants and the assessment of their environmental impacts, such as estimating the distributed PAH toxicity to benthic organisms (Hawthorne *et al.*, 2006) and the contribution of PAH to the total toxicity in the flowing water. While the proposed particle-facilitated pollutant transport model was applied to PAH in River Ammer, the framework can be transferred to predict the fate and exposure of other hydrophobic compounds in other rivers. The study illustrates that a thorough understanding of river hydraulics is neces-

sary to understand the fate of PAH in rivers, because the dynamics and spatial distribution of PAH depends on sediment transport, which itself depends on the shear stress exerted by the river flow.
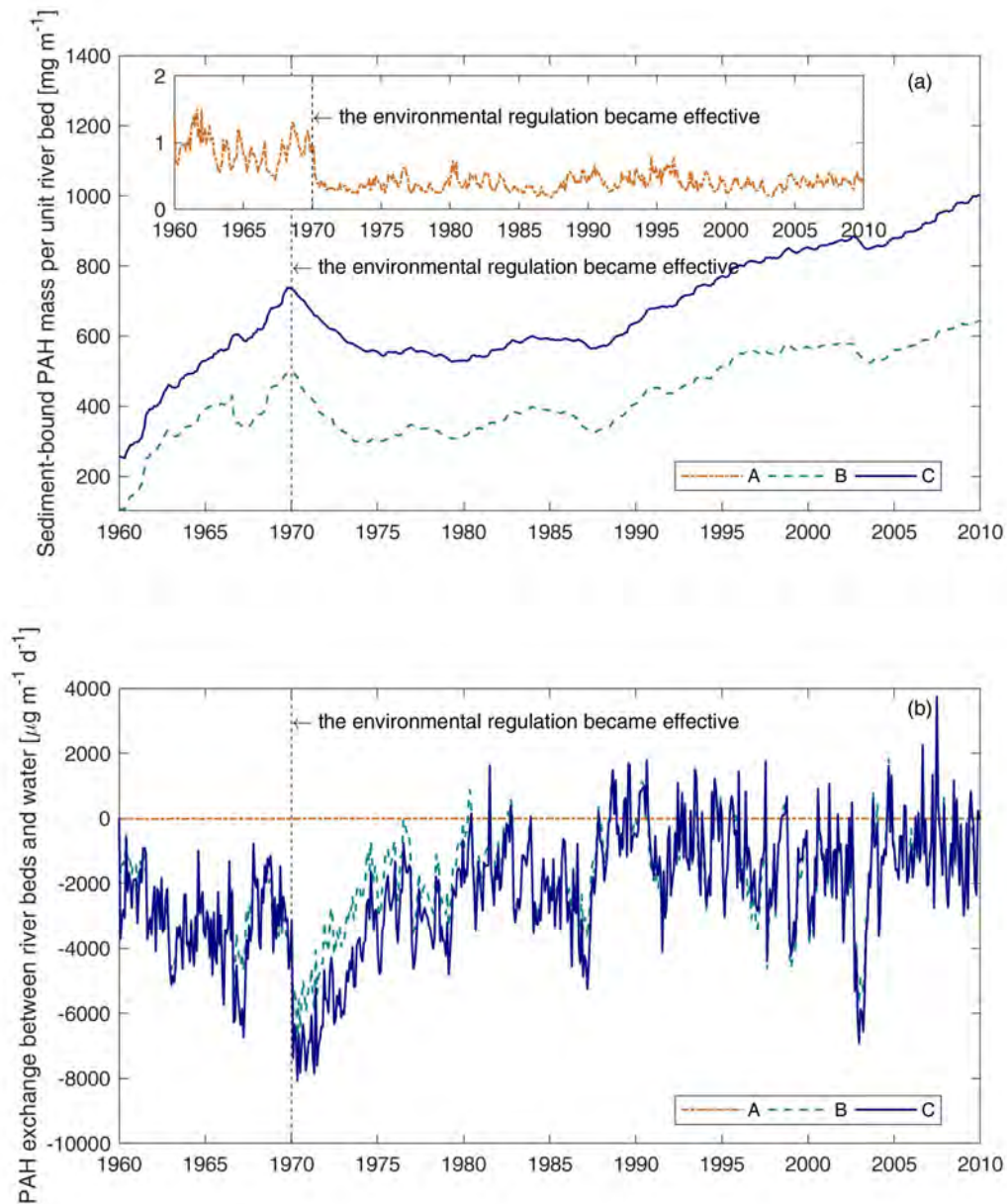
Figure 4.8: Time series of modelled sediment-bound PAH mass per unit river bed (a) and modelled PAH flux due to the exchange process between water and river beds (b) at locations A, B, and C (shown in Fig. 4.6) before and after the introduction of the environmental regulation in 1970. Positive values in figure (b) represent PAH flux from water to the river bed, negative values show the opposite direction.

Chapter 5

Fate of Dissolved Micropollutants in River Steinlach

In recent years, dissolved emerging micropollutants e.g., pharmaceuticals at concentrations in the range of nano- to micrograms per liter have become the major concern for water quality. The increasing detection of pharmaceuticals in rivers has drawn growing attentions. Understanding the fate of these compounds can help to evaluate the environmental impacts on river systems. I applied the one-dimensional reactive solute transport model with transient storage to investigate the fate of representative pharmaceuticals in the lowest section of River Steinlach, which is impacted by WWTP-effluents. Taking advantages of tracer experiments and a Lagrangian sampling campaign performed both at day and night, I could differentiate attenuation mechanisms for different pharmaceuticals. I estimated river hydraulic parameters and quantified the effect of flow rate on transient storage by fitting tracer breakthrough curves. Based on the sampling campaign I investigated the main attenuation processes of representative pharmaceuticals. Finally I quantitatively simulated the effect of flow rates on pharmaceutical removal.

5.1 Introduction

In industrialized countries, concerns about the water quality in rivers have shifted from nutrients to emerging micropollutants. With the development of better analytical techniques emerging contaminants, such as pharmaceuticals (Zhao *et al.*, 2010; Kunkel and Radke, 2012; Sim *et al.*, 2010), have been become detectable in rivers at concentrations in the range of nano- to micrograms per liter (Li *et al.*, 2016; Acuña *et al.*, 2015).

These compounds potentially have negative impacts on aquatic organisms and humans (Gelsleichter and Szabo, 2013; Grabicova *et al.*, 2017). However, common treatment of wastewater treatment plants (WWTPs) are not designed for their removal and they are not included in routine monitoring programmes. Their environmental fate and ecotoxicological effects are not well understood (Aristi *et al.*, 2016; Hughes *et al.*, 2012; Pal *et al.*, 2010).

WWTPs have been reported to be the main source of pharmaceuticals in streams (Musolff *et al.*, 2009; Phillips *et al.*, 2012; Launay *et al.*, 2016). Effluent and overflow of WWTPs bring incompletely removed pharmaceuticals into rivers, which then are diluted by the water from natural sources. Therefore, the fraction of WWTP effluent to the total river discharge essentially determines the magnitude of micropollutant concentrations downstream of the WWTP inlet. When the effluent constitutes a large fraction of total river flow, the environmental impacts increase. During dry seasons, WWTP effluent could contribute over 70% to the total discharge in rivers with low base flow, such as the Steinlach River (Guillet *et al.*, 2018). The discharge (a mixture of WWTP effluent and water from the catchment) controls the hydrodynamics of a river, which substantially affects transport and degradation of contaminants within the river (Cranswick *et al.*, 2014; Lewandowski *et al.*, 2011). Flow and pollutant transport may behave differently under low-flow conditions than under high-flow conditions.

The attenuation mechanisms of micropollutants in streams include adsorption onto bed sediments, photo-degradation, and bio-degradation (Barber *et al.*, 2013; Wang and Lin, 2014; Li *et al.*, 2013). Adsorption effects are normally qunatified by distribution coefficients between different phases; photo-degradation undergoes a diurnal pattern due to the fluctuations of solar radiation (Hanamoto *et al.*, 2013). While bio-degradation can in principle occur in water column, it is often concentrated in the hyporheic zone, that is, the top bed layer where river water infiltrates and exfiltrates back into the river, and in stagnant pool. These in comparison to the main channel practically immobile zones make up of the transient storage zone where the water resides over longer time periods and microorganisms have enough specific surface area to grow on (Burke *et al.*, 2014; Kunkel and Radke, 2008). Transient storage zones increase the travel time of contaminants and influence their attenuation. Tracer experiments can be used to estimate typical hydraulic parameters e.g., the mean flow velocity and dispersion coefficient, and coefficients parameterizing the effects of transient storage on the solute transport (Engelhardt *et al.*, 2011; Haggerty *et al.*, 2009; Knapp *et al.*, 2017; Briggs *et al.*, 2009). In Lagrangian

sampling the same water parcel is sampled on its trajectory along the stream. This sampling technique can give insights to transformation of solutes, unaffected by advection (Kunkel and Radke, 2011; Writer *et al.*, 2013; Schwientek *et al.*, 2016). Reactive transport models (Riml *et al.*, 2013) can be used to understand the entire system, but it is hard to quantify the effects of different processes. However, together with tracer experiments and Lagrangian sampling techniques targeting the contaminants, reactive transport models can be better verified so that the investigation of different processes becomes feasible.

5.2 Data Collection

5.2.1 Tracer Test

Several tracer tests were conducted in the Steinlach River. Fig. 1.3 shows the injection site and 4 downstream stations for measuring time-series of tracer concentrations. The tracer injection site is 492 *m* upstream from the first measuring station (MS1), which is sufficient to ensure that the tracer is well mixed over the cross-section when reaching MS1. The distance between the measuring stations, i.e., MS1-MS2, MS2-MS3 and MS3-MS4, are 410 *m*, 475 *m*, and 425 *m*, respectively. Sodium-fluorescein was used as tracer. At neutral pH it does not sorb. It undergoes photo-degradation but no biodegradation in rivers (Gutowski *et al.*, 2015), which makes it an ideal tracer during night and can reflect photo-degradation intensity during day. Two tracer campaigns were performed, in which tracer concentrations were recorded with a time resolution of 10 seconds at the 4 measuring stations. The first one was on August 7-8, 2015 with day and night samplings. Flow rates for both day and night samplings were quite stable, namely 0.18 m^3s^{-1} and 0.16 m^3s^{-1}, respectively. The second tracer-test campaign was on September 21, 2016 with night samplings, the flow rate was also stable during the campaign, namely 0.25 m^3s^{-1}. More information on sampling and measurements of the tracer test can be found in Guillet *et al.* (2018).

5.2.2 Measurements of Pharmaceuticals

River contaminants were measured on August 7-8, 2015 for both day and night campaigns. At MS1, 6 one-hour composite samples were taken by auto-samplers to measure hourly average pollutant concentrations. Triplicate grab samples were taken at a single

time at MS2. Single grab samples were used at MS3 and MS4. Details about the sample collection, storage, and analysis are reported by Guillet *et al.* (2018).

In this study, I have selected four representative pharmaceuticals to investigate the effects of different attenuation processes. They are the anticonvulsant carbamazepine, the antibiotic sulfamethoxazole, the beta-blocker metoprolol, and the antidepressant venlafaxine.

5.3 Model Setup

I applied the model of solute reactive transport with transient storage (see Sect. 2.5) to the Steinlach River (described in Sect. 1.2.2) to simulate the main attenuation processes for the representative pharmaceuticals listed above under steady-state flow conditions. The data of the tracer experiments and samplings of the pharmaceuticals are used to identify transient storage effects and different pollutant removal mechanisms.

5.3.1 Reactive Solute Transport Model

The reactive transport model is performed under steady-state flow conditions. The time step size is set to the temporal resolution of the tracer test. A finite volume discretization is used to solve the transport of solutes in the main channel, which is coupled with the transient storage area enabling the solute exchange between two compartments.

To fit the tracer breakthrough curves, the measured time-series of tracer concentrations at MS1 is used as the boundary condition and the initial condition is set to 0 since no tracer was present in the river before the tracer experiment. The measured time-series at MS2, MS3, and MS4 are used to calibrate model parameters.

For simulating the fate of pollutants in the river, pollutant measurements at MS1 are also used as boundary condition, but a continuous time-series of concentrations is reconstructed based on 6 continuous hourly-average concentrations by a method that minimizes the squared slope of the time series while meeting the values of the time-averaged concentrations and ensuring non-negativity of the reconstructed time series (Guillet *et al.*, 2018):

$$c_{rec}(t) = \arg\max_{c(t) \geq 0 \forall t} \int_0^T \left(\frac{dc(t)}{dt} \right)^2 dt \tag{5.1}$$

subject to

$$\frac{1}{\Delta t} \int_{(i-1)\Delta t}^{i\Delta t} c_{rec}(t)dt = c_{i,meas} \qquad (5.2)$$

in which $c_{rec}(t) \, [ngL^{-1}]$ is the reconstructed concentration at time $t \, [s]$. $c_{i,meas} \, [ngL^{-1}]$ is the i-th hourly-average concentration. Δt is 1 hour in this study, which is the averaging duration.

5.3.2 Parameter Estimation

I used DREAM$_{(ZS)}$ (see Sect. 2.6.1) to estimate the model parameters of conservative solute transport from the night-tracer tests and of the attenuation processes from the micropollutant measurements. DREAM$_{(ZS)}$ is a Markov chain Monte Carlo (MCMC) sampling algorithm, which efficiently estimates the posterior probability density function of model parameters given the data of dependent variables (Vrugt *et al.*, 2008, 2009; Vrugt, 2016).

To fit the tracer BTCs, I estimated the average velocities (v_1 - v_3) and longitudinal dispersion coefficients (D) between all measuring stations, the average fraction of transient storage area (f_{im}), the average exchange rate constant (k_{ex}), and the average photo-degradation rate constant of fluorescein (k_{pho}, only for day tracer BTCs) of the entire investigated river segment. For the pharmaceuticals of interest, I estimated the rate constants of photo-degradation (k_{pho}) and bio-degradation (k_{bio}). First I estimated the transport parameters from the day and night tracer BTCs. Then, keeping the hydraulic parameters determined from the night tracer BTCs, I estimated the bio-degradation rate constants of the target pharmaceuticals. Finally, I estimated the photo-degradation rate constants for the investigated pharmaceuticals based on the parameters of the day tracer BTCs and the bio-degradation rate constants. The fitted parameters are shown in sect. 5.4. The Nash-Sutcliffe Efficiency of the model fit is calculated from the MAP parameter set as well.

5.3.3 Pollutant Removal

The average pollutant removal during a time period is calculated as the ratio of removed pollutant mass over the total pollutant mass, see below:

$$R_{removal} = \frac{\int_0^T Q(t)c_0(t)dt - \int_0^T Q(t)c_r(t)dt}{\int_0^T Q(t)c_0(t)dt} \tag{5.3}$$

in which $R_{removal}$ $[-]$ is the average pollutant removal during time period T $[s]$. $Q(t)$ $[m^3 s^{-1}]$ represents the flow rate at time t. $c_0(t)$ $[ngL^{-1}]$ and $c_r(t)$ $[ngL^{-1}]$ stand for pollutant concentrations without and with removal processes at time t, respectively.

The pollutant removal is contributed by the photo- and bio-degradation:

$$R_{removal} = R_{removal}^{photo} + R_{removal}^{bio} \tag{5.4}$$

in which, $R_{removal}^{photo}$ $[-]$ and $R_{removal}^{bio}$ $[-]$ denote pollutant removals by photo- and bio-degradation, respectively. To separate the two contributions, measurements at day- and nighttime are needed. I further assume that rate constant of bio-degradation determined at night holds also for the daytime. Then, the remaining degradation can be attributed to photo-degradation.

To calculate the 24-hour average pollutant removal for the measurement campaign in August 7, 2015, I reconstructed the boundary condition of pharmaceutical concentrations as described in Sect. 5.3.1.

To investigate the influence of the flow rate on pollutant removal, I take the hydraulic parameters from the night tracer tests in 2015 and 2016. I assume that the input of pollutant mass flux from the WWTP does not depend on the two flow conditions, resulting in small pollutant concentrations for high flow rate. Furthermore, the photo- and bio-degradation rate constants are assumed to remain at the calibrated values determined from the pollutant measurements in 2015.

5.4 Results and Discussion

5.4.1 BTC Fitting and Effects of Flow Rates on Transient Storage

Figure 5.1 depicts the measured and modelled BTCs of two night tracer experiments in August 7, 2015 (Fig. 5.1a) and September 21, 2016 (Fig. 5.1b) in the Steinlach River. It can be seen that both BTCs are reproduced very well by the model. The simulated tracer concentrations and the shape of both BTCs are perfectly fitted. In particular, the first-arrival time, peak concentrations, and the long tailing are captured, implying that this model is verified very well. In Fig. 5.1a, the tracer concentrations at MS2 drop to 0 after 7 hours of injection, because the measurement sensor was clogged. This measurement artifact is not reflected in the model. I also tried to fit the normal advection-dispersion model to the tracer data but could not reproduce the main features of BTCs, especially the long tailing. This indicates that a transient-storage mechanism is necessary to simulate solute transport in the Steinlach River under low-flow conditions. The NSE values calculated with the MAP parameter set for the night tracer experiments in 2015 and 2016 are 0.996 and 0.998, respectively suggesting a very good model fit at nighttime when fluorescein is conservative. Table 5.1 lists the MAP parameters for the simulation.

Table 5.1: Estimated parameters by model fitting for night tracer tests in 2015 and 2016

Parameter	Unit	Definition	2015	2016
$v1$	$[ms^{-1}]$	MS1-MS2 velocity	0.097	0.130
$v2$	$[ms^{-1}]$	MS2-MS3 velocity	0.150	0.216
$v3$	$[ms^{-1}]$	MS3-MS4 velocity	0.122	0.169
D	$[m^2s^{-1}]$	dispersion coefficient	1.3	2.3
f_{im}	$[-]$	transient storage fraction	0.169	0.127
k_{ex}	$[s^{-1}]$	exchange rate constant	6.4×10^{-4}	2.5×10^{-4}
Q	$[m^3s^{-1}]$	river discharge	0.16	0.25

Table 5.2 shows the absolute transient storage area and relative transient storage fraction based on the model simulation. It can be seen that transient storage is relevant under low-flow conditions (flow rate < 0.16 $[m^3s^{-1}]$), when up to 17% of the cross-sectional area is in the transient storage (note that the mean discharge of this river is 1.84 m^3s^{-1}). The relative fraction of transient storage decreases with the increase in flow rate because the total cross-sectional area increases with increasing discharge. The absolute transient storage area decreases with the increase of flow rate, its percent change
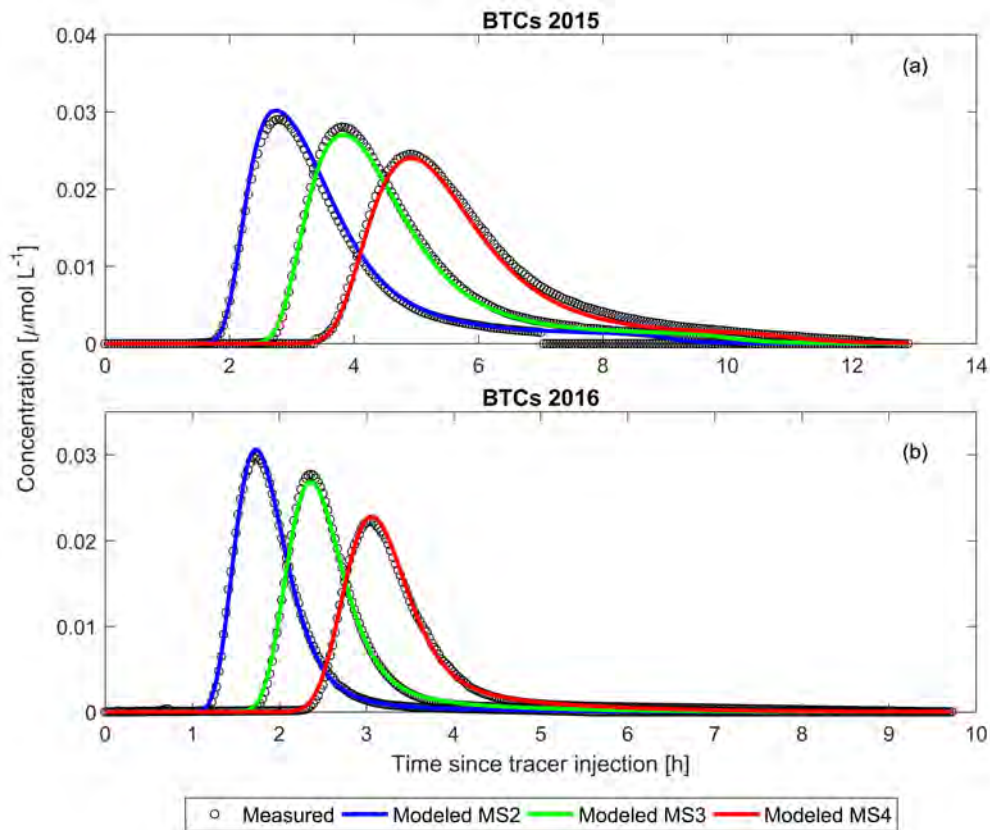
Figure 5.1: BTC fitting for the night tracer campaigns in 2015 and 2016.

is smaller than that of relative fraction of transient storage. The increase of flow rate may connect disconnected areas of the surface-water body so that the immobile area decreases. However, the increase in discharge should not affect the transient storage area in the hyporheic zones so that the absolute transient storage area decreases slower than the relative transient storage. I assume that when the flow rate increases significantly, the relative fraction of transient storage becomes so small that the effect of transient storage on solute transport may be neglected.

5.4.2 Attenuation of Representative Pharmaceuticals

Fluorescein tracer is reported to be photodegradable (Guillet *et al.*, 2018; Gutowski *et al.*, 2015). The time-series of solar radiation is accounted for in the model to capture the diurnal pattern of photo-degradation. Fig. 5.2 shows the measured and modelled BTCs of the

Table 5.2: Transient storage for night tracer tests in 2015 and 2016 with different flow conditions.

Year	Flow rate (Q, $m^3 s^{-1}$)	Relative transient storage fraction [-]	Absolute transient storage area [m^2]
2015	0.16	0.169	0.22
2016	0.25	0.127	0.18

day tracer experiment in August 7, 2015 in the Steinlach River. The measured data are fitted very well by the model considering solar radiation dependent photo-degradation. The main features of the BTCs (shape and tailings) are all reproduced. The NSE value is 0.991 for the model with the MAP parameter set, which indicates an excellent match between measured and modelled tracer concentrations. Compared with the night tracer experiment (Fig. 5.1a), it can be seen that photo-degradation is relevant in fluorescein transport at daytime. The fitted photo-degradation rate constant is slightly larger than that estimated by Guillet *et al.* (2018), who considered photo-degradation to affect fluorescein regardless of transient-storage effects, whereas in my model photo-degradation takes place only in the mobile water and not in the transient storage zones. The fitted photo-degradation rate coefficient of fluorescein provides a reference to estimate photo-degradation of other photo-sensitive compounds such as some pharmaceuticals.
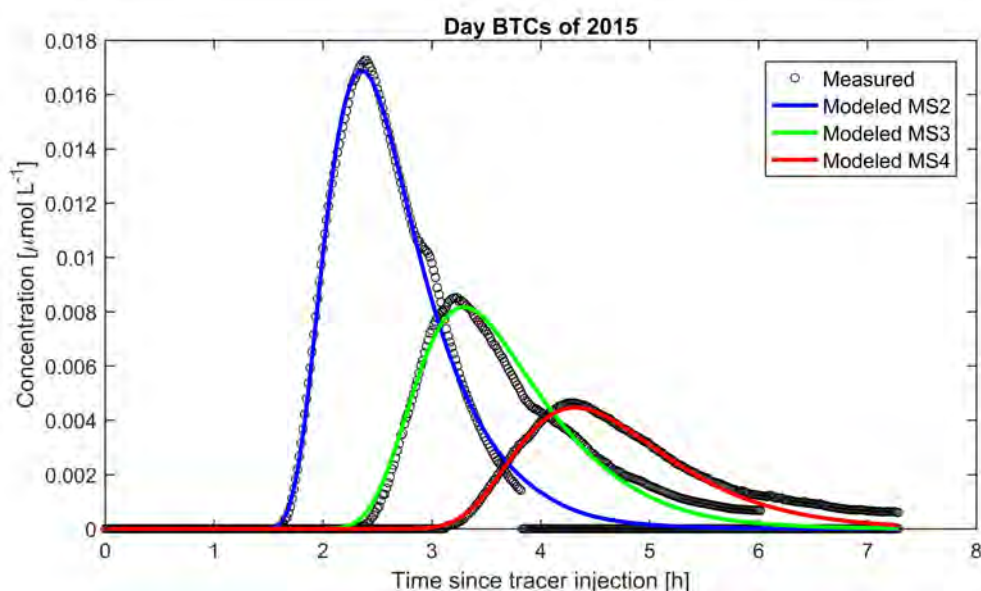
Figure 5.2: BTC fitting for the day tracer campaign in August 7, 2015.

Based on the hydraulic parameters calibrated by night and day tracer campaigns, first-order photo- and bio-degradation rate constants are achieved for the four representative pharmaceuticals (Carbamazepine, Metoprolol, Sulfamethoxazole, and Venlafaxine) by fitting measured concentrations. Fig. 5.3 shows that the trend of pharmaceutical measurements can be well reproduced both in the night and day campaigns.

Table 5.3 shows the calibrated photo- and bio-degradation rate constants of the four selected pharmaceuticals. According to table 5.3, the four pharmaceuticals can be classified into three groups. Carbamazepine is relatively conservative with very small photo- and bio-degradation rate constants. This is consistent with in-situ experiments and other modelling studies (Guillet *et al.*, 2018; Andreozzi *et al.*, 2003; Tiehm *et al.*, 2011). Sulfamethoxazole undergoes only bio-degradation in the Steinlach River. Xu *et al.* (2011) and Radke *et al.* (2009) also reported that the elimination of sulfamethoxazole in rivers is mainly caused by bio-degradation in sediments. The photo-degradation is hardly observed (Xu *et al.*, 2011). Photo- and bio-degradation processes are found both relevant for metoprolol and venlafaxine in this study, which has also been reported by Fono *et al.* (2006) and Liu *et al.* (2009a) in other river systems. However, photo- and bio-degradation rate constants are river-specific, and are influenced by the environmental conditions. Studies in other regions show that the two processes may be negligible (Aymerich *et al.*, 2016). Guillet *et al.* (2018) used a nonparametric transfer function approach to investigate the photo-dependent and photo-independent elimination processes, but cannot separate mobile and immobile water (e.g., photo-degradation should only influence water in mobile water that receives sunlight). In this study, photo- and bio-degradation processes take place in different compartments of the river. The bio-degradation rate constant is higher than that of Guillet *et al.* (2018) since only the water in immobile zone exhibits bio-degradation and the fraction of immobile water in my study is smaller than 17%.

Figure 5.4 depicts the modelled average removal of studied pharmaceuticals by photo- and bio-degradation during a 24-hour period in the Steinlach River. The pollutant removal was calculated for the 1310 meters long reach between the first (MS1) and last (MS4) measuring stations. The travel time of water from MS1 to MS4 is 3.2-3.6 hours. The total removal of carbamazepine by photo- and bio-degradation is very limited, resulting in a small total removal, $< 2.5\%$. This is consistent with the very small degradation rate constants and reflects the relatively conservative characteristics of carbamazepine. For sulfamethoxazole, only bio-degradation contributes to the total removal since photo-
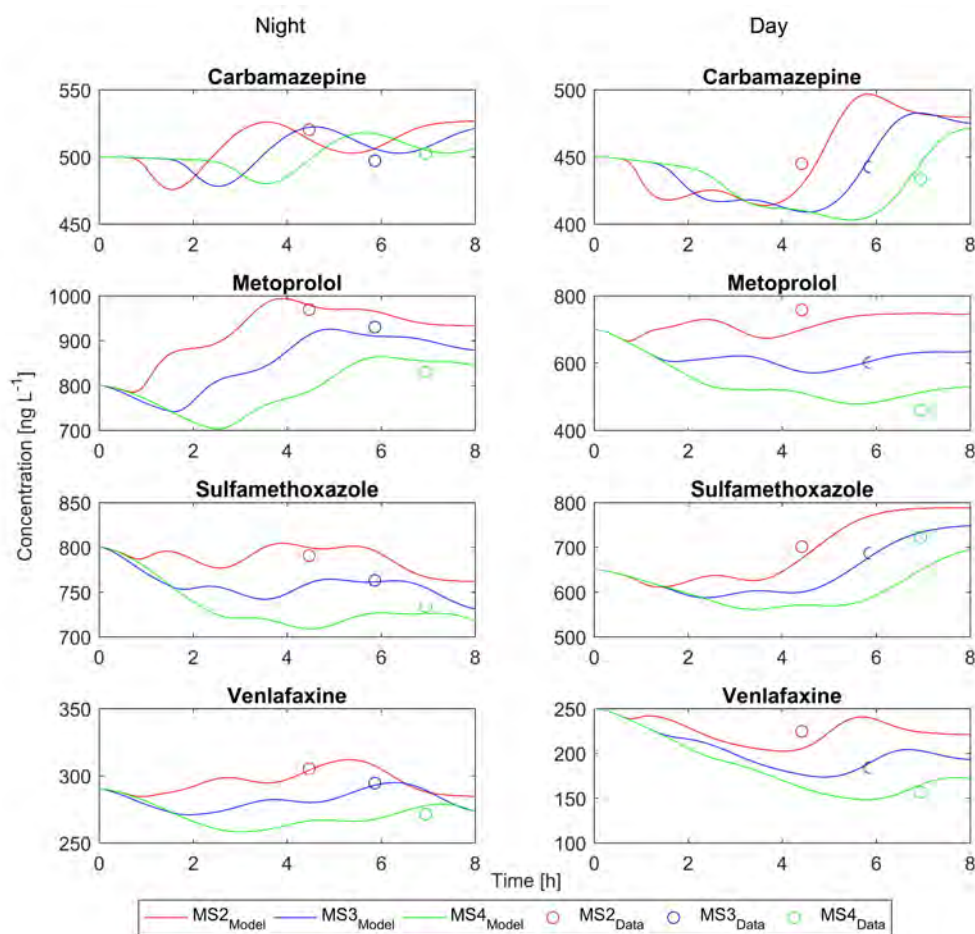
Figure 5.3: Measured and modelled pharmaceutical concentrations during night (left) and day (right) in August 7, 2015.

Table 5.3: Calibrated degradation rate constants of representative pharmaceuticals

Pharmaceuticals	photo-degradation rate constant* $[\times 10^{-5} s^{-1}]$	bio-degradation rate constant $[\times 10^{-4} s^{-1}]$
Carbamazepine	0.30	0.05
Metoprolol	2.3	1.4
Sulfamethoxazole	0	1
Venlafaxine	2.2	1.1

* shows the reference photo-degradation rate constants calculated with the global solar radiation of 500 $Jm^{-2}s^{-1}$.

degradation was found to be negligible in the Steinlach River. The total removal of

sulfamethoxazole over the reach is 13%, which is higher compared to studies for three Swedish rivers (Li *et al.*, 2016). This implies that the bio-degradation of sulfamethoxazole was enhanced in the Steinlach River. The reasons could be that i) the measurements were conducted in August when the water temperature was 20 to 25 $^\circ C$, which is the optimal temperature for microbial metabolism; ii) During the measurement campaign, WWTP effluent was estimated to account for over 70% of the total river discharge. The effluent could provide adequate substances for bacteria living in the transient storage zone; iii) the flow rate of the campaign was really low (0.16-0.18 $m^3 s^{-1}$) compared to the mean discharge of 1.84 $m^3 s^{-1}$. Thus, the effects of transient storage become important. Bio-degradation mainly occurs in hyporheic zones, the main component of transient storage areas. Meanwhile, the relative high transient storage fraction could increase the residence time of pollutants such that bio-degradation elimination may increase. For metoprolol and venlafaxine, studies have reported eliminations of metoprolol (Liu *et al.*, 2009a; Nödler *et al.*, 2014) and venlafaxine Rúa-Gómez and Püttmann (2013) in rivers by photo- and bio-degradation. In the Steinlach River, bio- and photo-degradation both contribute to the total removal of 23.2-26.5% in the reach. Their bio-degradation removal of 13.4-16.2% is similar to that of sulfamethoxazole. In addition metoprolol and venlafaxine undergo obvious removal by photo-degradation (9.9-10.3%) in the Steinlach River. Reasons for that may be: i) the water depth during the campaign was very shallow and the shading of the studied reach can be neglected. This ensures that water in the main channel can receive maximal solar radiation and the vertical attenuation of sunlight is insignificant; ii) solar radiation in August is intensive and the sunshine duration is large ca. 15 hours. In addition, during the campaign the sky was mostly clear. This provides a good external environment for photo-degradation. On the contrary, Aymerich *et al.* (2016) reported an insignificant load reduction of venlafaxine in a spanish river and Li *et al.* (2016) reported a wide range (from >5% to nearly 60%) of metoprolol depletion in four Swedish rivers. It can be seen that the degradation processes for pharmaceuticals that may be photo- and bio-degradable are substantially influenced by the local environment (e.g., temperature, solar radiation, proportion of WWTP effluents).

5.4.3 Effects of Flow Rates on Pharmaceutical Removals

Figure 5.5 shows simulated removals of four pharmaceuticals under two different flow conditions. The removals are 2.4-26.3% and 1.7-15.9% for river discharges of 0.18 and

Figure 5.4: Average removals of representative pharmaceuticals by photo- and bio-degradation from the entire studied river reach (between MS1 and MS4, 1310 m) for a 24-hour period in August 7, 2015.

0.25 $m^3 s^{-1}$, respectively. In the two scenarios, the WWTP effluent released to the river is assumed to be the same (pollutant mass flux and the effluent flow rate). However, the removal differs for the same pharmaceutical under the two investigated flow conditions. It can be seen that pharmaceutical removals decrease with the increase of discharge, but the relative decrease (the ratio of absolute removal decrease over the high removal) varies from 28% to 56% for different pharmaceuticals.

For sulfamethoxazole, the relative decrease of removal with the increase of the flow rate is the most significant. The removal at a discharge of 0.25 $m^3 s^{-1}$ is only half of that at a discharge of 0.18 $m^3 s^{-1}$. In Sect. 5.4.2, the degradation processes has been discussed. Sulfamethoxazole is biodegradable, while photo-degradation can be neglected. It can be derived that the elimination of sulfamethoxazole by bio-degradation decreases with the increase of river discharge. Because the total river discharge increases, but the WWTP effluent remains same, which results in a smaller contribution proportion of WWTP effluent to the total river discharge. There are essentially two effects explaining the decrease of the biodegradation removal with increasing discharge: (a) the immobile

water is less significant in relative terms at higher discharge, and (b) the flow velocity is higher, reducing the residence time.

For metoprolol and venlafaxine, the removal also decreases with the increase in river discharge. But the relative decrease of removal (38-40%) is smaller than in the case of sulfamethoxazole because these two compounds undergo both bio-degradation and photo-degradation. The elimination mass flux by bio-degradation decreases with the increase of river discharge. The elimination by photo-degradation also decreases because of reduction in residence time and a larger flow depth, but the reduction of the fraction of transient storage is actually beneficial. It should be noted that under both flow conditions, the flow depths are shallow, thus absorption of radiation in the water column can be neglected. By contrast, for larger river discharges, absorption of radiation by the water may no more be disregarded, not only because of a larger water depth but also because of increased turbidity. Conversely, high discharge typically occurs at times with high cloud coverage so that the solar radiation is small anyway.

The removal of carbamazepine is smaller than 2.5% in both scenarios. While a small decrease of carbamazepine removal is simulated with the increase of flow rates due to the reasons discussed above, the effect is practically negligible .

Overall I observed a decrease of pollutant removal with increasing river discharge. Kunkel and Radke (2012) reported a similar result that pharmaceutical elimination is higher in a sunny, dry weather period compared to a period with elevated discharge after a heavy rainfall. For pharmaceuticals mainly relying on bio-degradation, the flow rate has the biggest influence on the removal change. For pharmaceuticals with bio- and photo-degradation, the removal change is smaller compared to only biodegradable pollutants. For persistent pharmaceuticals, the absolute removal remains very small. These statements hold for shallow river systems. In deep rivers, transient-storage effects are typically negligible, solar radiation does not reach the ground, and solute turnover is dominated by processes in the water column rather than on the river bed.

5.5 Summary and Conclusion

Emerging micropollutants such as pharmaceuticals have increasingly been detected in streams and rivers. The transport and fate of these compounds pose new water quality issues to river management. In this chapter, I applied a one-dimensional solute reactive
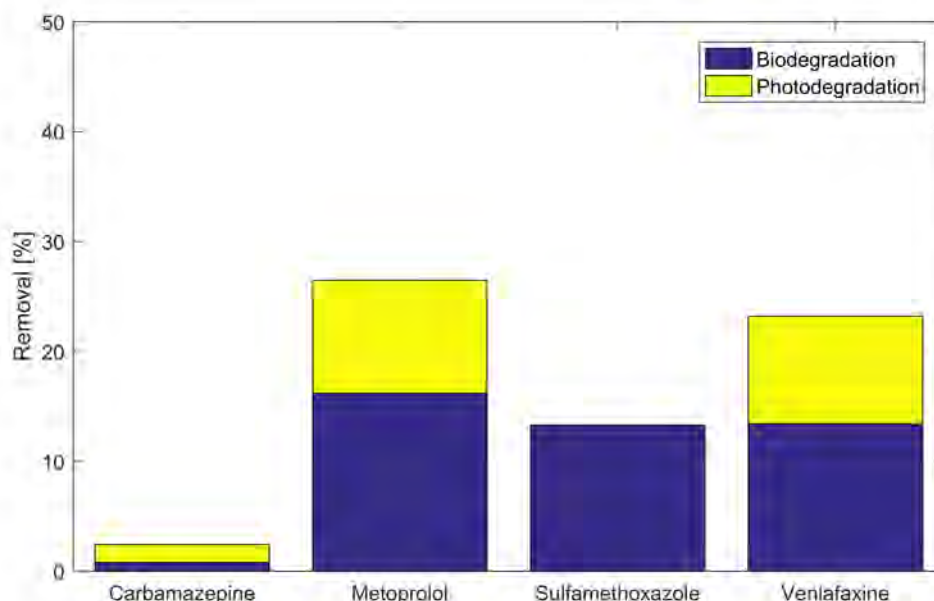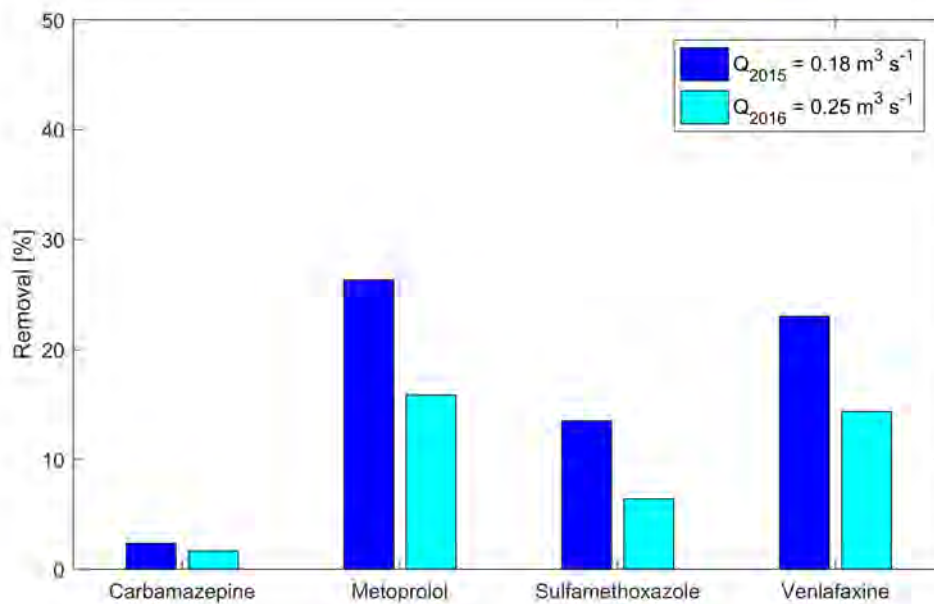
Figure 5.5: Comparisons of 24-hour average removals of representative pharmaceuticals from the entire studied river reach (between MS1 and MS4, 1310 m) under two different flow conditions.

transport model coupled with transient storage to the WWTP effluent-affected river, the Steinlach River in southwest Germany. The model helps to simulate four representative pharmaceuticals to investigate effects of different processes (e.g., transient storage, photo-degradation and bio-degradation) and flow rates on the pollutant removal.

Transient storage plays a significant role for flow and solute transport in rivers, especially under low-flow conditions. The increase in transient storage ratio increases the travel time and thus affects solute transport. The flow rate influences the transient storage. It is supposed that when the river discharge is large, the transient storage may be negligible. In the WWTP effluent-affected Steinlach River, carbamazepine is relatively conservative. Sulfamethoxazole is only biodegradable and the removal is around 13%. Metoprolol and venlafaxine undergo both photo- and bio-degradation leading to a total removal of 23-26%. The degradation processes are substantially affected by the local conditions. The pollutant removal decreases with the increase of flow rates. The influence is especially significant for pollutants that undergo only bio-degradation.

The study demonstrates that transient storage varies with flow rates and degradation

processes are significantly affected by local environment, which is important for estimating pharmaceutical removals. The model presented in this chapter provides a good tool to understand the fate of emerging contaminants and to evaluate their environmental impacts on the river system.

Chapter 6

Overall Conclusions and Outlook

This thesis has focused on understanding the catchment-scale transport of sediment, the long-term fate of micropollutants (PAH) undergoing particle-facilitated transport, and the transport and transformation of dissolved micropollutants (pharmaceuticals) in river systems. To address these research questions, I have developed an integrated sediment transport model, a particle-facilitated pollutant transport model, and a solute reactive transport model to reproduce the main environmental processes and applied these models to two tributaries to River Neckar, the Ammer River and the Steinlach River.

6.1 Conclusions

Through this PhD study, I came to major conclusions regarding the following aspects:

- **Catchment-scale sediment transport and dynamics:**

  Surface runoff characteristics affect particle contributions from different sources. In the dominantly groundwater-fed Ammer catchment, the weak rural surface runoff results in a small faction of rural particles to the annual suspended-sediment load, and thus urban particles dominate the annual load. The flow rate governs the relative contributions of different processes to the particle production. In-stream processes, i.e. bed erosion and bank erosion, are significant for sediment transport under high-flow conditions ($Q > 10\,m^3s^{-1}$). The channel slope significantly influences sediment deposition and erosion such that net sediment trapping can occur in very mild reaches, which was modelled in the Ammer River during the simulation period with events of a 2-year to 10-year return period. The river hydraulic

model is necessary to differentiate sediment sources and sinks of in-stream processes. The integrated sediment transport model provides the basis for studying the particle-facilitated transport.

- **Fate of PAH (sediment-bound micropollutants):**

Sediment supply and composition substantially influence PAH supply in a river system. Sediment-bound PAH are the dominant source of the annual PAH load. The high proportion of urban particles with high PAH content in the Ammer River determines the high urban PAH supply. PAH turnover is significantly affected by the river geometry. In steep reaches, turnover of sediments and PAH is fast, here sediment turnover governs the turnover of sediment-bound PAH. In mild reaches, by contrast, sediment turnover is slow such that diffusion of PAH from the sediment to the flowing water significantly influences PAH turnover. This results in a distinct difference of turnover between sediments and attached PAH in mild-slope reaches. The flow rate controls the in-stream redistribution of PAH by influencing PAH deposition and remobilization. PAH legacy could occur in river segments with slow sediment turnover. In these places, the highly contaminated particles can be trapped during high emission periods, then act as a secondary source after reduction of the pollutant input due to the implementation of environmental regulations. In the Ammer River, the PAH legacy may have remained 10-20 years after the environmental regulation in 1970s. A particle-facilitated transport model is essential to study the long-term fate of PAH in river systems.

- **Fate of pharmaceuticals (dissolved micropollutants):**

Under low-flow conditions, the transient storage plays a significant role in the transport and attenuation of dissolved micropollutants, such as pharmaceuticles, in river systems. The flow rate influences the importance of transient storage for the solute transport. The transient storage decreases with increasing flow rate and may become negligible when river discharge is large enough. The transient storage affects pollutant attenuation and removal. In River Steinlach, carbamazepine can be seen as relatively conservative, sulfamethoxazole is biodegradable but not photodegradable, whereas metoprolol and venlafaxine undergo both photo- and bio-degradation. The degradation processes are river-specific. The pollutant removal decreases with the increase of flow rates. The combination of tracer ex-

periments and a contaminant sampling scheme with a time-series at the upstream end and individual time points at downstream measurement stations helps with the model calibration and thus the better understanding of attenuation mechanisms of the investigated pharmaceuticals.

6.2 Outlook and Future Studies

The developed models have been applied to study the fate of micropollutants in sediment-bound (PAH) and dissolved form (pharmaceuticals) in two investigated rivers. This thesis focuses not only on identifying the main source of pollutants of interest, but also on investigating the main processes that control the transport and transformation of micropollutants. The fate of sediments, PAH, and pharmaceuticals have been discussed. Future studies may cover the following two aspects:

- **Model application**

  The particle-facilitated pollutant transport model provides a tool for studying hydrophobic compounds in rivers. Like the priority PAH, polychlorinated biphenyls (PCB) are also hydrophobic but persistant organic pollutants. PCB have been banned since the 1970s but are still widely occuring in rivers, particularly in River Ammer. The models developed in this thesis can help to study the fate of PCB in river systems.

  Methods have been developed to measure water and pollutant fluxes between river water and groundwater to show the interaction between the two compartments. The solute transport model with transient storage developed in this thesis can be further modified to include the interaction between river water and groundwater. Then it can help to understand the effects of the interacting process on in-stream pollutant transport.

  This thesis provides the temporal and spatial distribution of pollutant concentrations in rivers. It is useful and meaningful for the assessment of their environmental impacts, such as total toxicity on the aquatic environment.

- **Model improvement**

  In the Ammer catchment, the sediment transport model was calibrated and validated to the combined sediment contributions from sub-catchments of one gauge at

the outlet of the catchment. Currently, due to the lack of data for sub-catchments, it is difficult to verify sediment dynamics from different sub-catchments. To improve the model verification, installing few more gauging stations would be helpful to collect data from sub-catchments such that the assumptions on the main processes and behavior of sediment transport can be tested.

In chapter 4, I studied the annual PAH load from different processes and the long-term fate of sediment-bound PAH. In the model, the seasonality of PAH concentration on particles is not considered, whereas the average PAH concentration is simulated. If this seasonality does exist and is relevant, the PAH input module of the model can be improved.

To apply the sediment and pollutant transport models developed in this thesis to other study rivers, the additional processes that are necessary for local behaviors can be integrated as well. A good communication between modellers and field experimentalists can also help with the representation of the study system and the model verification.

Appendices

Appendix A

Table A1: Sensitivity analysis of the sediment transport model.

Parameter	Adjustment factor [-]	Rural contribution [%]	NSE for entire SS		NSE for SS $\geq 30mgL^{-1}$	
			Cali	Vali	Cali	Vali
M_{max}	-90%	7.0	0.21	0.09	-0.23	-0.39
	-70%	5.7	0.31	0.20	-0.05	-0.22
	-50%	4.9	0.38	0.27	0.10	-0.08
	-30%	4.2	0.43	0.32	0.22	0.03
	-10%	3.7	0.45	0.33	0.31	0.11
	+30%	3.0	0.43	0.25	0.42	0.17
	+50%	2.8	0.38	0.17	0.43	0.15
	+100%	2.3	0.14	-0.16	0.33	-0.01
	+200%	1.7	-0.79	-1.36	-0.37	-0.90
	+300%	1.3	-2.32	-3.29	-1.75	-2.50
K_w	-90%	6.9	0.22	0.10	-0.21	-0.38
	-70%	5.6	0.32	0.22	-0.02	-0.19
	-50%	4.8	0.40	0.29	0.13	-0.04
	-30%	4.2	0.44	0.44	0.24	0.06
	-10%	3.7	0.46	0.33	0.32	0.12
	+30%	3.1	0.43	0.25	0.41	0.14
	+50%	2.8	0.39	0.17	0.42	0.11
	+100%	2.4	0.23	-0.11	0.39	-0.05
	+200%	1.9	-0.26	-0.93	0.12	-0.63
	+300%	1.7	-0.86	-1.74	-0.23	-0.96

Parameter	Adjustment factor [-]	Rural contribution [%]	NSE for entire SS		NSE for SS $\geq 30mgL^{-1}$	
			Cali	Vali	Cali	Vali
C_h	-90%	0.4	0.50	0.32	0.34	0.13
	-70%	1.1	0.49	0.32	0.34	0.13
	-50%	1.1	0.49	0.32	0.34	0.13
	-30%	1.8	0.48	0.32	0.35	0.13
	-10%	2.5	0.47	0.32	0.35	0.14
	+30%	3.2	0.43	0.32	0.35	0.14
	+50%	4.5	0.40	0.32	0.35	0.14
	+100%	5.2	0.33	0.31	0.36	0.14
	+200%	6.7	0.10	0.30	0.36	0.14
	+300%	9.6	-0.20	0.29	0.36	0.14
τ_c	-90%	9.7	0.29	0.30	0.36	0.15
	-70%	7.8	0.35	0.31	0.36	0.15
	-50%	6.3	0.40	0.32	0.35	0.14
	-30%	5.0	0.43	0.32	0.35	0.14
	-10%	4.0	0.45	0.32	0.35	0.14
	+30%	2.5	0.47	0.32	0.35	0.13
	+50%	1.9	0.48	0.32	0.35	0.13
	+100%	1.1	0.49	0.32	0.34	0.13
	+200%	0.3	0.50	0.32	0.34	0.13
	+300%	0.1	0.50	0.32	0.34	0.13
Base Case	0%	3.5	0.46	0.32	0.35	0.14

Sediment source diagnosis based on the end-member-mixing analysis of sediment-bound PAH.

$$f_u + f_r + f_{bf} + f_{bd} + f_{bk} = 1 \qquad (A1)$$

$$c_u f_u + c_r f_r + c_{bf} f_{bf} + c_{bd} f_{bd} + c_{bk} f_{bk} = c_{p,ss} \qquad (A2)$$

Because $c_u = c_{bd}$, $c_r = c_{bf}$, and assuming f_{bk}=0.06 from the model simulation, then

$$c_u(f_u + f_{bd}) + c_r(f_r + f_{bf}) = 5.8 \qquad (A3)$$

Table A2: The PAH concentrations (the sum of 15 PAH) on different particles in the Ammer catchment.

Symbol	Description	Value $[mgkg^{-1}]$	Remarks
c_u	PAH concentration on urban particles	8.1	(Gocht *et al.*, 2005)
c_r	PAH concentration on rural particles	1	based on measurements
c_{bf}	PAH concentration on baseflow particles	1	assuming the same as rural particles
c_{bd}	PAH concentration on river bed particles	8.1	assuming the same as urban particles
c_{bk}	PAH concentration on river bank particles	0	regarded as clean particles
$c_{p,ss}$	Average PAH concentration on suspended particles at the gauge	5.5	(Schwientek *et al.*, 2013a)

$$f_u + f_{bd} = 0.68 \tag{A4}$$

$$f_r + f_{bf} = 0.26 \tag{A5}$$

$$f_{bf} = \frac{\sum_{Q_i \leq 1} Q_i c_{ss,i}}{\sum Q_i c_{ss,i}} = 0.23 \tag{A6}$$

$$f_r = 0.03 \tag{A7}$$

in which, f_u, f_r, f_{bf}, f_{bd}, and f_{bk} are the annual contribution fractions of urban, rural, baseflow, bed erosion, and bank erosion particles, respectively. Q_i and $c_{ss,i}$ are the i-th measured discharge and suspended sediment concentration.
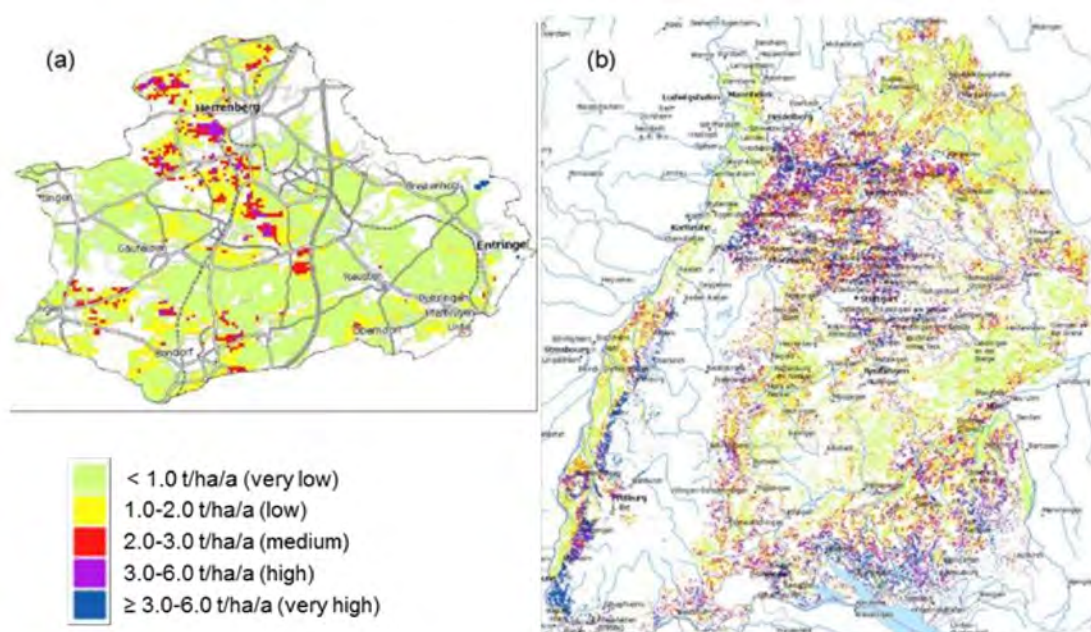
Figure A1: Soil erosion maps of the Ammer catchment (a) and the state of Baden-Württemberg (b). The white color in the maps represents forest. The original information can be found in http://maps.lgrb-bw.de/.

Table A3: The composition and octanol-water partition coefficient (K_{ow}) of investigated PAH

Rings	Fraction	K_{ow} $[Lkg^{-1}]$
3	15%	$10^3 - 10^5$
4	47%	$10^5 - 10^6$
≥ 5	38%	$10^6 - 10^7$

Appendix B

Calculation of the combined sediment-water partition coefficient (K_s) of investigated PAH

$$K_{ow}^{com} = \sum f_i K_{ow}^i \tag{A8}$$
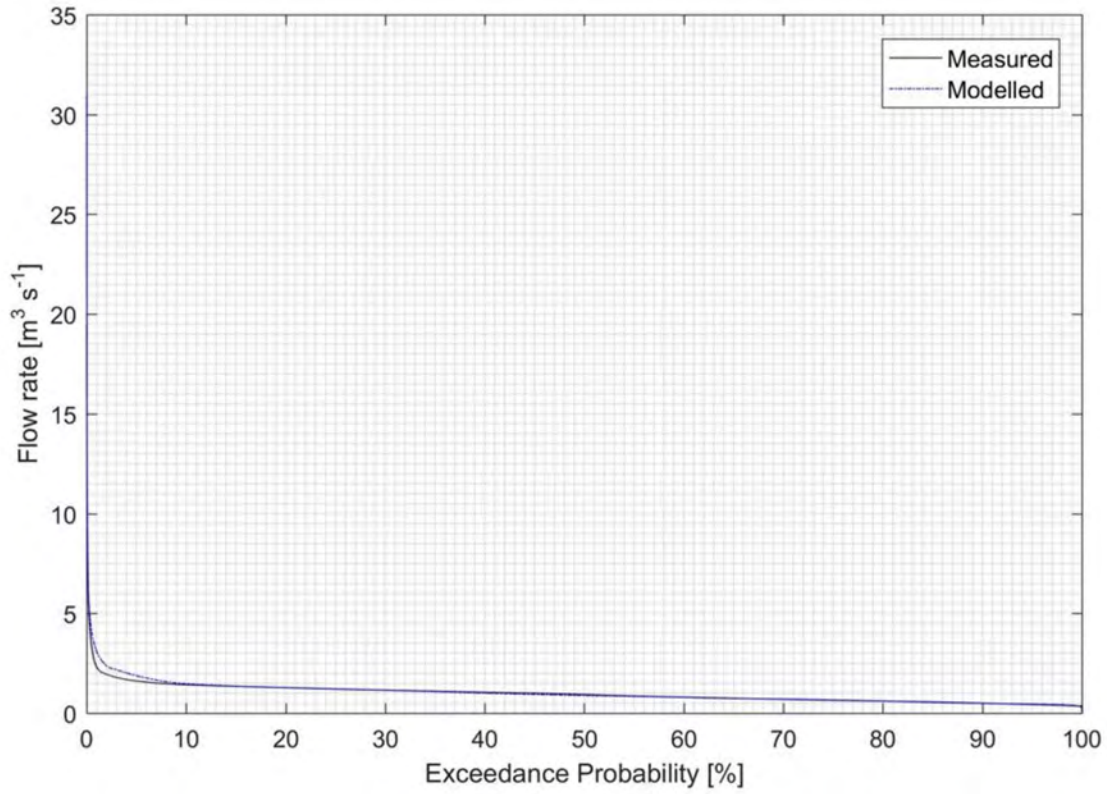
Figure A2: Flow duration curves of measured and modelled discharge of the Ammer River for year 2014-2016.

$$K_{oc} = 0.62 \times K_{ow}^{com} \tag{A9}$$

$$K_s = f_{oc}K_{oc} \tag{A10}$$

Providing Table A3 and Equations A8-A9, then:

$$K_{ow}^{com} = 4.3 \times 10^5 - 4.3 \times 10^6 \tag{A11}$$

$$K_{oc} = 2.7 \times 10^5 - 2.7 \times 10^6 \tag{A12}$$

$$K_s = 1.1 \times 10^4 - 1.1 \times 10^5 \tag{A13}$$

in which, K_{ow}^{com} $[Lkg^{-1}]$ is the combined octanol-water partition coefficient of the investigated PAH; K_{ow}^{i} $[Lkg^{-1}]$ and f_i $[-]$ represent the octanol-water partition coefficient and the fraction of the i-component PAH, respectively; K_{oc} $[Lkg^{-1}]$ denotes the organic carbon based partition coefficient, the equation of which is from Karickhoff *et al.* (1979); f_{oc} is the organic carbon content of the particles, 4% in our study.
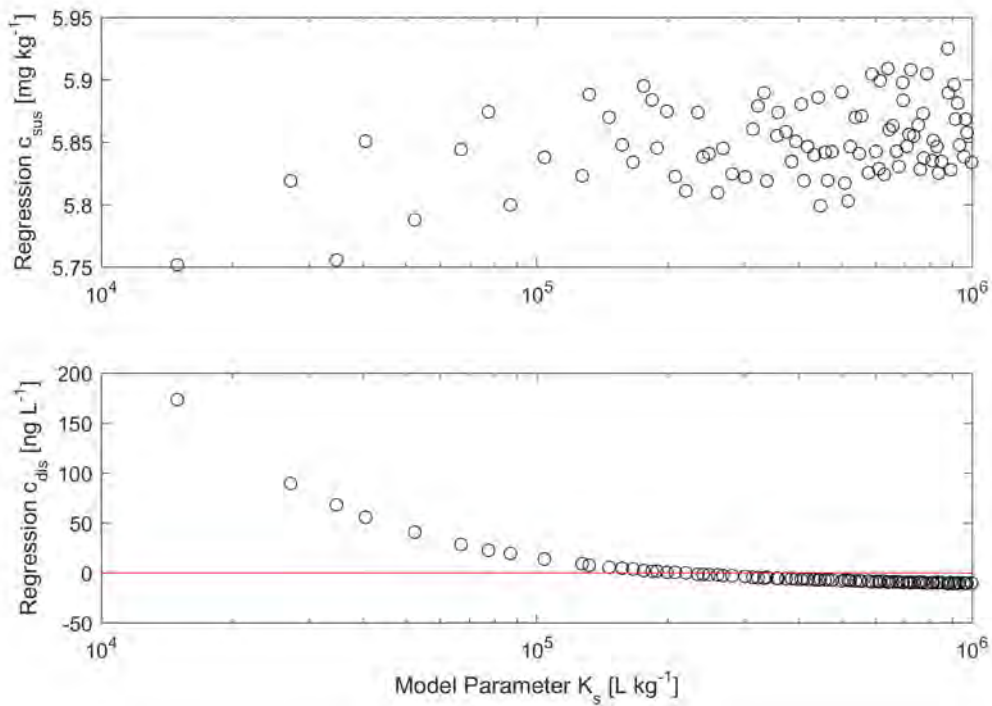
Figure A3: The influence of the model parameter K_s on the regression coefficient c_{sus}, suspended sediment-bound PAH concentrations, and c_{dis}, dissolved PAH concentrations.
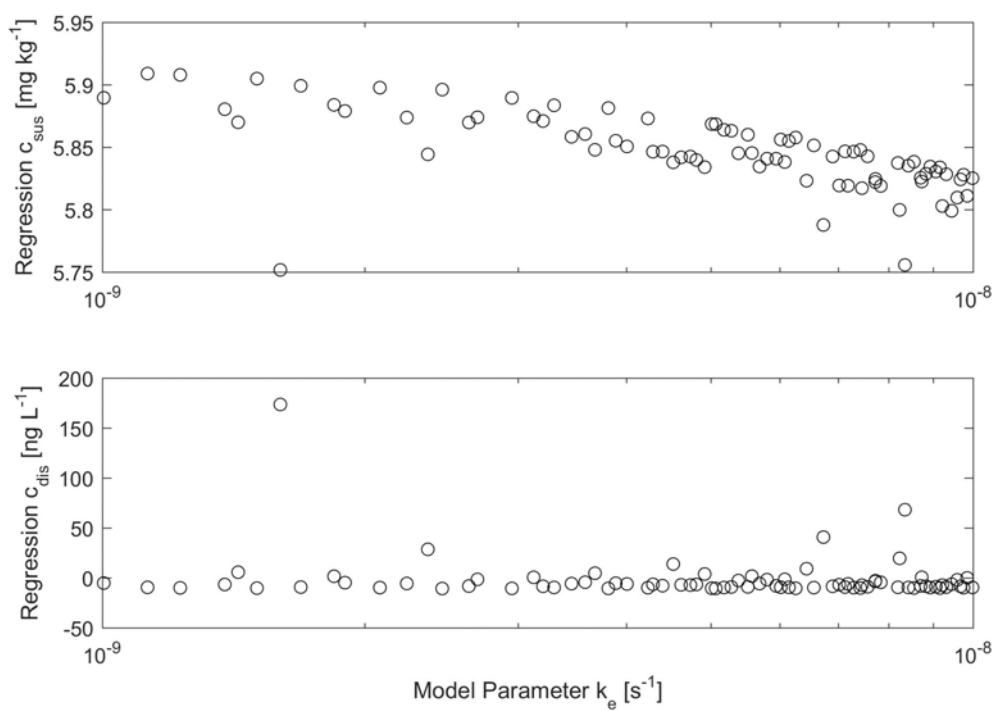
Figure A4: The influence of the model parameter k_e on the regression coefficient c_{sus}, suspended sediment-bound PAH concentrations, and c_{dis}, dissolved PAH concentrations.
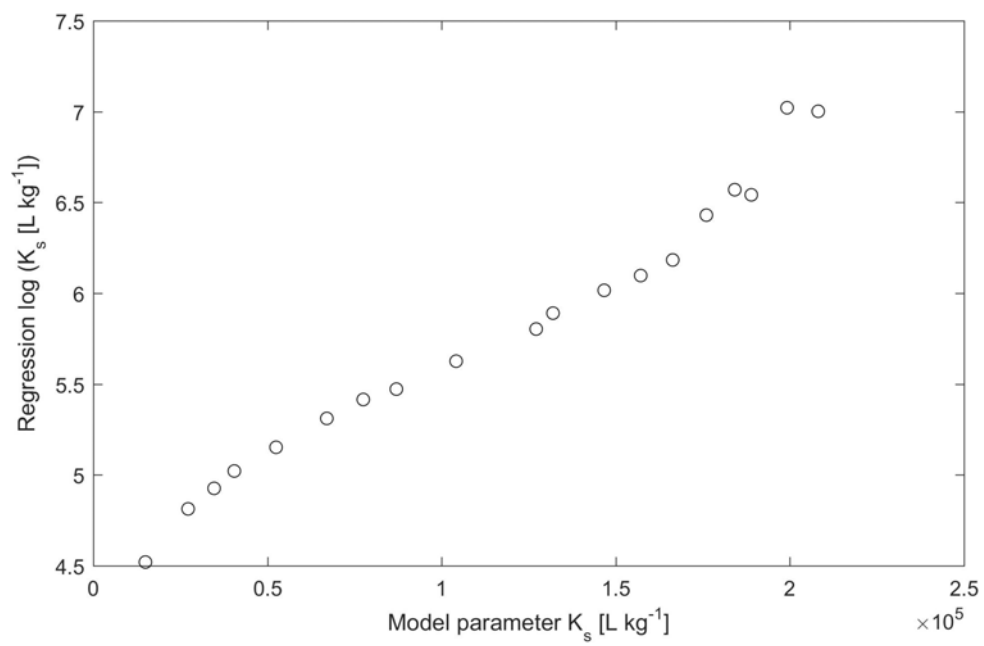
Figure A5: The influence of the model parameter K_s on the regression coefficient $log(K_s[Lkg^{-1}])$.

Bibliography

Acuña, V., von Schiller, D., García-Galán, M. J., Rodríguez-Mozaz, S., Corominas, L., Petrovic, M., Poch, M., Barceló, D., and Sabater, S. (2015). Occurrence and in-stream attenuation of wastewater-derived pharmaceuticals in iberian rivers. *Science of the Total Environment*, **503**, 133–141.

Agunbiade, F. O. and Moodley, B. (2014). Pharmaceuticals as emerging organic contaminants in umgeni river water system, kwazulu-natal, south africa. *Environmental monitoring and assessment*, **186**(11), 7273–7291.

Aisopou, A., Binning, P. J., Albrechtsen, H.-J., and Bjerg, P. L. (2015). Modeling the factors impacting pesticide concentrations in groundwater wells. *Groundwater*, **53**(5), 722–736.

Al-Yaseri, I., Morgan, S., and Retzlaff, W. (2012). Using turbidity to determine total suspended solids in storm-water runoff from green roofs. *Journal of Environmental Engineering*, **139**(6), 822–828.

Alder, A., McArdell, C., Golet, E., Kohler, H.-P., Molnar, E., Thi, N. A. P., Siegrist, H., Suter, M.-F., and Giger, W. (2004). Environmental exposure of antibiotics in wastewaters, sewage sludges and surface waters in switzerland. In *Pharmaceuticals in the Environment*, pages 55–66. Springer.

Álvarez-Romero, J. G., Wilkinson, S. N., Pressey, R. L., Ban, N. C., Kool, J., and Brodie, J. (2014). Modeling catchment nutrients and sediment loads to inform regional management of water quality in coastal-marine ecosystems: A comparison of two approaches. *Journal of environmental management*, **146**, 164–178.

Amalfitano, S., Corno, G., Eckert, E., Fazi, S., Ninio, S., Callieri, C., Grossart, H.-P., and Eckert, W. (2017). Tracing particulate matter and associated microorganisms in freshwaters. *Hydrobiologia*, **800**(1), 145–154.

Amvrosiadi, N., Seibert, J., Grabs, T., and Bishop, K. (2017). Water storage dynamics in a till hillslope: the foundation for modeling flows and turnover times. *Hydrological Processes*, **31**(1), 4–14.

Andreozzi, R., Raffaele, M., and Nicklas, P. (2003). Pharmaceuticals in stp effluents and their solar photodegradation in aquatic environment. *Chemosphere*, **50**(10), 1319–1330.

Arias-Estévez, M., López-Periago, E., Martínez-Carballo, E., Simal-Gándara, J., Mejuto, J.-C., and García-Río, L. (2008). The mobility and degradation of pesticides in soils and the pollution of groundwater resources. *Agriculture, Ecosystems & Environment*, **123**(4), 247–260.

Aristi, I., Casellas, M., Elosegi, A., Insa, S., Petrovic, M., Sabater, S., and Acuña, V. (2016). Nutrients versus emerging contaminants–or a dynamic match between subsidy and stress effects on stream biofilms. *Environmental pollution*, **212**, 208–215.

Aymerich, I., Acuña, V., Barceló, D., García, M., Petrovic, M., Poch, M., Rodriguez-Mozaz, S., Rodríguez-Roda, I., Sabater, S., von Schiller, D., *et al.* (2016). Attenuation of pharmaceuticals and their transformation products in a wastewater treatment plant and its receiving river ecosystem. *Water research*, **100**, 126–136.

Aziz, F., Syed, J. H., Malik, R. N., Katsoyiannis, A., Mahmood, A., Li, J., Zhang, G., and Jones, K. C. (2014). Occurrence of polycyclic aromatic hydrocarbons in the soan river, pakistan: insights into distribution, composition, sources and ecological risk assessment. *Ecotoxicol Environ Saf*, **109**, 77–84.

Bao, Z., Haberer, C., Maier, U., Beckingham, B., Amos, R. T., and Grathwohl, P. (2015). Modeling long-term uptake and re-volatilization of semi-volatile organic compounds (svocs) across the soil-atmosphere interface. *Sci Total Environ*, **538**, 789–801.

Barber, L. B., Keefe, S. H., Brown, G. K., Furlong, E. T., Gray, J. L., Kolpin, D. W., Meyer, M. T., Sandstrom, M. W., and Zaugg, S. D. (2013). Persistence and potential effects of complex organic contaminant mixtures in wastewater-impacted streams. *Environmental science & technology*, **47**(5), 2177–2188.

Barbosa, M. O., Moreira, N. F., Ribeiro, A. R., Pereira, M. F., and Silva, A. M. (2016). Occurrence and removal of organic micropollutants: an overview of the watch list of eu decision 2015/495. *Water research*, **94**, 257–279.

Bari, M. A., Kindzierski, W. B., and Cho, S. (2014). A wintertime investigation of atmospheric deposition of metals and polycyclic aromatic hydrocarbons in the athabasca oil sands region, canada. *Sci Total Environ*, **485-486**, 180–192.

Benotti, M. J., Trenholm, R. A., Vanderford, B. J., Holady, J. C., Stanford, B. D., and Snyder, S. A. (2008). Pharmaceuticals and endocrine disrupting compounds in us drinking water. *Environmental science & technology*, **43**(3), 597–603.

Bermúdez-Couso, A., Fernández-Calviño, D., Álvarez-Enjo, M. A., Simal-Gándara, J., Nóvoa-Muñoz, J. C., and Arias-Estévez, M. (2013). Pollution of surface waters by metalaxyl and nitrate from non-point sources. *Science of the Total Environment*, **461**, 282–289.

Beven, K. (2001). How far can we go in distributed hydrological modelling? *Hydrology and Earth System Sciences Discussions*, **5**(1), 1–12.

Bicknell, B. R., Imhoff, J. C., John L. Kittle, J., Jobes, T. H., and Anthony S. Donigian, J. (2001). Hydrological simulation program - fortran, version 12. Report, AQUA TERRA Consultants.

Bilotta, G. S. and Brazier, R. E. (2008). Understanding the influence of suspended solids on water quality and aquatic biota. *Water Res*, **42**(12), 2849–61.

Bishop, K., Seibert, J., Nyberg, L., and Rodhe, A. (2011). Water storage in a till catchment. ii: Implications of transmissivity feedback for flow paths and turnover times. *Hydrological Processes*, **25**(25), 3950–3959.

BKG (2009). Spatial data access act of 10 february 2009, federal law gazette [bgbl.] part i, p. 278. Technical report, Bundesamt für Kartographie und Geodäsie (BKG).

Bojes, H. K. and Pope, P. G. (2007). Characterization of epa's 16 priority pollutant polycyclic aromatic hydrocarbons (pahs) in tank bottom solids and associated contaminated soils at oil exploration and production sites in texas. *Regul Toxicol Pharmacol*, **47**(3), 288–95.

Bones, E. J. (2014). *Predicting critical shear stress and soil erodibility classes using soil properties*. Ph.D. thesis, Georgia Institute of Technology.

Bouchaoua, L., Manginb, A., and Chauve, P. (2002). Turbidity mechanism of water from a karstic spring: example of the ain asserdoune spring (beni mellal atlas, morocco). *Journal of Hydrology*, **265**, 34–42.

Bouteligier, R., Vaes, G., and Berlamont, J. (2002). Sensitivity of urban drainage wash-off models: compatibility analysis of hydroworks qm and mousetrapusing cdf relationships. *Journal of Hydroinformatics*, **4**(4), 235–243.

Boxall, A. B., Rudd, M. A., Brooks, B. W., Caldwell, D. J., Choi, K., Hickmann, S., Innes, E., Ostapyk, K., Staveley, J. P., Verslycke, T., *et al.* (2012). Pharmaceuticals and personal care products in the environment: what are the big questions? *Environmental health perspectives*, **120**(9), 1221.

Briggs, M. A., Gooseff, M. N., Arp, C. D., and Baker, M. A. (2009). A method for estimating surface transient storage parameters for streams with concurrent hyporheic storage. *Water Resources Research*, **45**(4).

Brirhet, H. and Benaabidate, L. (2016). Comparison of two hydrological models (lumped and distributed) over a pilot area of the issen watershed in the souss basin, morocco. *European Scientific Journal, ESJ*, **12**(18).

Brunner, G. W. (2016). Hec-ras, river analysis system hydraulic reference manual version 5.0. Report, Institute for Water Resources Hydrologic Engineering Center.

Burke, V., Greskowiak, J., Asmuß, T., Bremermann, R., Taute, T., and Massmann, G. (2014). Temperature dependent redox zonation and attenuation of wastewater-derived organic micropollutants in the hyporheic zone. *Science of the Total Environment*, **482**, 53–61.

Burns, E. E., Carter, L. J., Kolpin, D. W., Thomas-Oates, J., and Boxall, A. B. (2018). Temporal and spatial variation in pharmaceutical concentrations in an urban river system. *Water research*, **137**, 72–85.

Butler, M. P., Reed, P. M., Fisher-Vanden, K., Keller, K., and Wagener, T. (2014). Identifying parametric controls and dependencies in integrated assessment models using global sensitivity analysis. *Environmental modelling & software*, **59**, 10–29.

BwAm (2006). Weather data at weather station bondorf. Technical report, Agrarmeteorologie Baden-Württenmberg (BwAm).

Caille, F., Riera, J. L., and Rosell-Melé, A. (2011). Modelling nitrogen and phosphorus loads in a mediterranean river catchment (la tordera, ne spain). *Hydrology and Earth System Sciences Discussions, 2011, vol. 16, num. 8, p. 2417-2435.*

Campolongo, F. and Saltelli, A. (1997). Sensitivity analysis of an environmental model: an application of different analysis methods. *Reliability Engineering & System Safety*, **57**(1), 49–69.

Carpenter, T. M. and Georgakakos, K. P. (2006). Intercomparison of lumped versus distributed hydrologic model ensemble simulations on operational forecast scales. *Journal of hydrology*, **329**(1-2), 174–185.

Castaings, W., Dartus, D., Le Dimet, F.-X., and Saulnier, G.-M. (2009). Sensitivity analysis and parameter estimation for distributed hydrological modeling: potential of variational methods. *Hydrology and Earth System Sciences*, **13**(4), 503–517.

CDC (2017). Historical hourly station observations of precipitation for germany, version v005. Technical report, DWD Climate Data Center (CDC).

Chao, Y., Farrara, J. D., Zhang, H., Zhang, Y. J., Ateljevich, E., Chai, F., Davis, C. O., Dugdale, R., and Wilkerson, F. (2017). Development, implementation, and validation of a modeling system for the san francisco bay and estuary. *Estuarine, Coastal and Shelf Science*, **194**, 40–56.

Chen, H., Luo, Y., Potter, C., Moran, P. J., Grieneisen, M. L., and Zhang, M. (2017). Modeling pesticide diuron loading from the san joaquin watershed into the sacramento-san joaquin delta using swat. *Water research*, **121**, 374–385.

Chiffre, A., Degiorgi, F., Morin-Crini, N., Bolard, A., Chanez, E., and Badot, P.-M. (2015). Pah occurrence in chalk river systems from the jura region (france). pertinence of suspended particulate matter and sediment as matrices for river quality monitoring. *Environmental Science and Pollution Research*, **22**(22), 17486–17498.

Christensen, E. R. and Bzdusek, P. A. (2005). Pahs in sediments of the black river and the ashtabula river, ohio: source apportionment by factor analysis. *Water Res*, **39**(4), 511–24.

Clara, M., Kreuzinger, N., Strenn, B., Gans, O., and Kroiss, H. (2005). The solids retention time—a suitable design parameter to evaluate the capacity of wastewater treatment plants to remove micropollutants. *Water research*, **39**(1), 97–106.

Clark, L. A. and Wynn, T. M. (2007). Methods for determining streambank critical shear stress and soil erodibility: Implications for erosion rate predictions. *Transactions of the ASABE*, **50**, 95–106.

Cole, M., Lindeque, P., Fileman, E., Halsband, C., and Galloway, T. S. (2015). The impact of polystyrene microplastics on feeding, function and fecundity in the marine copepod calanus helgolandicus. *Environmental science & technology*, **49**(2), 1130–1137.

Colombo, J. C., Cappelletti, N., Lasci, J., Migoya, M. C., Speranza, E., and Skorupka, C. N. (2006). Sources, vertical fluxes, and equivalent toxicity of aromatic hydrocarbons in coastal sediments of the río de la plata estuary, argentina. *Environ Sci Technol*, **40**(3), 734–740.

Cranswick, R. H., Cook, P. G., and Lamontagne, S. (2014). Hyporheic zone exchange fluxes and residence times inferred from riverbed temperature and radon data. *Journal of hydrology*, **519**, 1870–1881.

Cui, S., Fu, Q., Guo, L., Li, Y.-F., Li, T.-x., Ma, W.-l., Wang, M., and Li, W.-l. (2016). Spatial–temporal variation, possible source and ecological risk of pcbs in sediments from songhua river, china: Effects of pcb elimination policy and reverse management framework. *Marine pollution bulletin*, **106**(1-2), 109–118.

De Lavenne, A., Thirel, G., Andréassian, V., Perrin, C., and Ramos, M.-H. (2016). Spatial variability of the parameters of a semi-distributed hydrological model. In *7th International Water Resources Management Conference of ICWRS*, volume 373, pages 87–94.

Denis, E. H., Toney, J. L., Tarozo, R., Anderson, R. S., Roach, L. D., and Huang, Y. (2012). Polycyclic aromatic hydrocarbons (pahs) in lake sediments record historic fire events: validation using hplc-fluorescence detection. *Organic geochemistry*, **45**, 7–17.

Devia, G. K., Ganasri, B., and Dwarakish, G. (2015). A review on hydrological models. *Aquatic Procedia*, **4**, 1001–1007.

DiBlasi, C. J., Li, H., Davis, A. P., and Ghosh, U. (2009). Removal and fate of polycyclic aromatic hydrocarbon pollutants in an urban stormwater bioretention facility. *Environ Sci Technol*, **43**(2), 494–502.

Doll, T. E. and Frimmel, F. H. (2003). Fate of pharmaceuticals—-photodegradation by simulated solar uv-light. *Chemosphere*, **52**(10), 1757–1769.

Dong, J., Xia, X., Wang, M., Lai, Y., Zhao, P., Dong, H., Zhao, Y., and Wen, J. (2015). Effect of water–sediment regulation of the xiaolangdi reservoir on the concentrations, bioavailability, and fluxes of pahs in the middle and lower reaches of the yellow river. *Journal of Hydrology*, **527**, 101–112.

Dong, J., Xia, X., Wang, M., Xie, H., Wen, J., and Bao, Y. (2016). Effect of recurrent sediment resuspension-deposition events on bioavailability of polycyclic aromatic hydrocarbons in aquatic environments. *Journal of Hydrology*, **540**, 934–946.

Doong, R. A. and Lin, Y. T. (2004). Characterization and distribution of polycyclic aromatic hydrocarbon contaminations in surface sediment and water from gao-ping river, taiwan. *Water Res*, **38**(7), 1733–44.

Engelhardt, I., Piepenbrink, M., Trauth, N., Stadler, S., Kludt, C., Schulz, M., Schüth, C., and Ternes, T. (2011). Comparison of tracer methods to quantify hydrodynamic exchange within the hyporheic zone. *Journal of hydrology*, **400**(1-2), 255–266.

Fadaei, H., Watson, A., Place, A., Connolly, J., and Ghosh, U. (2015). Effect of pcb bioavailability changes in sediments on bioaccumulation in fish. *Environmental science & technology*, **49**(20), 12405–12413.

Falconer, I. R., Chapman, H. F., Moore, M. R., and Ranmuthugala, G. (2006). Endocrine-disrupting compounds: A review of their challenge to sustainable and safe water supply and water reuse. *Environmental Toxicology: An International Journal*, **21**(2), 181–191.

Félix-Cañedo, T. E., Durán-Álvarez, J. C., and Jiménez-Cisneros, B. (2013). The occurrence and distribution of a group of organic micropollutants in mexico city's water sources. *Science of the Total Environment*, **454**, 109–118.

Fernández, P., Vilanova, R. M., Martínez, C., Appleby, P., and Grimalt, J. O. (2000). The historical record of atmospheric pyrolytic pollution over europe registered in the sedimentary pah from remote mountain lakes. *Environ Sci Technol*, **34**(10), 1906–1913.

Ferro, V. and Porto, P. (2000). Sediment delivery distributed (sedd) model. *Journal of Hydrologic Engineering*, **5**(4), 411–422.

Fick, J., Söderström, H., Lindberg, R. H., Phan, C., Tysklind, M., and Larsson, D. J. (2009). Contamination of surface, ground, and drinking water from pharmaceutical production. *Environmental Toxicology and Chemistry*, **28**(12), 2522–2527.

Flanagan, D. C. and Nearing, M. A. (1995). Usda - water erosion prediction project. Report, USDA-ARS National Soil Erosion Research Laboratory.

Focazio, M. J., Kolpin, D. W., Barnes, K. K., Furlong, E. T., Meyer, M. T., Zaugg, S. D., Barber, L. B., and Thurman, M. E. (2008). A national reconnaissance for pharmaceuticals and other organic wastewater contaminants in the united states—ii) untreated drinking water sources. *Science of the total Environment*, **402**(2-3), 201–216.

Fono, L. J., Kolodziej, E. P., and Sedlak, D. L. (2006). Attenuation of wastewater-derived contaminants in an effluent-dominated river. *Environmental science & technology*, **40**(23), 7257–7262.

Gelsleichter, J. and Szabo, N. J. (2013). Uptake of human pharmaceuticals in bull sharks (carcharhinus leucas) inhabiting a wastewater-impacted river. *Science of the total environment*, **456**, 196–201.

Gilley, J., Elliot, W., Laflen, J., and Simoanton, J. (1993). Critical shear stress and critical flow rates for initiation of rilling. *Journal of Hydrology*, **142**, 251–271.

Gocht, T., Steidle, D., and Grathwohl, P. (2005). Polyzyklische aromatische kohlenwasserstoffe in städtischen umweltkompartimenten. *Wasser und Abfall*, **7**(7-8), 10–15.

Gong, Y., Liang, X., Li, X., Li, J., Fang, X., and Song, R. (2016). Influence of rainfall characteristics on total suspended solids in urban runoff: A case study in beijing, china. *Water*, **8**(7), 278.

Gonzalez-Gaya, B., Zuniga-Rival, J., Ojeda, M. J., Jimenez, B., and Dachs, J. (2014). Field measurements of the atmospheric dry deposition fluxes and velocities of polycyclic aromatic hydrocarbons to the global oceans. *Environ Sci Technol*, **48**(10), 5583–92.

Grabicova, K., Grabic, R., Fedorova, G., Fick, J., Cerveny, D., Kolarova, J., Turek, J., Zlabek, V., and Randak, T. (2017). Bioaccumulation of psychoactive pharmaceuticals in fish in an effluent dominated stream. *Water research*, **124**, 654–662.

Grabowski, R. C., Droppo, I. G., and Wharton, G. (2011). Erodibility of cohesive sediment: The importance of sediment properties. *Earth-Science Reviews*, **105**(3-4), 101–120.

Gros, M., Petrović, M., and Barceló, D. (2007). Wastewater treatment plants as a pathway for aquatic contamination by pharmaceuticals in the ebro river basin (northeast spain). *Environmental toxicology and chemistry*, **26**(8), 1553–1562.

Guillet, G., Knapp, J. L., Merel, S., Cirpka, O. A., Grathwohl, P., Zwiener, C., and Schwientek, M. (2018). Fate of wastewater contaminants in rivers: using conservative-tracer based transfer functions to assess reactive transport. Science of the Total Environment (submitted).

Gutowski, L., Olsson, O., Lange, J., and Kümmerer, K. (2015). Photolytic transformation products and biological stability of the hydrological tracer uranine. *Science of the Total Environment*, **533**, 446–453.

Haggerty, R., Martí, E., Argerich, A., Von Schiller, D., and Grimm, N. B. (2009). Resazurin as a "smart" tracer for quantifying metabolically active transient storage in stream ecosystems. *Journal of Geophysical Research: Biogeosciences*, **114**(G3).

Hanamoto, S., Nakada, N., Yamashita, N., and Tanaka, H. (2013). Modeling the photochemical attenuation of down-the-drain chemicals during river transport by stochastic methods and field measurements of pharmaceuticals and personal care products. *Environmental science & technology*, **47**(23), 13571–13577.

Hanson, G. J. and Simon, A. (2001). Erodibility of cohesive streambeds in the loess area of the midwestern usa. *Hydrological Processes*, **15**, 23–38.

Hawthorne, S. B., Miller, D. J., and Kreitinger, J. P. (2006). Measurement of total poly-cyclic aromatic hydrocarbon concentrations in sediments and toxic units used for es-timating risk to benthic invertebrates at manufactured gas plant sites. *Environmental toxicology and chemistry*, **25**(1), 287–296.

Haygarth, P. M., Bilotta, G. S., Bol, R., Brazier, R. E., Butler, P. J., Freer, J., Gimbert, L. J., Granger, S. J., Krueger, T., Macleod, C. J. A., Naden, P., Old, G., Quinton, J. N., Smith, B., and Worsfold, P. (2006). Processes affecting transfer of sediment and colloids, with associated phosphorus, from intensively farmed grasslands: an overview of key issues. *Hydrological Processes*, **20**(20), 4407–4413.

Hublart, P., Ruelland, D., de Cortázar-Atauri, I. G., Gascoin, S., Lhermitte, S., and Iba-cache, A. (2016). Reliability of lumped hydrological modeling in a semi-arid moun-tainous catchment facing water-use changes. *Hydrology and Earth System Sciences*, **20**(9), 3691.

Huerta-Fontela, M., Galceran, M. T., and Ventura, F. (2011). Occurrence and removal of pharmaceuticals and hormones through drinking water treatment. *Water research*, **45**(3), 1432–1442.

Hughes, S. R., Kay, P., and Brown, L. E. (2012). Global synthesis and critical evaluation of pharmaceutical data sets collected from river systems. *Environmental science & technology*, **47**(2), 661–677.

Hwang, H.-M. and Foster, G. D. (2006). Characterization of polycyclic aromatic hydro-carbons in urban stormwater runoff flowing into the tidal anacostia river, washington, dc, usa. *Environmental Pollution*, **140**(3), 416 – 426.

Ibarra-Zavaleta, S. P., Landgrave, R., Romero-López, R., Poulin, A., and Arango-Miranda, R. (2017). Distributed hydrological modeling: Determination of theoretical hydraulic potential & streamflow simulation of extreme hydrometeorological events. *Water*, **9**(8), 602.

Johnston, R. and Smakhtin, V. (2014). Hydrological modeling of large river basins: how much is enough? *Water resources management*, **28**(10), 2695–2730.

Jungnickel, C., Stock, F., Brandsch, T., and Ranke, J. (2008). Risk assessment of biocides in roof paint. *Environmental science and pollution research*, **15**(3), 258.

Kaase, C. T. and Kupfer, J. A. (2016). Sedimentation patterns across a coastal plain floodplain: The importance of hydrogeomorphic influences and cross-floodplain connectivity. *Geomorphology*, **269**, 43–55.

Karickhoff, S. W., Brown, D. S., and Scott, T. A. (1979). Sorption of hydrophobic pollutants on natural sediments. *Water research*, **13**(3), 241–248.

Kasiotis, K. M. and Emmanouil, C. (2015). Advanced pah pollution monitoring by bivalves. *Environmental Chemistry Letters*, **13**(4), 395–411.

Kasprzyk-Hordern, B., Dinsdale, R. M., and Guwy, A. J. (2009). The removal of pharmaceuticals, personal care products, endocrine disruptors and illicit drugs during wastewater treatment and its impact on the quality of receiving waters. *Water research*, **43**(2), 363–380.

Kidd, K. A., Blanchfield, P. J., Mills, K. H., Palace, V. P., Evans, R. E., Lazorchak, J. M., and Flick, R. W. (2007). Collapse of a fish population after exposure to a synthetic estrogen. *Proceedings of the National Academy of Sciences*, **104**(21), 8897–8901.

Kim, M.-K. and Zoh, K.-D. (2016). Occurrence and removals of micropollutants in water environment. *Environmental Engineering Research*, **21**(4), 319–332.

Kim, S. D., Cho, J., Kim, I. S., Vanderford, B. J., and Snyder, S. A. (2007). Occurrence and removal of pharmaceuticals and endocrine disruptors in south korean surface, drinking, and waste waters. *Water research*, **41**(5), 1013–1021.

Kleywegt, S., Pileggi, V., Yang, P., Hao, C., Zhao, X., Rocks, C., Thach, S., Cheung, P., and Whitehead, B. (2011). Pharmaceuticals, hormones and bisphenol a in untreated source and finished drinking water in ontario, canada—occurrence and treatment efficiency. *Science of the Total Environment*, **409**(8), 1481–1488.

Knapp, J. L., González-Pinzón, R., Drummond, J. D., Larsen, L. G., Cirpka, O. A., and Harvey, J. W. (2017). Tracer-based characterization of hyporheic exchange and benthic biolayers in streams. *Water Resources Research*, **53**(2), 1575–1594.

Köck-Schulmeyer, M., Villagrasa, M., de Alda, M. L., Céspedes-Sánchez, R., Ventura, F., and Barceló, D. (2013). Occurrence and behavior of pesticides in wastewater treatment plants and their environmental impact. *Science of the total environment*, **458**, 466–476.

Krone, R. B. (1962). Flume studies of the transport of sediment in estuarial shoaling processes. Report, Univ. of Calif.

Kunkel, U. and Radke, M. (2008). Biodegradation of acidic pharmaceuticals in bed sediments: insight from a laboratory experiment. *Environmental science & technology*, **42**(19), 7273–7279.

Kunkel, U. and Radke, M. (2011). Reactive tracer test to evaluate the fate of pharmaceuticals in rivers. *Environmental science & technology*, **45**(15), 6296–6302.

Kunkel, U. and Radke, M. (2012). Fate of pharmaceuticals in rivers: deriving a benchmark dataset at favorable attenuation conditions. *Water research*, **46**(17), 5551–5565.

Lang, C., Tao, S., Zhang, G., Fu, J., and Simonich, S. (2007). Outflow of polycyclic aromatic hydrocarbons from guangdong, southern china. *Environ Sci Technol*, **41**(24), 8370–8375.

Lapworth, D., Baran, N., Stuart, M., and Ward, R. (2012). Emerging organic contaminants in groundwater: a review of sources, fate and occurrence. *Environmental pollution*, **163**, 287–303.

Launay, M. A., Dittmer, U., and Steinmetz, H. (2016). Organic micropollutants discharged by combined sewer overflows–characterisation of pollutant sources and stormwater-related processes. *Water research*, **104**, 82–92.

Léonard, J. and Richard, G. (2004). Estimation of runoff critical shear stress for soil erosion from soil shear strength. *Catena*, **57**(3), 233–249.

Lewandowski, J., Putschew, A., Schwesig, D., Neumann, C., and Radke, M. (2011). Fate of organic micropollutants in the hyporheic zone of a eutrophic lowland stream: results of a preliminary field study. *Science of the Total Environment*, **409**(10), 1824–1835.

LGRB (2011). Bodenkarte von baden-württemberg 1 v 50 000, geola – integrierte geowissenschaftliche landesaufnahme. Technical report, Regierungspräsidium Freiburg Landesamt für Geologie, Rohstoffe und Bergbau.

Li, Z., Gomez, E., Fenet, H., and Chiron, S. (2013). Chiral signature of venlafaxine as a marker of biological attenuation processes. *Chemosphere*, **90**(6), 1933–1938.

Li, Z., Sobek, A., and Radke, M. (2016). Fate of pharmaceuticals and their transformation products in four small european rivers receiving treated wastewater. *Environmental science & technology*, **50**(11), 5614–5621.

Liang, J., Fang, H., Wu, L., Zhang, T., and Wang, X. (2016). Characterization, distribution, and source analysis of metals and polycyclic aromatic hydrocarbons (pahs) of atmospheric bulk deposition in shanghai, china. *Water, Air, & Soil Pollution*, **227**(7).

Lima, A. L. C., Eglinton, T. I., and Reddy, C. M. (2003). High-resolution record of pyrogenic polycyclic aromatic hydrocarbon deposition during the 20th century. *Environmental Science & Technology*, **37**(1), 53–61.

Lindström, G., Johansson, B., Persson, M., Gardelin, M., and Bergström, S. (1997). Development and test of the distributed hbv-96 hydrological model. *Journal of hydrology*, **201**(1-4), 272–288

Liu, Q., Chai, F., Dugdale, R., Chao, Y., Xue, H., Rao, S., Wilkerson, F., Farrara, J., Zhang, H., Wang, Z., *et al.* (2018a). San francisco bay nutrients and plankton dynamics as simulated by a coupled hydrodynamic-ecosystem model. *Continental Shelf Research*, **161**, 29–48.

Liu, Q.-T., Cumming, R. I., and Sharpe, A. D. (2009a). Photo-induced environmental depletion processes of β-blockers in river waters. *Photochemical & Photobiological Sciences*, **8**(6), 768–777.

Liu, W.-C., Chang, S.-W., Jiann, K.-T., Wen, L.-S., and Liu, K.-K. (2007). Modelling diagnosis of heavy metal (copper) transport in an estuary. *Science of the total environment*, **388**(1-3), 234–249.

Liu, W.-C., Chen, W.-B., and Kimura, N. (2009b). Impact of phosphorus load reduction on water quality in a stratified reservoir-eutrophication modeling study. *Environmental monitoring and assessment*, **159**(1-4), 393–406.

Liu, Y., Beckingham, B., Ruegner, H., Li, Z., Ma, L., Schwientek, M., Xie, H., Zhao, J., and Grathwohl, P. (2013). Comparison of sedimentary pahs in the rivers of ammer (germany) and liangtan (china): differences between early- and newly-industrialized countries. *Environ Sci Technol*, **47**(2), 701–9.

Liu, Y., Zarfl, C., Basu, N. B., Schwientek, M., and Cirpka, O. A. (2018b). Contributions of catchment and in-stream processes to suspended sediment transport in a dominantly groundwater-fed catchment. *Hydrology and Earth System Sciences*, **22**(7), 3903–3921.

LUBW (2010). Erstellung von hochwassergefahrenkarten des landes baden-württemberg. Technical report, LUBW (Landesanstalt für Umwelt, Messungen und Naturschutz, Karlsruhe).

Luo, Y., Guo, W., Ngo, H. H., Nghiem, L. D., Hai, F. I., Zhang, J., Liang, S., and Wang, X. C. (2014). A review on the occurrence of micropollutants in the aquatic environment and their fate and removal during wastewater treatment. *Science of the Total Environment*, **473**, 619–641.

Mai, Qi, Zeng, E. Y., Yang, Zhang, G., Fu, Sheng, Peng, and Wang (2003). Distribution of polycyclic aromatic hydrocarbons in the coastal region off macao, china: assessment of input sources and transport pathways using compositional analysis. *Environ Sci Technol*, **37**(21), 4855–4863.

Manamsa, K., Crane, E., Stuart, M., Talbot, J., Lapworth, D., and Hart, A. (2016). A national-scale assessment of micro-organic contaminants in groundwater of england and wales. *Science of the Total Environment*, **568**, 712–726.

Manickum, T. and John, W. (2014). Occurrence, fate and environmental risk assessment of endocrine disrupting compounds at the wastewater treatment works in pietermaritzburg (south africa). *Science of the Total Environment*, **468**, 584–597.

Margot, J., Kienle, C., Magnet, A., Weil, M., Rossi, L., De Alencastro, L. F., Abegglen, C., Thonney, D., Chèvre, N., Schärer, M., *et al.* (2013). Treatment of micropollutants in municipal wastewater: ozone or powdered activated carbon? *Science of the total environment*, **461**, 480–498.

Meus, P., Moureaux, P., Gailliez, S., Flament, J., Delloye, F., and Nix, P. (2013). In situ monitoring of karst springs in wallonia (southern belgium). *Environmental Earth Sciences*, **71**(2), 533–541.

Meyer, T. and Wania, F. (2008). Organic contaminant amplification during snowmelt. *Water Res*, **42**(8-9), 1847–65.

Modugno, M., Gioia, A., Gorgoglione, A., Iacobellis, V., Forgia, G., Piccinni, A., and Ranieri, E. (2015). Build-up/wash-off monitoring and assessment for sustainable management of first flush in an urban area. *Sustainability*, **7**(5), 5050–5070.

Morgan, R. P. C., Quinton, J. N., Smith, R. E., Govers, G., Poesen, J. W. A., Auerswald, K., Chisci, G., Torri, D., and Styczen, M. E. (1998). The european soil erosion model (eurosem): A dynamic approach for predicting sediment transport from fields and small catchments. *Earth Surface Processes and Landforms*, **23**(6), 527–544.

Mukherjee, D. P. (2014). Dynamics of metal ions in suspended sediments in hugli estuary, india and its importance towards sustainable monitoring program. *Journal of Hydrology*, **517**, 762–776.

Musolff, A., Leschik, S., Möder, M., Strauch, G., Reinstorf, F., and Schirmer, M. (2009). Temporal and spatial patterns of micropollutants in urban receiving waters. *Environmental pollution*, **157**(11), 3069–3077.

Nam, S.-W., Jo, B.-I., Yoon, Y., and Zoh, K.-D. (2014). Occurrence and removal of selected micropollutants in a water treatment plant. *Chemosphere*, **95**, 156–165.

Neitsch, S. L., Arnold, J. G., Kiniry, J. R., and Williams, J. R. (2011). Soil and water assessment tool theoretical documentation version 2009. Technical report, Texas Water Resources Institute.

Nerantzaki, S., Giannakis, G., Efstathiou, D., Nikolaidis, N., Sibetheros, I., Karatzas, G., and Zacharias, I. (2015). Modeling suspended sediment transport and assessing the impacts of climate change in a karstic mediterranean watershed. *Science of the Total Environment*, **538**, 288–297.

Nguyen, T. T., Keupers, I., and Willems, P. (2018). Conceptual river water quality model with flexible model structure. *Environmental Modelling & Software*, **104**, 102–117.

Nödler, K., Tsakiri, M., and Licha, T. (2014). The impact of different proportions of a treated effluent on the biotransformation of selected micro-contaminants in river water microcosms. *International journal of environmental research and public health*, **11**(10), 10390–10405.

Norton, J. (2015). An introduction to sensitivity assessment of simulation models. *Environmental Modelling & Software*, **69**, 166–174.

Oros, D. R., Ross, J. R., Spies, R. B., and Mumley, T. (2007). Polycyclic aromatic hydrocarbon (pah) contamination in san francisco bay: a 10-year retrospective of monitoring in an urbanized estuary. *Environ Res*, **105**(1), 101–18.

Osenbrück, K., Gläser, H.-R., Knöller, K., Weise, S. M., Möder, M., Wennrich, R., Schirmer, M., Reinstorf, F., Busch, W., and Strauch, G. (2007). Sources and transport of selected organic micropollutants in urban groundwater underlying the city of halle (saale), germany. *Water research*, **41**(15), 3259–3270.

Osorio, V., Marcé, R., Pérez, S., Ginebreda, A., Cortina, J. L., and Barceló, D. (2012). Occurrence and modeling of pharmaceuticals on a sewage-impacted mediterranean river and their dynamics under different hydrological conditions. *Science of the total environment*, **440**, 3–13.

Pal, A., Gin, K. Y.-H., Lin, A. Y.-C., and Reinhard, M. (2010). Impacts of emerging organic contaminants on freshwater resources: review of recent occurrences, sources, fate and effects. *Science of the total environment*, **408**(24), 6062–6069.

Park, Y.-J., Sudicky, E. A., Brookfield, A. E., and Jones, J. P. (2011). Hydrologic response of catchments to precipitation: quantification of mechanical carriers and origins of water. *Water Resources Research*, **47**(12).

Partheniades, E. (1965). Erosion and deposition of cohesive soils. *Journal of the Hydraulics Division*, **91**(1), 105–139.

Patil, S., Sivapalan, M., Hassan, M. A., Ye, S., Harman, C. J., and Xu, X. (2012). A network model for prediction and diagnosis of sediment dynamics at the watershed scale. *Journal of Geophysical Research*, **117**.

Patrolecco, L., Ademollo, N., Capri, S., Pagnotta, R., and Polesello, S. (2010). Occurrence of priority hazardous pahs in water, suspended particulate matter, sediment and common eels (anguilla anguilla) in the urban stretch of the river tiber (italy). *Chemosphere*, **81**(11), 1386–92.

Pechlivanidis, I., Jackson, B., McIntyre, N., and Wheater, H. (2011). Catchment scale hydrological modelling: a review of model types, calibration approaches and uncertainty analysis methods in the context of recent developments in technology and applications. *Global NEST journal*, **13**(3), 193–214.

Peraza-Castro, M., Sauvage, S., Sanchez-Perez, J. M., and Ruiz-Romera, E. (2016). Effect of flood events on transport of suspended sediments, organic matter and particulate metals in a forest watershed in the basque country (northern spain). *Sci Total Environ*, **569-570**, 784–97.

Petrovic, M., de Alda, M. J. L., Diaz-Cruz, S., Postigo, C., Radjenovic, J., Gros, M., and Barcelo, D. (2009). Fate and removal of pharmaceuticals and illicit drugs in conventional and membrane bioreactor wastewater treatment plants and by riverbank filtration. *Philosophical Transactions of the Royal Society of London A: Mathematical, Physical and Engineering Sciences*, **367**(1904), 3979–4003.

Phillips, P., Chalmers, A., Gray, J., Kolpin, D., Foreman, W., and Wall, G. (2012). Combined sewer overflows: an environmental source of hormones and wastewater micropollutants. *Environmental science & technology*, **46**(10), 5336–5343.

Phillips, P. J., Schubert, C., Argue, D., Fisher, I., Furlong, E. T., Foreman, W., Gray, J., and Chalmers, A. (2015). Concentrations of hormones, pharmaceuticals and other micropollutants in groundwater affected by septic systems in new england and new york. *Science of the Total Environment*, **512**, 43–54.

Pianosi, F., Beven, K., Freer, J., Hall, J. W., Rougier, J., Stephenson, D. B., and Wagener, T. (2016). Sensitivity analysis of environmental models: A systematic review with practical workflow. *Environmental Modelling & Software*, **79**, 214–232.

Ping, J., Yan, S., Gu, P., Wu, Z., and Hu, C. (2017). Application of mike she to study the impact of coal mining on river runoff in gujiao mining area, shanxi, china. *PloS one*, **12**(12), e0188949.

Piro, P. and Carbone, M. (2014). A modelling approach to assessing variations of total suspended solids (tss) mass fluxes during storm events. *Hydrological Processes*, **28**(4), 2419–2426.

Price, O. R., Hughes, G. O., Roche, N. L., and Mason, P. J. (2010). Improving emissions estimates of home and personal care products ingredients for use in eu risk assessments. *Integrated environmental assessment and management*, **6**(4), 677–684.

Prieto-Rodríguez, L., Oller, I., Klamerth, N., Agüera, A., Rodríguez, E., and Malato, S. (2013). Application of solar aops and ozonation for elimination of micropollutants in municipal wastewater treatment plant effluents. *Water research*, **47**(4), 1521–1528.

Purcaro, G., Moret, S., and Conte, L. S. (2013). Overview on polycyclic aromatic hydrocarbons: occurrence, legislation and innovative determination in foods. *Talanta*, **105**, 292–305.

Quesada, S., Tena, A., Guillen, D., Ginebreda, A., Vericat, D., Martinez, E., Navarro-Ortega, A., Batalla, R. J., and Barcelo, D. (2014). Dynamics of suspended sediment borne persistent organic pollutants in a large regulated mediterranean river (ebro, ne spain). *Sci Total Environ*, **473-474**, 381–90.

Quinton, J. N. and Catt, J. A. (2007). Enrichment of heavy metals in sediment resulting from soil erosion on agricultural fields. *Environ. Sci. Technol.*, **41**, 3495–3500.

Radke, M., Lauwigi, C., Heinkele, G., Mürdter, T. E., and Letzel, M. (2009). Fate of the antibiotic sulfamethoxazole and its two major human metabolites in a water sediment test. *Environmental science & technology*, **43**(9), 3135–3141.

Rajapaksha, A. U., Vithanage, M., Lim, J. E., Ahmed, M. B. M., Zhang, M., Lee, S. S., and Ok, Y. S. (2014). Invasive plant-derived biochar inhibits sulfamethazine uptake by lettuce in soil. *Chemosphere*, **111**, 500–504.

Rakowska, M. I., Kupryianchyk, D., Smit, M. P., Koelmans, A. A., Grotenhuis, J. T., and Rijnaarts, H. H. (2014). Kinetics of hydrophobic organic contaminant extraction from sediment by granular activated carbon. *Water Res*, **51**, 86–95.

Reungoat, J., Macova, M., Escher, B., Carswell, S., Mueller, J., and Keller, J. (2010). Removal of micropollutants and reduction of biological activity in a full scale reclamation plant using ozonation and activated carbon filtration. *Water research*, **44**(2), 625–637.

Riml, J., Wörman, A., Kunkel, U., and Radke, M. (2013). Evaluating the fate of six common pharmaceuticals using a reactive transport model: Insights from a stream tracer test. *Science of the total environment*, **458**, 344–354.

Romero, C. C., Stroosnijder, L., and Baigorria, G. A. (2007). Interrill and rill erodibility in the northern andean highlands. *Catena*, **70**(2), 105–113.

Rossman, L. A. and Huber, W. C. (2016). Storm water management model, reference manual, volume iii – water quality. Report, U.S. Environmental Protection Agency.

Rúa-Gómez, P. C. and Püttmann, W. (2013). Degradation of lidocaine, tramadol, venlafaxine and the metabolites o-desmethyltramadol and o-desmethylvenlafaxine in surface waters. *Chemosphere*, **90**(6), 1952–1959.

Rügner, H., Schwientek, M., Beckingham, B., Kuch, B., and Grathwohl, P. (2013). Turbidity as a proxy for total suspended solids (tss) and particle facilitated pollutant transport in catchments. *Environmental Earth Sciences*, **69**(2), 373–380.

Rügner, H., Schwientek, M., Egner, M., and Grathwohl, P. (2014a). Monitoring of event-based mobilization of hydrophobic pollutants in rivers: calibration of turbidity as a proxy for particle facilitated transport in field and laboratory. *Sci Total Environ*, **490**, 191–8.

Rügner, H., Schwientek, M., Egner, M., and Grathwohl, P. (2014b). Monitoring of event-based mobilization of hydrophobic pollutants in rivers: calibration of turbidity as a proxy for particle facilitated transport in field and laboratory. *Sci Total Environ*, **490**, 191–8.

Rujner, H., Leonhardt, G., Marsalek, J., and Viklander, M. (2018). High-resolution modelling of the grass swale response to runoff inflows with mike she. *Journal of Hydrology*, **562**, 411–422.

Sabiha, C., Azzedine, H., Larbi, D., Bachir, S., Sebaiti Bdra, A., Imen, A., and Sami, L. (2014). A new conceptual water integrated model for the seybouse basin, annaba region. *Desalination and Water Treatment*, **52**(10-12), 2102–2113.

Sámano, M. L., García, A., Revilla, J. A., and Álvarez, C. (2014). Modeling heavy metal concentration distributions in estuarine waters: an application to suances estuary (northern spain). *Environmental earth sciences*, **72**(8), 2931–2945.

Santoke, H. and Cooper, W. J. (2017). Environmental photochemical fate of selected pharmaceutical compounds in natural and reconstituted suwannee river water: Role of reactive species in indirect photolysis. *Science of the Total Environment*, **580**, 626–631.

Scanlon, T. M., Kiely, G., and Xie, Q. (2004). A nested catchment approach for defining the hydrological controls on non-point phosphorus transport. *Journal of Hydrology*, **291**(3-4), 218–231.

Schimmelpfennig, S., Kirillin, G., Engelhardt, C., Dünnbier, U., and Nützmann, G. (2016). Fate of pharmaceutical micro-pollutants in lake tegel (berlin, germany): the impact of lake-specific mechanisms. *Environmental Earth Sciences*, **75**(10), 893.

Schoknecht, U., Gruycheva, J., Mathies, H., Bergmann, H., and Burkhardt, M. (2009). Leaching of biocides used in facade coatings under laboratory test conditions. *Environmental science & technology*, **43**(24), 9321–9328.

Schwarzenbach, R. P., Escher, B. I., Fenner, K., Hofstetter, T. B., Johnson, C. A., Von Gunten, U., and Wehrli, B. (2006). The challenge of micropollutants in aquatic systems. *Science*, **313**(5790), 1072–1077.

Schwientek, M., Rügner, H., Beckingham, B., Kuch, B., and Grathwohl, P. (2013a). Integrated monitoring of particle associated transport of pahs in contrasting catchments. *Environ Pollut*, **172**, 155–62.

Schwientek, M., Osenbrück, K., and Fleischer, M. (2013b). Investigating hydrological drivers of nitrate export dynamics in two agricultural catchments in germany using high-frequency data series. *Environmental Earth Sciences*, **69**(2), 381–393.

Schwientek, M., Guillet, G., Rügner, H., Kuch, B., and Grathwohl, P. (2016). A high-precision sampling scheme to assess persistence and transport characteristics of micropollutants in rivers. *Science of the Total Environment*, **540**, 444–454.

Schwientek, M., Rügner, H., Scherer, U., Rode, M., and Grathwohl, P. (2017). A parsimonious approach to estimate pah concentrations in river sediments of anthropogenically impacted watersheds. *Sci Total Environ*, **601-602**, 636–645.

Selle, B., Schwientek, M., and Lischeid, G. (2013). Understanding processes governing water quality in catchments using principal component scores. *Journal of Hydrology*, **486**, 31–38.

Seo, Y., Kim, S., Kisi, O., and Singh, V. P. (2015). Daily water level forecasting using wavelet decomposition and artificial intelligence techniques. *Journal of Hydrology*, **520**, 224–243.

Shen, H., Tao, S., Wang, R., Wang, B., Shen, G., Li, W., Su, S., Huang, Y., Wang, X., Liu, W., Li, B., and Sun, K. (2011). Global time trends in pah emissions from motor vehicles. *Atmos Environ (1994)*, **45**(12).

Sherman, L. K. (1932). Streamflow from rainfall by the unit-graph method. *Eng. News Record*, **108**, 501–505.

Shin, M.-J., Guillaume, J. H., Croke, B. F., and Jakeman, A. J. (2013). Addressing ten questions about conceptual rainfall–runoff models with global sensitivity analyses in r. *Journal of Hydrology*, **503**, 135–152.

Siddiqui, A. and Robert, A. (2010). Thresholds of erosion and sediment movement in bedrock channels. *Geomorphology*, **118**(3-4), 301–313.

Sim, W.-J., Lee, J.-W., and Oh, J.-E. (2010). Occurrence and fate of pharmaceuticals in wastewater treatment plants and rivers in korea. *Environmental Pollution*, **158**(5), 1938–1947.

Singer, H., Jaus, S., Hanke, I., Lück, A., Hollender, J., and Alder, A. C. (2010). Determination of biocides and pesticides by on-line solid phase extraction coupled with mass spectrometry and their behaviour in wastewater and surface water. *Environmental pollution*, **158**(10), 3054–3064.

Singh, R., Wagener, T., Crane, R., Mann, M., and Ning, L. (2014). A vulnerability driven approach to identify adverse climate and land use change combinations for critical hydrologic indicator thresholds: Application to a watershed in pennsylvania, usa. *Water Resources Research*, **50**(4), 3409–3427.

Slaets, J. I. F., Schmitter, P., Hilger, T., Lamers, M., Piepho, H.-P., Vien, T. D., and Cadisch, G. (2014). A turbidity-based method to continuously monitor sediment, carbon and nitrogen flows in mountainous watersheds. *Journal of Hydrology*, **513**, 45–57.

Song, X., Zhang, J., Zhan, C., Xuan, Y., Ye, M., and Xu, C. (2015). Global sensitivity analysis in hydrological modeling: Review of concepts, methods, theoretical framework, and applications. *Journal of hydrology*, **523**, 739–757.

Stein, E. D., Tiefenthaler, L. L., and Schiff, K. (2006). Watershed-based sources of polycyclic aromatic hydrocarbons in urban storm water. *Environmental Toxicology and Chemistry*, **25**(2), 373–385.

Stuart, M., Lapworth, D., Crane, E., and Hart, A. (2012). Review of risk from potential emerging contaminants in uk groundwater. *Science of the Total Environment*, **416**, 1–21.

Ter Braak, C. J. (2006). A markov chain monte carlo version of the genetic algorithm differential evolution: easy bayesian computing for real parameter spaces. *Statistics and Computing*, **16**(3), 239–249.

Teutschbein, C. and Seibert, J. (2012). Bias correction of regional climate model simulations for hydrological climate-change impact studies: Review and evaluation of different methods. *Journal of Hydrology*, **456**, 12–29.

Tiedeken, E. J., Tahar, A., McHugh, B., and Rowan, N. J. (2017). Monitoring, sources, receptors, and control measures for three european union watch list substances of emerging concern in receiving waters–a 20 year systematic review. *Science of The Total Environment*, **574**, 1140–1163.

Tiehm, A., Schmidt, N., Stieber, M., Sacher, F., Wolf, L., and Hoetzl, H. (2011). Biodegradation of pharmaceutical compounds and their occurrence in the jordan valley. *Water Resources Management*, **25**(4), 1195–1203.

Tijani, J. O., Fatoba, O. O., and Petrik, L. F. (2013). A review of pharmaceuticals and endocrine-disrupting compounds: sources, effects, removal, and detections. *Water, Air, & Soil Pollution*, **224**(11), 1770.

Tijani, J. O., Fatoba, O. O., Babajide, O. O., and Petrik, L. F. (2016). Pharmaceuticals, endocrine disruptors, personal care products, nanomaterials and perfluorinated pollutants: a review. *Environmental chemistry letters*, **14**(1), 27–49.

Tiwari, M. K. and Chatterjee, C. (2010). Development of an accurate and reliable hourly flood forecasting model using wavelet–bootstrap–ann (wbann) hybrid approach. *Journal of Hydrology*, **394**(3-4), 458–470.

Tobiszewski, M. and Namiesnik, J. (2012). Pah diagnostic ratios for the identification of pollution emission sources. *Environ Pollut*, **162**, 110–9.

Torresi, E., Plósz, B. G., Christensson, M., and Smets, B. F. (2017). *Removal of micropollutants in Moving Bed Biofilm reactors (MBBRs): Microbial-diversity-and-functional-relationships*. Ph.D. thesis, Department of Environmental Engineering.

Tsakiris, G. and Alexakis, D. (2012). Water quality models: an overview. *European Water*, **37**, 33–46.

UBA (2009). Corine land cover (clc2006). Technical report, Umweltbundesamt (German Environmental Protection Agency) (DLR-DFD 2009).

Van Metre, P. C. and Mahler, B. J. (2003). The contribution of particles washed from rooftops to contaminant loading to urban streams. *Chemosphere*, **52**(10), 1727–1741.

Van Metre, P. C. and Mahler, B. J. (2014). Pah concentrations in lake sediment decline following ban on coal-tar-based pavement sealants in austin, texas. *Environmental science & technology*, **48**(13), 7222–7228.

Verlicchi, P., Al Aukidy, M., and Zambello, E. (2012). Occurrence of pharmaceutical compounds in urban wastewater: removal, mass load and environmental risk after a secondary treatment—a review. *Science of the total environment*, **429**, 123–155.

Verliefde, A., Cornelissen, E., Amy, G., Van der Bruggen, B., and Van Dijk, H. (2007). Priority organic micropollutants in water sources in flanders and the netherlands and assessment of removal possibilities with nanofiltration. *Environmental pollution*, **146**(1), 281–289.

Vithanage, M., Rajapaksha, A. U., Tang, X., Thiele-Bruhn, S., Kim, K. H., Lee, S.-E., and Ok, Y. S. (2014). Sorption and transport of sulfamethazine in agricultural soils amended with invasive-plant-derived biochar. *Journal of environmental management*, **141**, 95–103.

Vrugt, J. A. (2016). Markov chain monte carlo simulation using the dream software package: Theory, concepts, and matlab implementation. *Environmental Modelling & Software*, **75**, 273–316.

Vrugt, J. A., Ter Braak, C. J., Clark, M. P., Hyman, J. M., and Robinson, B. A. (2008). Treatment of input uncertainty in hydrologic modeling: Doing hydrology backward with markov chain monte carlo simulation. *Water Resources Research*, **44**(12).

Vrugt, J. A., Ter Braak, C., Diks, C., Robinson, B. A., Hyman, J. M., and Higdon, D. (2009). Accelerating markov chain monte carlo simulation by differential evolution with self-adaptive randomized subspace sampling. *International Journal of Nonlinear Sciences and Numerical Simulation*, **10**(3), 273–290.

Vulava, V. M., Cory, W. C., Murphey, V. L., and Ulmer, C. Z. (2016). Sorption, photodegradation, and chemical transformation of naproxen and ibuprofen in soils and water. *Science of the Total Environment*, **565**, 1063–1070.

Vulliet, E. and Cren-Olivé, C. (2011). Screening of pharmaceuticals and hormones at the regional scale, in surface and groundwaters intended to human consumption. *Environmental pollution*, **159**(10), 2929–2934.

Vulliet, E., Cren-Olivé, C., and Grenier-Loustalot, M.-F. (2011). Occurrence of pharmaceuticals and hormones in drinking water treated from surface waters. *Environmental Chemistry Letters*, **9**(1), 103–114.

Wakeham, S. G., Forrest, J., Masiello, C. A., Gélinas, Y., Alexander, C. R., and Leavitt, P. R. (2004). Hydrocarbons in lake washington sediments. a 25-year retrospective in an urban lake. *Environ Sci Technol*, **38**(2), 431–439.

Wang, J.-Z., Guan, Y.-F., Ni, H.-G., Luo, X.-L., and Zeng, E. Y. (2007). Polycyclic aromatic hydrocarbons in riverine runoff of the pearl river delta (china): concentrations, fluxes, and fate. *Environ Sci Technol*, **41**(16), 5614–5619.

Wang, Q., Li, S., Jia, P., Qi, C., and Ding, F. (2013). A review of surface water quality models. *The Scientific World Journal*, **2013**.

Wang, X.-H. and Lin, A. Y.-C. (2014). Is the phototransformation of pharmaceuticals a natural purification process that decreases ecological and human health risks? *Environmental pollution*, **186**, 203–215.

136

Wicke, D., Cochrane, T. A., and O'Sullivan, A. (2012). Build-up dynamics of heavy metals deposited on impermeable urban surfaces. *J Environ Manage*, **113**, 347–54.

Winterwerp, J. C., van Kesteren, W. G. M., van Prooijen, B., and Jacobs, W. (2012). A conceptual framework for shear flow-induced erosion of soft cohesive sediment beds. *Journal of Geophysical Research: Oceans*, **117**(C10), n/a–n/a.

Wischmeier, H. and Smith, D. (1978). Predicting rainfall erosion losses. Report, USDA Science and Education Administration.

Writer, J. H., Antweiler, R. C., Ferrer, I., Ryan, J. N., and Thurman, E. M. (2013). In-stream attenuation of neuro-active pharmaceuticals and their metabolites. *Environmental science & technology*, **47**(17), 9781–9790.

Xu, B., Mao, D., Luo, Y., and Xu, L. (2011). Sulfamethoxazole biodegradation and biotransformation in the water–sediment system of a natural river. *Bioresource technology*, **102**(14), 7069–7076.

Xu, Z.-x., Li, L., and Zhao, J. (2017). A distributed eco-hydrological model and its application. *Water Science and Engineering*, **10**(4), 257–264.

Yan, B., Bopp, R. F., Abrajano, T. A., Chaky, D., and Chillrud, S. N. (2014). Source apportionment of polycyclic aromatic hydrocarbons (pahs) into central park lake, new york city, over a century of deposition. *Environ Toxicol Chem*, **33**(5), 985–92.

Yan, J., Wang, L., Fu, P. P., and Yu, H. (2004). Photomutagenicity of 16 polycyclic aromatic hydrocarbons from the us epa priority pollutant list. *Mutation Research/Genetic Toxicology and Environmental Mutagenesis*, **557**(1), 99–108.

Yang, Y., Ligouis, B., Pies, C., Grathwohl, P., and Hofmann, T. (2008). Occurrence of coal and coal-derived particle-bound polycyclic aromatic hydrocarbons (pahs) in a river floodplain soil. *Environ Pollut*, **151**(1), 121–9.

Yang, Y., Ok, Y. S., Kim, K.-H., Kwon, E. E., and Tsang, Y. F. (2017). Occurrences and removal of pharmaceuticals and personal care products (ppcps) in drinking water and water/sewage treatment plants: A review. *Science of the Total Environment*, **596**, 303–320.

Yuceer, M. and Coskun, M. (2016). Modeling water quality in rivers: a case study of beylerderesi river in turkey. *APPLIED ECOLOGY AND ENVIRONMENTAL RESEARCH*, **14**(1), 383–395.

Zhang, M. and Yu, G. (2017). Critical conditions of incipient motion of cohesive sediments. *Water Resour. Res.*, **53**, 7798–7815.

Zhang, W., Keller, A. A., and Wang, X. (2009). Analytical modeling of polycyclic aromatic hydrocarbon loading and transport via road runoff in an urban region of beijing, china. *Water Resources Research*, **45**(1).

Zhang, Y., Guo, C.-S., Xu, J., Tian, Y.-Z., Shi, G.-L., and Feng, Y.-C. (2012). Potential source contributions and risk assessment of pahs in sediments from taihu lake, china: comparison of three receptor models. *Water research*, **46**(9), 3065–3073.

Zhang, Y., Xiao, W., and Jiao, N. (2016). Linking biochemical properties of particles to particle-attached and free-living bacterial community structure along the particle density gradient from freshwater to open ocean. *Journal of Geophysical Research: Biogeosciences*, **121**(8), 2261–2274.

Zhao, J.-L., Ying, G.-G., Liu, Y.-S., Chen, F., Yang, J.-F., Wang, L., Yang, X.-B., Stauber, J. L., and Warne, M. S. J. (2010). Occurrence and a screening-level risk assessment of human pharmaceuticals in the pearl river system, south china. *Environmental Toxicology and Chemistry*, **29**(6), 1377–1384.

Zhu, Y., Tao, S., Sun, J., Wang, X., Li, X., Tsang, D. C., Zhu, L., Shen, G., Huang, H., Cai, C., *et al.* (2019). Multimedia modeling of the pah concentration and distribution in the yangtze river delta and human health risk assessment. *Science of The Total Environment*, **647**, 962–972.